Characterization of proneural bHLH transcription factor target genes in *X. laevis*

Doctoral Thesis

Dissertation for the award of the degree
"Doctor rerum naturalium (Dr. rer. nat.)"
in the GGNB program “Genes and Development”

at the Georg August University Göttingen
Faculty of Biology

submitted by

Esther Adjoa Essel
born in Accra, Ghana

Göttingen, April 2022

Members of the Thesis Committee:

Dr. Kristine A. Henningfeld (Supervisor, Reviewer)
Institute for Cell biochemistry and Institute for Molecular biology
University of Goettingen

Prof. Dr. Gregor Bucher (Reviewer)
Department of Evolutionary Developmental Genetics
University of Goettingen

Prof. Dr. Heike Krebber
Institute for Microbiology and Genetic
Department of Molecular Genetics
University of Goettingen

Examination board Members:

Prof. Dr. E. A Wimmer
Department of Developmental Biology
University of Goettingen

Prof. Dr. Thomas Dresbach
Department of Anatomy and Embryology
University of Goettingen

Prof. Dr. Joerg Grosshans
Department of Genetics
Philipps-University Marburg

Table of content

List of figures

List of tables

List of Appendices

Abbreviations

A	Adenine
aa	amino acid
ARE	Adenylate-uridylate-rich element
BCNE center	blastula Chordin- and Noggin-expressing center
bHLH	basic helix-loop-helix
BMP	bone morphogenetic protein
bp	base pairs
C	Cytosine
CC	noninjected control caps
cDNA	complementary DNA
CE	noninjected control embryos
Co MO	control morpholino
dll1	Notch ligand delta1
DNA	deoxyribonucleic acid
EDTA	ethylenediaminetetraacetic acid
et al.	et alii
EtOH	ethanol
FGF	Fibroblast growth factors
for	forward
G	Guanine
g	gram
GFP	green fluorescent protein
h	hour/hours
hb	hindbrain
l	liter
LB	Luria Bertani
m	millimeter
M	molar
MAB	maleic acid buffer
MAPK	mitogen-activated protein kinase
mb	midbrain
min	minutes
miR	microRNA

MO	morpholino
n	nano
neurog2	neurogenin 2
ng	nanogram
NICD	intracellular domain of the Notch receptor
nl	nanolitre
p	pico
PBS	phosphate buffered saline
PCR	polymerase chain reaction
pH	negative decade logarithm of hydrogen ion concentration
RBP	RNA binding protein
REST	RE1 Silencing Transcription Factor
rev	reverse
RNA	ribonucleic acid
RNase	ribonuclease
RNAseq	RNA sequencing
rpm	rounds per minute
RT	room temperature
RT-PCR	reverse transcriptase PCR
s	seconds
sc	spinal cord
St	stage
T	Thymine
TAE	Tris-acetate-EDTA
Tm	melting temperature
tp	trigeminal placodes
U	units
v	volume
WMISH	whole mount in situ hybridizations
X. laevis	*Xenopus laevis*
xg	times gravity
X-Gal	5-bromo-4-chloro-3-indolyl-β-d-galactopyranoside
%	percent
°C	celsius degree

µ	micro
3’UTR	3’ untranslated region
5’UTR	5’ untranslated region

Acknowledgement

I thank God for how far I have come. He has been my source and sustainer all through.

My heartfelt gratitude goes to Dr. Kristine Henningfeld for her great supervisory skills and invaluable support throughout my PhD journey. She showed interest not only in the outcomes of my research work but my general wellbeing as well.

I would like to also thank my thesis committee members Prof. Dr. Gregor Bucher and Prof. Dr. Heike Krebber for their invaluable contribution toward this work.

I am very grateful to Prof. Dr. Wimmer, Prof. Dr. Dresbach and Prof. Dr. Joerg Grosshans for been part of my examination board.

I would like to express my gratitude to Dr. Sven Richts for his support and company during the entire period of my studies and Mona Capito-Honemann for her technical support.

I appreciate all former lab members especially Katja Ditter for her enormous technical support as well as members of the TAL for the immense help with sequencing.

I am highly indebted to the Government of Ghana and the DAAD through whose joint sponsorship this PhD journey was began and sustained and the GGNB for the doctoral training finishing grant.

A special thanks go to my husband, Mr. Nicholas Taylor. for his phenomenal support throughout this journey and my daughter Aseda Annan Taylor for giving me several reasons to persevere in the very tough times.

To the Sokpor family, I say thank you for the support especially at the beginning of my studies.

Finally, to my extended family and friends, I appreciate all the help I received from you in the entire journey.

Abstract

Zc3h12c is a member of the Zc3h12 endoribonuclease family (also known as MCPIP/Regnase), which contains four members (Zc3h12a-c). This family of proteins is characterized by the presence of a single centrally located CCCH-type zinc finger domain, which mediates RNA binding, and an N-terminally located NYN/PIN domain responsible for RNase activity. Members of this family are best described for their role in modulating inflammation, through negative feedback via destruction of specific mRNAs encoding proinflammatory cytokines.

In this thesis, the role of the RNase Zc3h12c as a novel regulator of early neural development in *X. laevis* is described. In ectodermal explants, Zc3h12c localizes as granule-like structures in the cytoplasm. Transcripts of *zc3h12c* are first detected by WMISH to the bilateral stripes of primary neurogenesis in open neural plate stage embryos. The temporal expression of *zc3h12c* is preceded by the proneural gene *neurog2,* but parallels that of the neural zinc finger transcription factor *myt1.* In tailbud stages embryos, *zc3h12c* transcripts are specifically expressed in the nervous system including the brain, eye and intermediate zone of the spinal cord where cells are actively undergoing differentiation. Consistent with its expression, *zc3h12c* is positively regulated by Neurog2, both in the embryo and in animal caps. Overexpression of Zc3h12c increases the number of primary neurons within the neurogenic stripes in an RNase dependent manner. Results from loss of function experiments in embryos and animal caps show that Zc3h12c acts downstream of Neurog2 and is essential for primary neuron differentiation. A transcriptome analysis of animal caps directed to undergo neurogenesis through Neurog2 expression in the presence or absence of Zc3h12c (MO knockdown) was performed. Zc3h12c knockdown only influenced a subset of Neurog2 downstream genes. The knockdown of Zc3h12c did not disrupt the Neurog2-induction of genes involved in the early phase of neuronal differentiation,

including most neural transcription factors (*e.g. ebf2, ebf3, tlx3, myt1, neurod4*). However, later acting neuronal genes like *tubb2b* and those encoding cytoskeletal binding proteins and other aspects of neuronal maturation and function were preferentially disrupted. The knockdown of Zc3h12c resulted in the upregulation of several *hes* genes, indicating elevated Notch signaling. However, the loss of neuronal differentiation upon knockdown of Zc3h12c could not be rescued through the inhibition of Notch signaling suggesting additional mechanisms. Zc3h12c knockdown also upregulated genes involved in promoting the cell cycle, including several cyclins, which suggests that the failure of neural progenitors to undergo neuronal differentiation upon Zc3h12c knockdown may be due to the inability to exit the cell cycle.

1 Introduction

During embryogenesis, multiple intrinsic and extrinsic regulators act together to control the competence, differentiation and maturation of individual cells. The development of a functional nervous system requires the precise regulation of neuron production, the failure of which forms the basis of several neurological diseases (Fan & Pang, 2017). As the molecular mechanisms by which a progenitor cell attains a neuronal fate during early neural development may be conserved in adult neurogenesis, gaining an understanding of these events is of fundamental importance to the development of therapeutic interventions.

The African clawed frog, *Xenopus laevis* (*X. laevis*) is an ideal model system for neurodevelopmental studies (Borodinsky, 2017; Droz & McLaughlin, 2017; Dubey & Saint-Jeannet, 2017; Exner & Willsey, 2021; Lee-Liu *et al*., 2017). The first neurons are borne in a simple characteristic pattern at the open neural plate stage. Additionally, the external nature of development offers early access to embryos allowing their manipulation through microinjection and lipofection experiments. Various material can be directly injected including mRNA or DNA for gain of function experiments and antisense morpholino oligonucleotides (MO), mRNA encoding dominant negative mutants and the CRISPR-Cas9 system for loss of function studies (Mimoto & Christian, 2011) . Moreover, the availability of a detailed fate map permits the injection into single blastomeres allowing the direct targeting of specific tissues and regions of the embryo (Moody, 1987). With the help of lineage tracing dyes and fluorescent probes, the injected side of the embryo can be identified and the observed phenotype compared to that of the uninjected side of the same embryo. This allows the detection of weaker phenotypes that may have been missed in inter-embryonic comparisons (Exner & Willsey, 2021). Animal caps are pluripotent cells that are obtained from the blastula

stage embryo and these cells are an excellent system for the *in vitro* differentiation studies (Borchers & Pieler, 2010; Green, 1999). Importantly, the basics of nervous system development is conserved between *X. laevis* and higher vertebrates including humans (Exner & Willsey, 2021).

1.1 Early neural genes

In *X. laevis* embryos, the process of neural induction creates a population of neural precursor cells in the ectoderm of the neural plate (Sharpe, 1990). Expressed in these neural precursor cells are several transcription factors (Moody & Je, 2002; Rogers *et al*., 2009; Sasai, 1998) including members of the Sox (Sox2-3, Sox15) (Mizuseki *et al*., 1998a; Mizuseki *et al*., 1998b; Rogers *et al*., 2009), Zic (Zic1-3) (Mizuseki *et al*., 1998a; Nakata *et al*., 1997; Nakata *et al*., 1998) and Iroquois (iro1-3) (Bellefroid *et al*., 1998; Gómez-Skarmeta *et al*., 1998) families as well as the coiled-coil protein, Geminin (Kroll *et al*., 1998) and forkhead box protein FoxD5 (Sullivan *et al*., 2001). In addition to their ability to expand the neural plate, these genes function by promoting the immature undifferentiated neural state (Sox2, Sox3, Foxd5, Geminin, Zic2) or the onset of differentiation (Sox15, Sox11, Iro1-3, Zic1, Zic3) (Rogers *et al*., 2009).

1.2 Neurogenesis in *Xenopus*

In *X. laevis* two phases of neurogenesis, interspersed by a period of quiescence, occurs (Hartenstein, 1989; Thuret *et al*., 2015). The first, termed primary neurogenesis, gives rise to neurons that are responsible for the earliest movements and responses in the embryo and is initiated at the open neural plate stage (Thuret *et al.*, 2015). The second phase known as secondary neurogenesis, takes place during metamorphosis and replaces most primary neurons and gives rise to the adult nervous system

(Schlosser, 2002; Wullimann *et al*., 2005). At the open neural plate stage, primary neurogenesis produces scattered post-mitotic neurons organised in three longitudinal domains on each side of the dorsal midline (Chitnis *et al*., 1995; Hartenstein, 1989). Following folding of the neural plate, the medial, intermediate and lateral domains would occupy a ventral to dorsal position in the neural tube (Chitnis *et al*., 1995). The ventrally located medial domain will give rise to motor neurons, the intermediate domains to interneurons and the lateral domain to the dorsally located sensory neurons (Rohon-Beard) (Chitnis *et al*., 1995; Hartenstein, 1989).

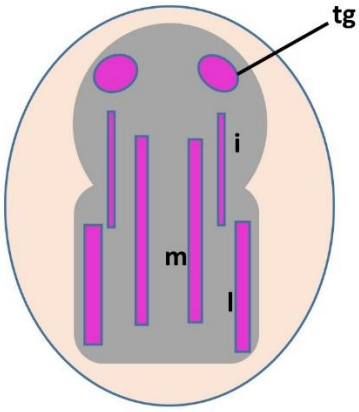

Figure 1.1 Primary neurogenesis.

In *X. laevis*, a subset of neural precursors at the open neural plate stage begin to differentiate giving rise to the first-born neurons. These first neurons arise in three longitudinal strips on each side of the dorsal midline and also in the trigeminal placode (tg). m, i, l indicates the medial, intermediate neurogenic stripes.

1.3 Proneural genes

Members of the basic helix-loop-helix family (bHLH) of transcription factors have multiple crucial regulatory roles during the establishment of the nervous system (Kageyama & Nakanishi, 1997; Lee, 1997). Structurally, bHLH transcription factors are characterized by a HLH domain, which is used for dimerization and interactions with

other proteins, and a basic domain. The basic domain is responsible for DNA binding at E-box motifs (CANNTG) within the regulatory regions of target genes (Bertrand *et al*., 2002; Massari & Murre, 2000). Based on the pattern of expression, bHLH transcription factors are into categorized into two classes: class I bHLH transcription factors/E proteins have a ubiquitous expression, while class II factors are tissue-specific (Bertrand *et al*., 2002; Meredith & Johnson, 2000). The tissue-specific bHLH proteins require dimerization with the class I bHLH for DNA binding and gene regulation (Bertrand *et al*., 2002; Meredith & Johnson, 2000).

A subclass of class II bHLH transcription factors encoded by homologues of the *Drosophila Atonal* and *Achaete-Scute* gene families initiate the neuronal determination and play essential roles during neuronal differentiation, subtype specification and maturation (Baker & Brown, 2018; Bertrand *et al*., 2002). These proneural factors are both necessary and sufficient to initiate the cellular changes that drive pan-neuronal differentiation and neuronal subtype specification during development (Guillemot, 2007). Moreover, they are sufficient to reprogram specific neural and non-neural cell types to develop into functional neurons (Masserdotti *et al*., 2016). Proneural genes have a transient expression in neural progenitor cells and hence exert their proneural effects through the induction of a cascade of downstream genes in a sequence leading from determination to differentiation (Bertrand *et al*., 2002).

The Neurogenin family of the atonal-like bHLH transcription factors is made up of three members, Neurog1, Neurog2 and Neurog3. In *X. laevis*, all three *neurogs* have the onset of their expression at late gastrula stages within the induced neural ectoderm (Sommer *et al*., 1996; Nieber *et al*., 2009). While transcripts of *neurog1* and *neurog2* are expressed in the three longitudinal stripes of primary neurogenesis in open neural

plate stages (Ma *et al*., 1996; Nieber *et al*., 2009), those of *neurog3* are limited to the medial domain (Nieber *et al*., 2009).

During primary neurogenesis, Neurog2 induces several genes including *neurod* (Lee *et al*. 1995; Vernon *et al*. 2003), *ath3* (Takebayashi *et al*., 1997), *ebf2* (Dubois *et al*.,1998), *ebf3* (Pozzoli *et al*., 2001), *myt1* (Bellefroid *et al*., 1996), *numbl* (Nieber *et al*., 2013) and *seb4r* (Boy *et al*., 2004), which positively regulate the neurogenic process. Neurog2 also couples cell cycle exit with neuronal differentiation by inducing the expression of genes encoding the cell cycle inhibitors Gadd45-γ and Pak3 (de la Calle-Mustienes *et al*., 2002; Souopgui *et al*., 2002). Neurog2 also induces the expression of *dll1,* which mediates Notch signaling and exerts a negative regulatory effect on differentiation (Ma *et al*., 1996).

1.4 Lateral inhibition

The neural plate is thought to consist of a population of proliferating cells with equal differentiating potentials (Beatus & Lendahl, 1998). The Notch signaling pathway acts through intercellular communication between adjacent cells to regulate differentiation. The induction of *dll1* by Neurog2 in a progenitor cell fated to undergo differentiation (signaling-sending cell), activates Notch signaling in neighbouring cells (signal receiving cell) through its interaction with the extracellular component of the Notch transmembrane protein (Bray, 2006; Kiyota & Kinoshita, 2002). Subsequently, Notch is processed leading to the release and translocation of the Notch intracellular domain (NICD) into the nucleus (Bray, 2006; Chitnis *et al*., 1995). The formation of a complex between NICD and Rbpj, a DNA binding protein, induces the expression of the *hes* genes (*hes1* and *hes5*). Hes1 and Hes5 are bHLH transcriptional repressor proteins, which repress *neurog2* and other genes required for neuronal differentiation (Wettstein

et al., 1997). This results in the inhibition of neuronal differentiation and the maintenance of the progenitor state in the signal receiving cell (Cau *et al*., 2000; Louvi & Artavanis-Tsakonas, 2006; Schneider *et al*., 2001). Meanwhile the induction of Neurog2 in the signal giving cell activates downstream differentiation genes that leads to its differentiation. Consequently, through the process of lateral inhibition, the signal sending cell acquires a neuronal fate, while neighboring cells maintain their progenitor identity or become glia giving rise to a scattered pattern of differentiated neurons (Chitnis *et al*., 1995; Ma *et al*., 1996). The sensitivity of proneural genes to lateral inhibition, therefore, has an effect on the pattern of the generated primary neurons (Chitnis & Kintner, 1996).

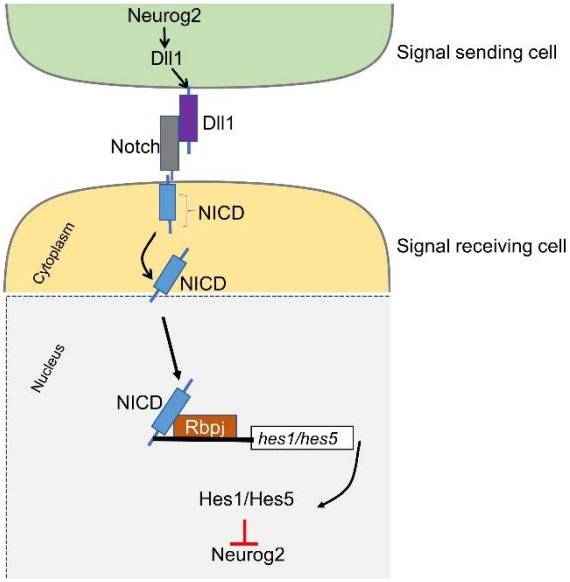

Figure 1.2 Notch signaling.

Neurog2 induces the expression of dll1, which leads to downstream effects and the subsequent localization of NICD to the nucleus where its interaction with Rbpj drives the expression of the hes genes. The Hes proteins in turn, inhibits Neurog2, which results in the maintenance of the progenitor state.

1.5 Post-transcriptional regulation of neurogenesis

Gene regulation at the post-transcriptional level has been identified as a crucial aspect of nearly all stages of neurogenesis (DeBoer *et al*. 2013; Pilaz & Silver 2015) with

dysregulation underlying a variety of diseases (Cooper *et al*., 2009; Lara-Pezzi, *et al*., 2017; Saffary & Xie 2011). Multiple different mediators control post-transcriptional gene regulation including noncoding RNAs (microRNAs and long noncoding RNAs) and RNA binding proteins (RBP) (Änkö & Neugebauer 2012; Gao, 2010; Han *et al*., 2016; Ramos *et al*., 2015).

1.5.1 MicroRNAs in neurogenesis

The dynamic function of microRNAs (miRNAs) in neurogenesis has been reviewed by Lang and Shi (2012). By regulating their target RNAs, miRNAs control the neurogenic path by influencing neural stem cell and progenitor proliferation, differentiation and maturation. The function of miRNAs such as miR-125, miR-134, and miR-184 enhance the proliferation of neural progenitors, while others like let7, miR-9, miR-124 and miR-137 induces neural stem cells and progenitors to differentiate into specific cell types (Lang & Shi, 2012). Yet others, including miR-128, miR-125b, and miR-132 promotes the maturation of differentiated neurons (Bian & Sun, 2011; Lang & Shi, 2012).

1.5.2 RNA binding proteins in the context of neurogenesis

RNA binding proteins have been shown to play crucial roles during the establishment of the vertebrate nervous system. RNA binding proteins have been identified which regulate stem cell division and maintenance, progenitor division and fate decision as well as neuronal function (Zahr *et al*., 2019).

1.5.2.1 Maintenance of progenitor state

Stau2, is involved in regulating the balance between stem cell maintenance and differentiation during mammalian neurogenesis by regulating the localization of proneurogenic mRNAs like *prox1* in mammalian neural stem cells (Vessey *et al*., 2012). *In vivo*, Stau2 is enriched in radial glial progenitors (RGP) as part of an RNA

complex involving Pum2, a translational repressor, DDX1, a RNA helicase and *prox1* and *β-actin*, targets of Stau2. The knockdown of Stau2, Pum2, or DDX1, decreases radial glial progenitors and enhances neurogenesis. Stau2 knockdown alters *prox1* mRNA localization and expression of *prox1* mRNA, and a mutation that interferes with its binding to target RNAs is unable to promote the self-renewal of RGP (Vessey *et al*., 2012).

Tristetraprolin (TTP/Zfp36) is a member of the ZFP36 family of RNA-binding proteins, known to destabilize, through AU-rich *cis*-elements (AREs) in the 3' UTR, mRNAs encoding a wide range of cytokines, growth factors and proto-oncogenes (Sanduja *et al*., 2012). TTP has been identified as a post-transcriptional repressor of genes specific to the nervous system (Dai *et al*., 2015). TTP limited steady-state abundance of a considerable number of ARE-containing neuronal mRNAs in non-neuronal cells and its downregulation was essential to upregulate such transcripts in cells undergoing neural differentiation (Dai *et al*., 2015). In *Xenopus* the overexpression of a TTP paralogue, Zfp36l1 inhibited neural induction and differentiation and resulted in severe defects in the neural tube during neural development (Xia *et al*., 2012).

Drosha, another RBP with a ribonuclease activity is a known core player of the RNA microRNA microprocessor, processing pri-microRNA to pre-microRNA in the miRNA biogenic pathway (Han *et al*., 2004; Nguyen *et al*., 2015). Independent of its microRNA processing role, Drosha has been found to sustain the embryonic and hippocampal neural stem cell pool by directly destabilizing mRNAs of the transcription factors Neurogenin 2 (Ngn2) and NeuroD1 (Knuckles *et al*., 2012). Accordingly, loss of Drosha led to loss of stemness and precocious differentiation.

1.5.2.2 Neuronal differentiation

REST/NRSF, is a transcriptional repressor of neuron specific genes in neural progenitor cells. The RBP nR100/SRRM4 promotes through alternate splicing, the expression of REST4, an isoform of REST with greatly reduced repressive activity. The relieve of REST targets from REST repression due to REST4's weak repressive activity, leads to their activation and hence neuronal differentiation (Raj *et al*., 2011).

In mouse, the fragile X mental retardation protein (FMRP) regulates the fate of adult neural progenitor cells by translationally regulating the expression of GSK3β thereby modulating the Want/β-catenin signaling pathway and its downstream effector, Neurog1 (Luo *et al*. 2010).

In *Xenopus*, Seb4r exhibits proneural activity during primary neurogenesis and retinogenesis. *Seb4r* is induced at the open neural plate stage by the proneural factor Neurog2 (Ngnr1) and the differentiation gene NeuroD but inhibited by the Notch/Delta pathway (Boy *et al*., 2004).

Rbmx function is required for neural differentiation and its knockdown inhibits neurogenesis and causes mispatterning of the anterior neural plate in Xenopus (Dichmann *et al*., 2008).

MARF1 belongs to the NYN/PIN-like domain, RNase domain family (Anantharaman & Aravind, 2006). Overexpression of the somatic form of MARF1(sMARF1) promoted differentiation in E12.5 neuronal progenitors and increased neurons *in vivo* (Kanemitsu *et al*., 2017). This positive effect of sMARF1 on neurogenesis in the cortex was mediated by the PIN domain as the overexpression of a mutant lacking the PIN domain *in vitro* had no effect on differentiation or proliferation in progenitor cells contrary to the WT sMARF1 which promoted differentiation and inhibited proliferation.

1.6 Post-transcription regulation of gene expression by RNA binding proteins

RNA binding proteins (RBPs) play essential roles in the post-transcriptional regulation of gene expression by controlling all aspects of RNA metabolism including splicing, processing, nuclear export, localization, translation and stability (Doyle & Kiebler 2012; Glisovic *et al.* 2008). Accordingly, the interruption of the RBP-RNA interaction, due to alterations in the expression of the RBP or modifications (mutations) within RBPs or their mRNA targets may have pathogenic consequences (Brinegar & Cooper, 2016; Kelaini *et al*., 2021; Lukong *et al*., 2008; Nussbacher *et al*., 2019; Zhou *et al*., 2014). For instance, the aggregation of Fused in Sarcoma (FUS) and TAR DNA-binding protein (TDP-43), predominantly nuclear RBPs, in the cytoplasm in amyotrophic lateral sclerosis (ALS) disrupt their interaction with RNA and have pathogenic roles in ALS (Brinegar & Cooper, 2016).

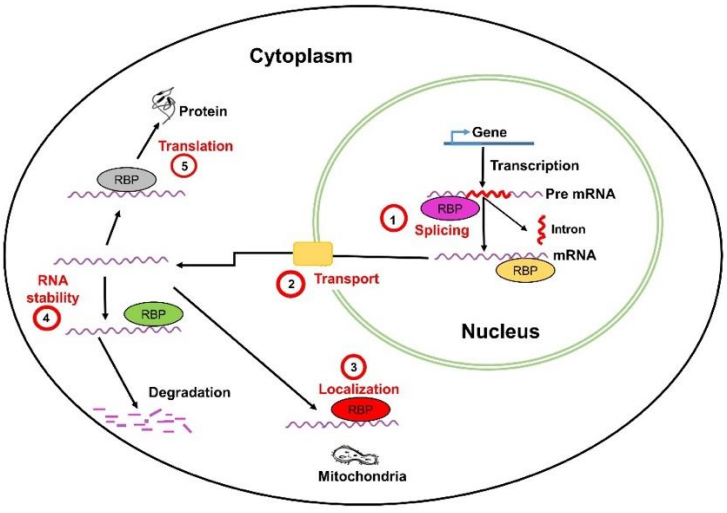

Figure 1.3 Schematic diagram of the essential role of RBP in the post-transcriptional regulation of gene expression.

RBPs are involved in the regulation of all aspect of RNA metabolism including splicing, transport, localization, stability and translation.

RBPs bind to specific cis-acting elements present in their target RNAs, the locations of which may provide clues as to the effects of the RBP´s regulation on the RNA. For

instance, the binding of an RBP to sequences within the coding regions may regulate splicing (Kelaini *et al*., 2021) or repress translation (Brummer *et al.,*2013), while binding to the 5'UTR (Kelaini *et al*., 2021) or 3´UTR (Kelaini *et al*., 2021; Brummer *et al.,* 2013) may have roles in the processing or stability of target RNA.

A variety of domains mediate the binding of RBPs to RNA and even though single domains can sufficiently interact with RNA, several RBPs possess multiple RNA-binding domains (Lunde *et al*., 2007). The combination of the same or different binding domains form diverse macromolecular binding surfaces that determine the binding specificity of RBPs (Lunde *et al*., 2007). Of the many identified binding domains of RBPs, the best described includes RNA recognition motifs (RRMs), K homology (KH) domains and zinc fingers domains (Letunic *et al*., 2009). Other RPBs without conventional RNA binding domains have also been identified. The mode of RNA binding by these novel RBPs and their functions have been reviewed (Hentze *et al*., 2018).

In addition to the binding domains, RBPs possess additional domains, which mediate their interaction with other proteins as well as the post-translational modification of the RBPs themselves. Post-translational modification of RBPs by mechanisms such as phosphorylation, arginine methylation and small ubiquitin-like modification (SUMO) can alter RNA binding, function and localization of ribonucleoprotein complex (Glisovic *et al*. 2008).

1.6.1 Zc3h12c Family

The Zc3h12 family of RNA binding protein comprises four members (Zc3h12a-d). The family is also known as MCPIP (Monocyte chemoattractant protein-induced protein) or Regnase, in which instance members are designated MCPIP/Regnase 1-4. The

Zc3h12c members were first identified by Liang *et al.* (2008) in macrophages to be induced in response to lipopolysaccharide-activated toll-like receptors and to modulate the inflammation response.

Structurally, members possess an N-terminal NYN/PIN domain with RNase activity and a single CCCH zinc finger domain immediately downstream of the RNase domain for RNA binding (Fu & Blackshear, 2017). The most studied member of the family is Zc3h12a.

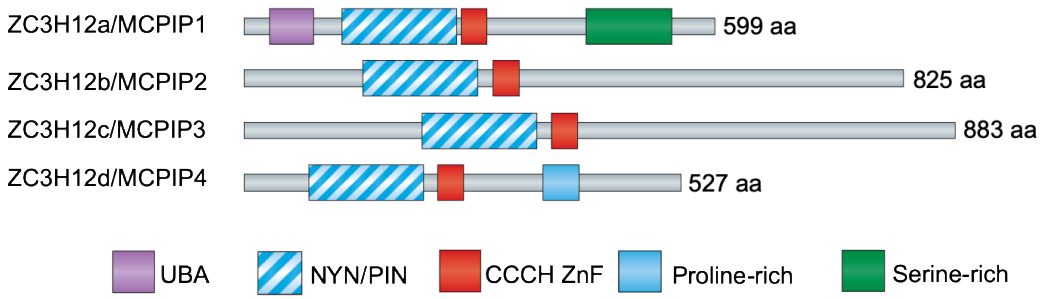

Figure 1.4 Schematic structure of human Zc3h12 family members.

(Fu & Blackshear, 2017, modified). NYN/PIN, RNase, ribonuclease domain; UBA, ubiquitin-associated domain.

The post-transcriptional regulation of gene expression by Zc3h12a is well studied in the context of inflammation where it regulates, through its endonuclease activity, the turnover of mRNA transcripts of several pro-inflammatory cytokines and bring about the modulation of inflammation (Garg *et al*., 2015; Kochan *et al*., 2016; Li *et al*., 2012; Matsushita *et al*., 2009; Uehata & Akira, 2013). Consequently, mice deficient in Zc3h12a present with severe anemia and inflammatory response and died prematurely (Liang *et al.,* 2010; Matsushita *et al.,* 2009). Target mRNAs of Zc3h12a include *il-6*, *il-2*, *il-1β*, *il-8*, *il12b*, *ier-3*, *calcr* and *c/ebpβ* (Garg *et al*., 2015; Kochan *et al*., 2016; Li *et al*., 2012; Matsushita *et al*., 2009; Uehata & Akira, 2013).

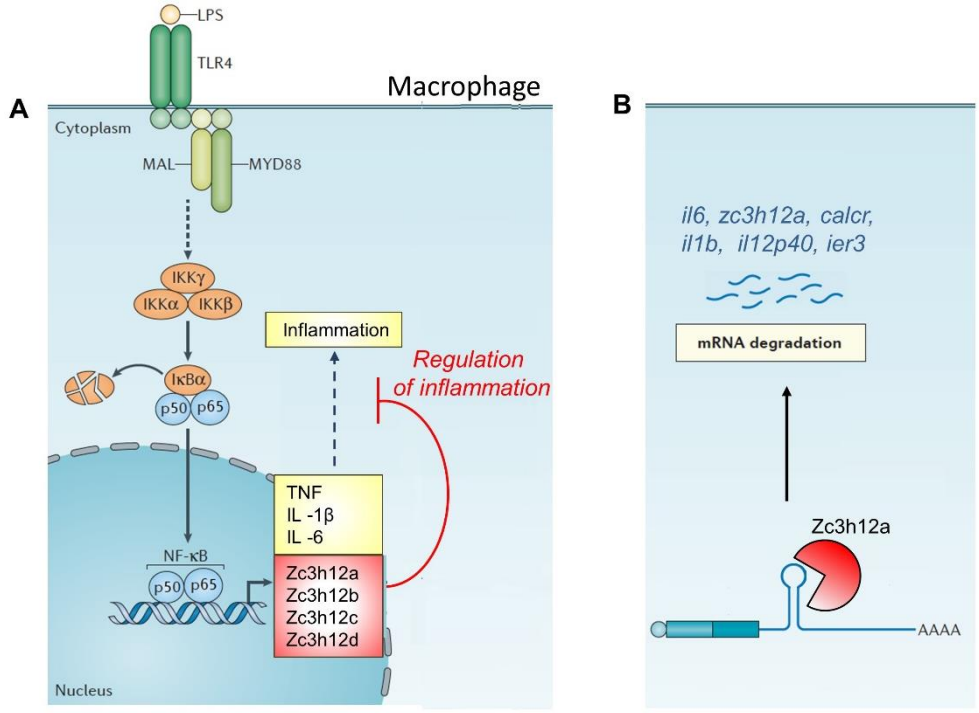

Figure 1.5 Zc3h12a members regulate inflammation.

(A) The activation of toll-like receptors by lipopolysaccharide (LPS) results in the activation of the transcription factor, NFκB, which activates expression of pro-inflammatory cytokines such as IL-6, IL-1β and TNF leading to inflammation. In addition, NFκB also activates the expression of members of the Zc3h12 family leading to the modulation of inflammation. **(B)** Zc3h12 members, represented here by Zc3h12a, bind stem-loop structures in the 3'UTR of target mRNAs and degrade them (Fu and Blackshear, 2017, modified).

1.6.1.1 Zc3h12a

Zc3h12a is expressed in response to toll-like receptor ligands, pro-inflammatory cytokines (TNF, Il-1β and Ccl2), as well as chemical stimulation (Liang *et al*., 2008; (Iwasaki *et al*., 2011; Mao *et al*., 2017) via the activation of the NFκB and ERK pathways (Kasza *et al*., 2010). Signaling-induced Zc3h12a in turn exerts a negative feedback effect on the inducing signals (Mao *et al*., 2017). Zc3h12a expression is regulated at the transcript level by miRNAs such as miR-9 (Yao *et al*., 2014) and interestingly, Zc3h12a itself (Wawro *et al*., 2016) in a 3'UTR-dependent manner. Post-translationally, Zc3h12a is regulated by IKK-mediated phosphorylation and subsequent proteasomal degradation, as well as cleavage by the paracaspase

mucosa-associated lymphoid tissue 1 (Mao *et al*., 2017; Tanaka *et al*., 2019; Uehata & Takeuchi, 2020).

Zc3h12a localizes to the cytoplasm as granule-like structures to P bodies and to the endoplasmic reticulum (Mino *et al*., 2015; Suzuki *at al*., 2011; von Gamm *et al*., 2019). Zc3h12a binds translationally active mRNAs, effecting their degradation in cooperation with the helicase UPF1, similar to nonsense-mediated mRNA decay (Mino *et al*., 2015). Zc3h12a recognizes stem-loop structures in the 3'UTR of target mRNAs with a canonical three consensus motif comprising a pyrimidine–purine–pyrimidine loop (e.g. UAU or UAC) (Li *et al*., 2012; Yoshinaga & Takeuchi, 2019). In addition to 3' UTR-dependent regulation of target mRNAs, Zc3h12a also interacts with RNA via intronic, coding as well as 5' UTR regions (Jiang *et al*., 2016; Mino *et al*., 2015). For instance, Zc3h12a degraded *Il17ra* and *tet* genes in HEK293T cells by binding sequences within the coding region (Garg *et al*., 2015; Jiang *et al*., 2016). Target binding is increased in the presence of the zinc finger (ZF) domain but is not greatly affected by the N-terminal domain (NTD) (Yokogawa *et al*. 2016). The NTD associates with the PIN domain to significantly enhance RNase activity (Yokogawa *et al*. 2016). The lack of this interaction results in an insufficient enzymatic activity by the PIN domain. The PIN domain forms a head-to-tail oligomer and the dimer interface overlaps with the NTD binding site (Yokogawa *et al*. 2016). *In vitro*, oligomerization of the PIN domain and NTD binding are crucial to the endonuclease activity of Zc3h12a as mutations that disrupt oligomerization do not have enzymatic activity (Yokogawa *et al*. 2016).

The catalytic center of the Zc3h12a PIN domain consists of four aspartic acid residues that chelate Mg^{2+} (Anantharaman & Aravind, 2006; Habacher & Ciosk, 2017). The spatial orientation of these residues relative to one another, as well as their physiochemical properties are essential for enzymatic activity (Habacher & Ciosk,

2017). Therefore, mutating one of the aspartic acid residues completely abolishes the RNase activity of Zc3h12a (Matsushita *et al*., 2009, Wawro *et al*., 2017). The well-known point mutation in human Zc3h12a is that associated with the aspartic acid residue at position 141 (Matsushita *et al*., 2009).

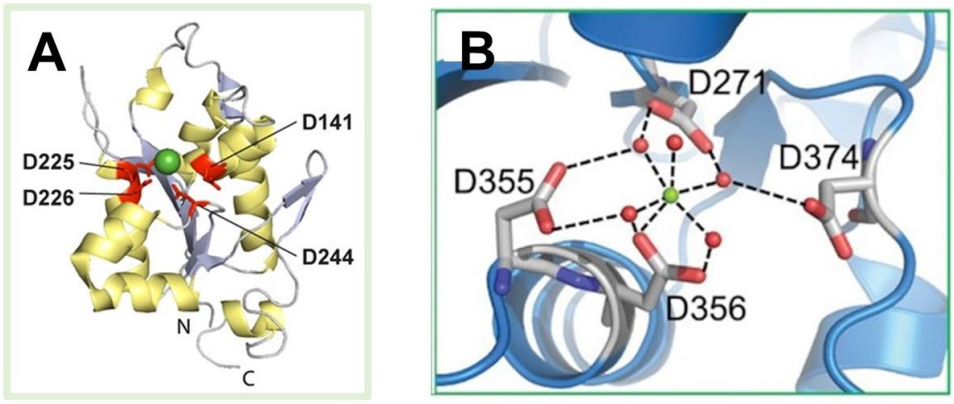

Figure 1.6 RNase domain of Zc3h12 members.

The crystal structure of the RNase domain of human ZC3H12A (**A**) and mouse Zc3h12c (**B**). The four aspartic acid residues are shown in red **(A**) and as two the arms of a Y (**B**). Green structure represents magnesium ion. N and C show the amino and carboxylic ends respectively of the ZC3H12A. Modified from Habacher & Ciosk, 2017 and Garg *et al*., 2021.

In addition to its role in mRNA degradation during inflammation, Zc3h12a has been reported to regulate, also via its RNase activity, other processes such as miRNA processing (Suzuki *et al*., 2011), viral RNA degradation (Lin *et al*., 2013), body fat metabolism (Habacher *et al*., 2016) and early cortical neurogenesis (Jiang *et al*., 2016). Zc3h12a has also been implicated in other RNase-independent roles including transcription, deubiquitinating and translational silencing (Behrens *et al*., 2018; Liang *et al*., 2010).

1.6.1.2 Other Zc3h12 members

Similar to Zc3h12a, the other members of the Zc3h12 family, Zc3h12b, Zc3h12c and Zc3h12d play important roles in the inflammation pathway and *in vitro*, share with Zc3h12a a set of common target mRNAs (Liu *et al*., 2021; Wawro *et al*., 2017; Wawro *et al*., 2019; Zhou *et al*., 2014). These targets include *il-6, tnf*, *ier3.* Additionally, all three family members target *zc3h12a*. Regulation of target mRNAs by Zc3h12b, Zc3h12c and Zc3h12d is also 3' UTR-dependent, with Zc3h12d recognizing the same structural elements as Zc3h12a (Wawro *et al*., 2017; Wawro *et al*., 2019). Point mutation in a conserved aspartic acid residue within their catalytic center abolishes their RNase activity (Wawro *et al*., 2017; Wawro *et al*., 2019).

An intact NYN/PIN-like domain has been shown to be crucial for the biological activity of Zc3h12b and Zc3h12d (Wawro *et al*., 2017; Wawro *et al*.,2019). Zc3h12b, like Zc3h12a, localizes to the cytoplasm in the form of small granule-like structures (Suzuki *et al*., 2011; Wawro *et al*., 2019). Although Zc3h12c also localizes to the cytoplasm, the pattern of localization is not so clear. Whereas one study in macrophages reported a granule-like pattern and suggested an endosomal localization (von Gamm *et al*., 2019), another in U251-MG, observed a diffused localization (Wawro *et al*., 2021).

Non-inflammatory related roles have also been ascribed to Zc3h12b, Zc3h12c and Zc3h12d. Zc3h12b inhibits proliferation by halting the cell cycle in the G2 phase in a NYN/PIN domain-independent manner (Wawro *et al*., 2019). Zc3h12d has been identified as a marker for tumor progression (Minagawa *et al*., 2009) and Zc3h12c, in addition to been involved in the pathology of psoriasis (Tsoi *et al*., 2012; Wawro *et al*., 2021), may function as a suppressor of metastasis in human colorectal cancer by inhibiting cell migration (Suk *et al*., 2018).

1.7 Aim

Post-transcriptional regulation of gene expression has been shown in recent years to play crucial roles in most aspects of development and cellular function. Dysfunction of post-transcriptional regulatory events is the basis of diverse diseases (Brinegar & Cooper, 2016; ; Kelaini *et al*., 2021; Lukong *et al*., 2008; Nussbacher *et al*., 2019; Zhou et al., 2014). In this thesis, the role of the RNase Zc3h12c during embryogenesis will be studied. We have previously identified zc3h12c in a screen for early genes induced by the proneural bHLH transcription factor Neurog2 (Hedderich, 2012). Zc3h12a, the best characterized member of the Zc3h12 family, has been implicated in early cortical neurogenesis (Jiang *et al*., 2016), however, no such role has yet been reported for the other family members, including Zc3h12c. Therefore, in this study the role of Zc3h12c during neural development will be elucidated primarily using *X. laevis* as a model system. Specifically, the expression of *zc3h12c* during embryogenesis will be determined and gain and loss of function analysis performed to determine its role during neurogenesis.

2 Materials and Methods

2.1 Materials

2.1.1 Model Organism

All experimental studies were performed with the African clawed frog, *Xenopus laevis.* Both pigmented male and female X. *laevis* were procured from Nasco (Ft. Atkinson, USA).

2.1.2 Bacteria

Standard molecular biology methods were performed using the chemical competent *Escherichia coli* strand XL1-Blue (recA1, endA1, gyrA96, thi-1, hsdR17, supE44, relA1, lac [F'proAB, $lacI^qZ\Delta M15$, Tn10(Tetr)]^c) obtained from Stratagene GmbH (Heidelberg, Germany).

2.1.3 Chemicals

Standard chemicals used, unless otherwise stated, were ordered from the following companies: ApplChem, Merck, Roche, Roth, Sigma-Aldrich and New England Biolabs.

2.1.4 Antibiotics and Media

Bacteria culture medium was made by dissolving 32 g Luria Bertani (LB) in 1 l dH_2O. The LB medium was autoclaved at 121 °C and then cooled down to 50 °C. Ampicillin (working concentration: 100 µg/ml, diluted from a 100 mg/ml in dH_2O stock solution) was added and the medium transferred to petri dishes and stored at 4 °C.

2.1.5 Oligonucleotides

Oligonucleotides were ordered from Sigma-Aldrich or Integrated DNA Technologies.

Table 2.1 RT-PCR primers

Gene	Primers		T_A ˚C	Cycles *
	Forward	Reverse		
odc	5´-GCCATTGTGAAGACTC TCTCCATTC-3´	5´-TTCGGGTGATTCCTTG CCAC-3´	57	26
tubb2b	5´-ACACGGCATTGATCCT ACAG-3´	5´-AGCTCCTTCGGTGTAA TGAC-3´	56	32
zc3h12c	5'-GGTTACTCGGAAGAACAG G-3' or 5'-GGTTACTCTGAAGAACAG G-3'	5'-ACTTAATCCCACGGCAAG -3'	50	45

* Indicates approximate number of cycles. Cycle number varied in individual experiments.

Table 2.2 Sequencing oligonucleotides

Oligonucleotide	Sequence
Ex1ForZc3h12C	5´-GGTTACTCGGAAGAACAGG-3´
Ex2revZc3h12C	5´-ACTTAATCCCACGGCAAG-3´
GR7	5´-ATCCTGCATATAACACTTC-3´
pCS2+ upstream	5´-GACGCAAATGGGCG-3´
Seq_pmirGLO_for	5´-TGTTCGTGGACGAGGTGC-3´
Seq_pmirGLO_rev	5´-GGTTATGCTAGTTATTGCTCAGCG-3´
Sp6	5´-ATTTAGGTGACACTATAG-3´
T7	5´-TAATACGACTCACTATAGGG-3´
zc3h12c seq fw1	5´-GGTAGCAAGAGTGAGAATGAAC-3´
zc3h12c.SEx2 for1	5´-GGTTACTCTGAAGAACAGG-3´
Zc3h12c.S_forSeq1	5´-GACCTGACACATGTAGCAGC-3´
Zc3h12c.SL_Ex1for	5´-TGACATGTAGCAGCTTCATGG-3´

2.1.6 Morpholino Oligonucleotides (MOs)

All MOs were obtained from Gene Tools LLC (Philomath, OR, USA).

Table 2.3 List of Morpholino Oligonucleotides.

Oligonucleotide	Sequence
zc3h12c.L MO	5´-GCCACATCTTTTCAACTTACCTCAT-3´
zc3h12c.S MO	5´-GCCACATCATTCCACCTTACCTCAT-3´
Standard control MO	5´-CCTCTTACCTCAGTTACAATTTATA-3´

Morpholinos were dissolved in RNase-free water into 20 ng/nl stock solution, divided into 10 ul aliquots and stored at 4 ^{o}C. Prior to use, the morpholinos were heated at 65 ^{o}C for 10 min.

2.1.7 Sense RNA constructs

Table 2.4 Sense RNA constructs

Insert	Vector	Restriction enzyme	Polymerase	Reference
Neurog2-GR	GR-p3'HGR	SfiI	T3	Perron *et al.,* 1999
DN-Rbpj	pCS2+	NotI	SP6	Wettstein *et al*., 1997
LacZ	pCS2+	NotI	SP6	Chitnis *et al*., 1995
H2B-cherry	pCS2+	NotI	SP6	Kashef *et al.,* 2009
MT-Zc3h12c.S	MT-pCS2+	NotI	Sp6	This thesis
MT-Zc3h12c.S^{D249N}	MT-pCS2+	NotI	Sp6	This thesis
MT-Zc3h12c.S-GR	MT-GR-pCS2+	NotI	SP6	This thesis
MT-Zc3h12c.S^{D249N}-GR	MT-GR-pCS2+	NotI	SP6	This thesis
Zc3h12c.S-GFP	GFP-pCS2+	NotI	SP6	This thesis
Zc3h12c.S^{D249N}-GFP	pCS2+GFP	NotI	SP6	This thesis

2.1.8 Reporter constructs

Table 2.5 Reporter constructs.

Insert	Vector	Reference
pmirGLO-IL6-3'UTR	pmirGLO	Kochan *et al*., 2015
pmirGLO-Empty	pmirGLO	Kochan *et al*., 2015

2.1.9 Antisense constructs

Table 2.6 Antisense constructs.

Insert	Vector	Restriction enzyme	RNA polymerase	Reference
tubb2b	pBst KS	BamHI	T3	Chitnis *et al*., 1995
sox2	pBluescript SK	EcoRI	T7	Mancilla & Mayor, 1996
neurog2	pBluescript II	BamHI	T3	Ma *et al*., 1996
myt1	pGem-T	ClaI	T7	Bellefoid *et al*., 1996
zc3h12c	pGem-T easy	ApaI	SP6	This thesis

2.1.10 Intermediate constructs and templates

Underlined nucleotides in primer sequences represents restriction sites within the primers.

2.1.10.1 Zc3h12c.S-pGEM-T easy (1)

The construct contains the full-length coding sequence (2364 bp) of *zc3h12c.S*, amplified from a *X. laevis* cDNA mix with the primers, for: 5'-ATGTCTGTCTGCTCCCCT-3' and rev: 5'-TCAGTATCCATACTGGGATTTC-3' and cloned into the pGEM-T easy vector (prepared by K. Ditter).

2.1.10.2 Zc3h12c.S-pGEM-T easy (2)

Zc3h12c.S-pGEM-T easy contains the full-length coding sequence (2364 bp) of *zc3h12c.S* amplified from MT-Zc3h12c.S-pCS2+ with the primers for: 5'-GACTCGAGTCTGTCTGCTCCCCTC-3' and rev: 5'-CACTCGAGGTATCCATACTGGGATTTCTC-3'. The PCR product was cloned into the pGEM-T easy vector (prepared by K. Ditter and E. Essel).

2.1.10.3 Zc3h12c.S^{D249N}-pGEM-T easy

Zc3h12c.S^{D249N}-pGEM-T easy contains the full-length coding sequence (2364 bp) of *zc3h12c.S* with a point mutation in the aspartic acid residue at position 249 to asparagine. The coding sequence of *zc3h12c.S* was amplified from MT-Zc3h12c.S^{D249N}-pCS2+ with the primers for: 5'-GCCTCGAGATGTCTGTCTGCTCCCCT-3' and rev: 5'-ATCAATTGTCAGTATCCATACTGGGATTTC-3' and cloned into the pGEM-T easy vector (prepared by K. Ditter and E. Essel).

2.1.10.4 Zc3h12c.S-pCS2+

The full-length coding sequence (2364 bp) of *zc3h12c.S* was PCR amplified from Zc3h12c.S-pGEM-T easy (1) using the primers, for: 5'-GAGGATCCATGTCTGTCTGCTCCCCT-3' and rev: 5'-ATCTCGAGTCAGTATCCATACTGG-3' and cloned into the pCS2+ vector at the BamHI and XhoI sites (prepared by K. Ditter).

2.1.10.5 Zc3h12c.S^{D249N}-pCS2+

The construct comprises the full-length coding sequence (2364 bp) of *zc3h12c.S* with a point mutation in the aspartic acid residue at position 249 to asparagine. The mutation was generated with the QuickChange XL Site Directed Mutagenesis Kit

(Stratagene) using the primers (mutation indicated in red), up: 5'-CCTAAGACCTATTGTCATTAATGGCAGCAACGTTGCAATG-3' and down: 5'-CATTGCAACGTTGCTGCCATTAATGACAATAGGTCTTAGG-3' and Zc3h12c.S-pCS2+ as template (prepared by K. Ditter).

2.1.10.6 FLAG-Zc3h12c.S-pCS2+ (1)

The construct contains the full-length coding sequence of *zc3h12c.S* (2364 bp) with an N-terminal FLAG tag. The coding sequence of *zc3h12c.S* was amplified from Zc3h12c.S-pCS2+ with the primers for: 5'-GCCTCGAGATGTCTGTCTGCTCCCCT-3' and rev: 5'-ATCAATTGTCAGTATCCATACTGGGATTTC-3' and cloned into the FLAG-pCS2+ vector using the XhoI and MfeI restriction sites in the insert and the XhoI and EcoRI sites in the vector (prepared by K. Ditter and E. Essel).

2.1.10.7 FLAG-Zc3h12c.S^{D249N}-pCS2+ (1)

The construct consists of the full-length coding sequence (2364 bp) of *zc3h12c.S* with a point mutation in the aspartic acid residue at position 249 to asparagine and a FLAG tag located at the N-terminus. The coding sequence of *zc3h12c.S* was amplified from Zc3h12c.S^{D249N}-pCS2+ with the primers for: 5'-GCCTCGAGATGTCTGTCTGCTCCCCT-3' and rev: 5'-ATCAATTGTCAGTATCCATACTGGGATTTC-3' and cloned into the FLAG-pCS2+ vector using the XhoI and MfeI restriction sites in the insert and the XhoI and EcoRI sites in the vector (prepared by K. Ditter and E. Essel).

2.1.10.8 FLAG-Zc3h12c.S-pCS2+ (2)

FLAG-Zc3h12c.S-pCS2+ consists of the full-length coding sequence of *zc3h12c.S* (2364 bp) with an N-terminus FLAG tag. The QuickChange XL Site Directed Mutagenesis Kit (Stratagene) was used to generate a mutation in FLAG-Zc3h12c.S-

pCS2+ (1) with the primers (mutation indicated in red) up: 5'-CGACGATGACAAGAATGGAATGTCTGTCTGCTCCC-3' and down: 5'-GGGAGCAGACAGACATTCCATTCTTGTCATCGTCG-3'. The resulting product was then amplified with the primers, for: 5'-GGCTCGAGTCAGTATCCATACTGGGATTTC-3' and rev: 5'-GGCTCGAGATGTCTGTCTGCTCCC-3' and cloned into the FLAG-pCS2+ vector at the XhoI restriction site (prepared by K. Ditter and E. Essel).

2.1.10.9 FLAG-Zc3h12c.S^{D249N}-pCS2+ (2)

FLAG-Zc3h12c.S^{D249N}-pCS2+ consists of the full-length coding sequence (2364 bp) of *zc3h12c.S* with a point mutation in the aspartic acid residue at position 249 to asparagine and fused at its N-terminus with a FLAG tag. The QuickChange XL Site Directed Mutagenesis Kit (Stratagene) was used to generate a mutation in Zc3h12c.S^{D249N}-pGEM-T easy with the primers (mutation indicated in red) up: 5'-CGACGATGACAAGAATGGAATGTCTGTCTGCTCCC-3' and down: 5'-GGGAGCAGACAGACATTCCATTCTTGTCATCGTCG-3' The resulting product was then amplified with the primers, for: 5'-GGCTCGAGTCAGTATCCATACTGGGATTTC-3' and rev: 5'-GGCTCGAGATGTCTGTCTGCTCCC-3' and cloned into the FLAG-pCS2+ vector at the XhoI restriction site (prepared by K. Ditter and E. Essel).

2.1.11 Overexpression constructs/Sense RNA

2.1.11.1 Zc3h12c.S-GFP-pCS2+

The construct contains the full-length coding sequence (2364 bp) of *zc3h12c.S* fused at its C-terminus with the green florescent protein (GFP) (717 bp). The coding sequence of *zc3h12c.S* was PCR amplified from Zc3h12c.S-pCS2+ with the primers for: 5' CGGGATCCATGTCTGTCTGCTCCCCT-3' and rev: 5'-CAGGATCCGTATCCATACTGGGATTTCTCC-3' and cloned into the GFP-pCS2+

vector using the BamHI restriction site. Sense RNA was prepared by linearization with NotI and transcription with SP6 RNA polymerase (prepared by K. Ditter and E. Essel).

2.1.11.2 Zc3h12c.S^{D249N}-GFP-pCS2+

The construct contains the coding sequence (2364 bp) of *zc3h12c.S* with a point mutation in the aspartic acid residue at position 249 to asparagine and fused at its C terminus with GFP (717 bp). The coding sequence of *zc3h12c.S* was PCR amplified from Zc3h12c.S^{D249N}-pCS2+ with the primers, for: 5'-CGGGATCCATGTCTGTCTGCTCCCCT-3' and rev: 5'-CAGGATCCGTATCCATACTGGGATTTCTCC-3'. The PCR product was cloned into the GFP pCS2+ vector using the BamHI restriction site. Sense RNA was prepared by linearization with NotI and transcription with SP6 RNA polymerase (prepared by K. Ditter and E. Essel).

2.1.11.3 MT-Zc3h12c.S-pCS2+

The construct contains the full-length coding sequence of *zc3h12c.S* with a N-terminal 6x Myc tag (MT). The coding sequence of *zc3h12c.S* was PCR amplified from FLAG-Zc3h12c.S-pCS2+ (2) using the primers for: 5'-GGCTCGAGATGTCTGTCTGCTCCC-3' and rev: 5'-GGCTCGAGTCAGTATCCATACTGGGATTTC- 3' and then cloned into the MT-pCS2+ vector at the XhoI restriction site (prepared by K. Ditter).

2.1.11.4 MT-Zc3h12c.S^{D249N}-pCS2+

MT-Zc3h12c.S^{D249N}-pCS2+ contains the full-length coding sequence of *zc3h12c.S* with a point mutation in the aspartic acid residue at position 249 to asparagine and fused at its N-terminus with a 6x Myc tag (MT). The coding sequence of *zc3h12c.S* was PCR amplified from FLAG-Zc3h12c.S^{D249N}-pCS2+ (2) using the primers for: 5'-GGCTCGAGATGTCTGTCTGCTCCC-3' and rev: 5'-

GGCTCGAGTCAGTATCCATACTGGGATTTC- 3' and then cloned into the MT-pCS2+ vector at the XhoI restriction site (prepared by K. Ditter).

2.1.11.5 MT-Zc3h12c.S-GR-pCS2+

The construct contains the full-length coding sequence (2364 bp) of *zc3h12c.S* with a N-terminal 6x Myc tag (MT) and fused at its C-terminus to the glucocorticoid receptor (GR). The coding sequence of *zc3h12c.S* was excised from Zc3h12c.S-pGEM-T easy (2) and subcloned into the MT-GR-pCS2+ vector using the XhoI restriction site. Sense RNA was prepared by linearization with NotI and transcription with SP6 RNA polymerase (prepared by K. Ditter and E. Essel).

2.1.11.6 MT-Zc3h12c.S^{D249N}-GR-pCS2+

The construct contains the full-length coding sequence (2364 bp) of *zc3h12c.S* with a point mutation in the aspartic acid residue at position 249 to asparagine, a N-terminal 6x Myc tag and fused at its C-terminus to the Glucocorticoid receptor (GR). The coding sequence of *zc3h12c.S* was excised from Zc3h12c.S^{D249N}-pGEM-T easy and cloned into the MT-GR-pCS2+ using the XhoI restriction site. Sense RNA was prepared by linearization with NotI and transcription with SP6 RNA polymerase (prepared by K. Ditter and E. Essel).

2.1.12 Antisense RNA constructs

2.1.12.1 Zc3h12c-pGEM-T easy

A 657 bp fragment of the coding sequence of *zc3h12c* was PCR amplified from a *X. laevis* cDNA library (primers, for: 5'-CATGTCTAGAAGCAGCCAG-3' and rev: 5'-ACTGAGAACCTGAGCGAGG-3') and cloned into the pGEM-T easy vector. Antisense RNA was prepared by linearization with ApaI and transcription with SP6 RNA

polymerase (prepared by D. Hernandez).

2.2 Methods

2.2.1 DNA methods

2.2.1.1 Chemical transformation and cultivation of bacteria cells

LB-medium: Bacto tryptone 10 g (1%); Bacto Yeast Extract (0.5%); NaCl 10 g (17.1 mM); dH_2O to 1 l; pH to 7.5

LB-agar: Agar 15 g (1.5%) to 1 l LB-medium

Ampicillin: Stock solution 100 mg/ml in dH_2O; stored at -20 ^oC; working solution 100 ug/ml

To amplify plasmid DNA for analytical and preparative purposes, chemical competent *E. coli* XL1-Blue were used. Bacterial cell suspension (200 µl) was thawed on ice, mixed with 10 µl of ligation mixture and incubated on ice for 30 min. The bacterial cells were heat-shocked for 90 sec at 42 ^oC and then incubated for 3 min on ice. LB-medium (800 µl) was added and the solution was incubated with mild shaking (4000 rpm) for 45 min at 37 ^oC. The bacteria cells were then pelleted by centrifugation at 7000 rpm for 30 sec and then resuspended in 100 µl LB-medium and seeded on LB-agar plates supplemented with ampicillin. Colonies were grown overnight at 37 ^oC. Single colonies were picked and cultivated in LB-medium containing ampicillin (Sambrook & Russel, 2001) at 37 ^oC and 200 rpm.

2.2.1.2 Plasmid DNA preparations

For the plasmid preparation in analytical amounts (~ 20 ug), the “GeneJET™ Plasmid DNA Miniprep” kit (Thermo Scientific) was used. For the isolation of plasmid DNA in

preparative amounts (~ 200 ug) the “NucleoBondXtra® Midi” kit (Machery-Nagel) was used according to the manufacturer's instructions. The DNA concentration was measured with the NanoDrop-2000c spectrometer.

2.2.1.3 DNA restriction digestion

For the purposes of cloning or preparation of templates (for making sense or antisense RNA) DNA was restricted with the appropriate fast digest restriction enzyme (Thermo Scientific) following the manufacturer’s protocol. The digestions were performed with 2 - 5 U of the appropriate enzymes per ug DNA and incubated at 37 °C for at least

1 h.

2.2.1.4 Agarose gel electrophoresis

TAE (Tris/Acetate/EDTA): 40 mM Tris Acetate; 2 mM EDTA; pH 8.5

2x RNA loading dye: 95% Formamide; 18 mM EDTA; 0.025% of each SDS, Xylene Cyanol and Bromophenol Blue (Thermo Scientific).

To analyze DNA restrictions and PCR products or assess the quality of sense and antisense RNA, agarose gel electrophoresis was performed (Sharp *et al*., 1973) Depending on the size of the DNA or RNA fragment to be analyzed, agarose gels consisting of 0.8 - 2.2 % were prepared by boiling agarose powder (Roth) in 1x TAE buffer. To help with visualization of the separated products after electrophoresis, ethidium bromide (0.5 ug/ml) was added to the agarose/TAE solution before the gel was cast. Standard DNA ladders (Fast Ruler DNA ladder, Fermentas) were used to define the sizes of DNA fragments. Prior to loading, RNA-samples were mixed with 2 µl RNA loading dye. The DNA reactions mixtures are set up with a buffer containing a loading dye and are therefore directly loaded onto the gel. 1x TAE buffer is used as

running buffer. A ChemiDoc (Bio-Rad) chamber using an Intas camera and software was used for documentation of images from the gel.

2.2.1.5 Purification of DNA fragments from agarose gel, PCR and digestions

To purify DNA fragments from agarose gel after PCR or restriction digestions, the “Invisorb Fragment cleanup” kit (Invitek) was used according to the manufacturer's instructions.

2.2.1.6 Polymerase chain reactions (PCR)

To increase the quantity of DNA or cDNA for cloning or analytical purposes, the DNA or cDNA was PCR amplified (Mullis *et al*.,1986; Saiki *et al*., 1985). The PCR reaction is composed of the DNA or cDNA template, oligonucleotides with complementary sequence to the ends of the segment to be amplified, nucleotides and DNA polymerase. The reaction proceeds in three sequential steps (denaturation, annealing and elongation) which are then repeated. Denaturing involves the heating of the DNA template to 95 ^{o}C to render it single stranded. The oligonucleotides then bind to the complementary sequence of the single stranded DNA at a lower temperature specific for their size and composition (annealing) and are extended by the DNA polymerase at 72 ^{o}C (elongation). Depending on the purpose of amplification, the kind of polymerase used, as well as the length and composition of the oligonucleotides varied.

2.2.1.7 PCR for cloning

For molecular cloning, the Phusion High Fidelity PCR enzyme Mix (Thermo Scientific), which contains Taq DNA Polymerase and an additional thermostable DNA polymerase with a 3’ ~ 5’ exonuclease ‘’proof-reading’’ activity was used. This was to ensure a reduction in the incidence of point mutations during the amplification process. A 100 µl PCR reaction was set up comprising the following:

Volume (µl)	Final conc.	Component
1	250 ng	250 ng/ µl
20	1x	5x High Fidelity Buffer with 15 mM $MgCl_2$
2	0.2 mM	10 mM dNTP Mix (Thermo Scientific)
2	0.2 uM	10 uM oligonucleotide mix
1	0.02 U	Phusion High Fidelity PCR enzyme Mix (Thermo Scientific)
to 100	-	HPLC water

The amplification process took place in a thermocycler (Biometra GmbH) under these conditions:

Initial denaturation	98 °C	30 sec	
Denaturation	98 °C	10 min	10x
Annealing	45 °C	30 sec	
Elongation	72 °C	1 min	
Denaturation	97 °C	10 sec	10x
Annealing	60 °C	30 sec	
Elongation	92 °C	1 min	
Final elongation	72 °C	10 min	

2.2.1.8 Semi-quantitative PCR

Analyses of temporal gene expression patterns or alterations due to microinjections or chemical treatments, were done by means of the semi-quantitative PCR using cDNA in a 12.5 µl reaction comprising:

Volume (µl)	Final conc.	Component
2.5	~125 ng	~50 ng/ul cDNA
2.5	1x	5x Flexi Go Taq buffer with 25 mM $MgCl_2$
0.625	0.5 uM	10 uM gene specific oligonucleotides mix
0.1	0.5 U	Go Taq Polymerase (Promega)
to 12.5 µl		HPLC water

The PCR was carried out per the conditions below:

Initial denaturation	95 °C	2 min	
Denaturation	95 °C	45 sec	~25x
Annealing	X °C	45 sec	
Elongation	72 °C	45 sec	
Final elongation	72 °C	5 min	

X = oligonucleotides specific annealing temperature.

2.2.1.9 Fragment Analysis

To determine the effect of CRISPR/Cas9 or *zc3h12c*-MO knockdown on the *zc3h12c* gene, fragment analysis was first performed on PCR amplified genomic DNA or CDNA. For accurate quantitation of NGS library, the De Novix dsDNA High Sensitivity Assay (Biozym) was used. The NGS Diluent Marker (22 ul) was added to the NGS library (2 ul) and the size of the final NGS library determined by using the NGS fragment kit (1-6000 bp, Cat # DNF-473) and run on the 5200 Fragment Analyzer System (Agilent).

2.2.1.10 DNA sequencing

To determine the effect of a manipulation at the genomic level or to control prepared constructs, 1.2 ug of DNA was used. Sequencing was done by the SEQLAB Sequence Laboratories Göttingen GmbH.

2.2.2 RNA methods

2.2.2.1 *In vitro* preparation of capped sense RNA for injection

Capped sense RNAs were synthesized with the SP6 mMessage mMachine Kit (Thermo Scientific) according to the manufacturer's instructions. A total of 20 µl transcription reaction volume was incubated for 2 h at 37 °C after which digestion of DNA was done for 30 min using 1 U Turbo DNase I. Following the manufacturer's instructions, synthesized sense RNAs were then purified using the Illustra RNAspin

Mini kit (GE Healthcare) and eluted with 30 µl RNase free water at 80 °C. RNA concentration was determined on a NanoDrop 2000c spectrophotometer (Thermo Scientific) and the quality verified by running 300 ng on a 2% agarose gel. The RNAs were stored at -80 °C in 2-4 µl aliquots depending on the concentration.

2.2.2.2 *In vitro* synthesis of labeled antisense RNA

To detect endogenous transcripts by means of whole mount in situ hybridization, antisense RNA probes were prepared in 25 µl volume reaction as below:

Volume (µl)	Component
~12.5	1 ug DNA template
5	5x transcription buffer (Fermentas)
4	ATP, GTP, CTP, UTP, Dig-UTP (10 mM each) (Boehringer)
1	DTT (0.75 M)
1	Ribolock RNase inhibitor (40 U/ µl) (Thermo Scientific)
1.5	RNA polymerase (20 U/ µl Fermentas)
25 µl	

The reaction mixture was incubated for 3 h at 37 ^{o}C after which DNase treatment was performed by incubated mixture with 2 U/ µl Turbo DNasel (Ambion) for 30 min at 37 ^{o}C. Anti-sense RNA was purified with the RNeasy® Mini Kit (Qiagen) and eluted in 100 µl RNase-free water at 80 ^{o}C for 2 min. RNA quality was analyzed on a 1% agarose gel after which the remaining was dissolved in 1 ml of hybridization mix and stored at -20 ^{o}C.

2.2.2.3 RNA isolation from whole embryos and ectodermal explants

Trizol® reagent (Thermo Sicientific)

To extract total RNA for downstream application, four embryos or thirty-fifty ectodermal explants were macerated in 400 µl Trizol using a sterile Omnican® 40 syringe (Braun). Samples were incubated at RT for 10 min during which time each sample was vortexed

for 30 sec. Chloroform (80 µl) (Roth) was added to samples and incubated at RT for 5 min while each sample was vortex again for 30 sec. Samples were centrifuged at 13000 rpm for 10 min at 4 ^{o}C to separate the phases. The upper phase was transferred into a new tube and 200 µl of chloroform added. The mixture was vortexed for 30 sec and then centrifuged at 13000 rpm for 5 min at 4 ^{o}C. The upper phase was again transferred into a new tube, 200 µl of isopropanol was added to precipitate nucleic acids and incubated overnight at -20 ^{o}C. Samples were centrifuged at 13000 rpm for 30 min at 4 ^{o}C to pellet nucleic acids. The pellets were washed with 400 ul of 75% ethanol and centrifuged at 13000 rpm for 5 min at 4 ^{o}C. The ethanol was discarded and samples re-centrifuged to remove residual solution. The pellets were air-dried for a few minutes and dissolved in 20 µl RNase free water consisting of the following: 17 µl RNase free water, 2 µl 10x DNase buffer and 1 µl DNase I (2U) (Thermo Scientific) to remove genomic DNA. The RNA samples were incubated at 37 ^{o}C for 45 min after which 0.5 µl DNase 1 (1 U) was added again to the samples and incubated at 37 ^{o}C for 30 min. DNase treatment was stopped by incubating the samples at 70 ^{o}C for 10 min. To control for complete digestion of genomic DNA, PCR was performed with 1 µl of 100 ng/µl dilution of the RNA samples using primers for the housekeeping gene *odc* and the products run on a 1% agarose gel.

2.2.2.4 Reverse transcription

Following the isolation of total RNA, 10 µl of cDNA was prepared in a reaction mix comprising 100 ng of total RNA, 1x Go Taq flexi buffer (Promega), 5 mM MgCl2 (Thermofisher), 2.5 mM random hexamer (Invitrogen), 1 mM dNTP mix (Thermo Scientific), 0.8 U Ribolock RNase inhibitor (Thermo Scientific), and 2 U M-MLV reverse transcriptase (Invitrogen). The reaction took place in a thermocycler (Biometra) under the following cycling conditions: 10 min at 20 °C, 1 h at 42 °C, 5 min at 99 °C.

2.2.2.5 Transcriptome analysis (RNA-sequencing)

2.2.2.5.1 RNA isolation

To isolate total RNA for sequencing, the trizol-based method described above (2.2.2.3) was applied with a few modifications. The precipitated RNA was air dried and resuspended in 50 µl solution of RNase free water (43 µl), 10x DNase buffer (5 µl), 1.5 U DNaseI (0.75 µl) and 20 U of RNase inhibitor (0.5 µl) and incubated at 37 °C for 45 min. 1 U DNaseI (0.5 µl) was added again to the isolated RNA and incubated for an additional 30 min at 37 °C. To stop the DNase treatment, the RNA solution was brought to a 200 µl volume by the addition of 150 µl RNase-free water, phenol-chloroform-isoamyl alcohol (200 µl) was then added, vortexed and centrifuged 13000 rpm for 10 min at 4 °C. The upper phase was transferred to a new tube, 1/10 vol 5 M ammonium acetate and 1 vol, 2-propanol were added and incubated overnight at -20 °C. RNA was pelleted by centrifugation at 13000 rpm for 30 min at 4 °C. The pellet was washed with 400 µl 70% ethanol, air-dried and dissolved in 15 µl RNase-free water. RNA quality was analyzed by using Nanodrop. To verify that the RNA was not contaminated with genomic DNA, a PCR was performed with 1 µl RNA samples (100 ng/µl) with oligonucleotides for housekeeping gene *odc*.

2.2.2.5.2 Sample preparation and sequencing

RNA-samples were prepared in three biological replicates and sequenced by the University Medical Center Göttingen (UMG) -NGS Integrative Genomic Core Unit (NIG). For sequencing, the RNA-samples were prepared with the "TruSeq RNA Sample Prep Kit v2" according to the manufacturer's protocol (Illumina). Single read (50 bp) sequencing was conducted using a HiSeq 4000 (Illumina). Three independent biological replicates were analyzed for each condition. Sequencing quality was checked and approved via the FastQC software version 0.11.9 (Andrews, 2019).

Sequence images were transformed to BCL files with the Illumina BaseCaller software and samples were demultiplexed to FASTQ files with bcl2fastq (version 2.20). Sequences were aligned to the genome reference sequence of *X. laevis* (genome build 10.1, available at Xenbase, http://www.xenbase.org/). Alignment was performed using the STAR alignment software (Dobin *et al*., 2013; version 2.5.2a) allowing for 2 mismatches within 50 bases. Subsequently, counting of uniquely mapping hits was conducted with featureCounts (Liao *et al*., 2013). Data was preprocessed and analyzed in the R/Bioconductor environment version 4.1.0 (www.bioconductor.org) using the DEseq2 package (Anders & Huber, 2010, version 1.32.0). Specifically, the data was normalized and tested for differentially expressed genes based on a generalized linear model assuming negative binomial data distribution. Candidate genes were filtered using an absolute log2 fold-change >1 and FDR-corrected p-value < 0.05.

2.2.2.5.3 Gene Ontology Analysis

Gene Ontology enrichment analysis plots were created using ShinyGo v0.76 (http://bioinformatics.sdstate.edu/go/) (Ge *et al*., 2020) using Human Biological Process assignments. FDR cutoff 0.05.

2.2.3 Protein methods

2.2.3.1 Preparation of protein lysate

Extraction Buffer IPP 145 (10x stock): 100 mM Tris HCl, pH 7.5; 145 mM NaCl: 1% NP 40 (Nonidet 40) Substitute (stored at RT)

Lysis buffer: 1x IPP145 solution; 5% Glycerol; Protease inhibitor tablet ‘Complete’ (Roche, according to manufacturer’s instruction).

To verify that sense RNAs transcribed from overexpression constructs get translated into proteins *in vivo*, western blot analyses were performed. Embryos injected with the desired sense RNA were lysed in lysis buffer (10 µl per embryo) using an embryo homogenizer and incubated on ice for 15 min. Samples were then centrifuged for 5 min at 4 °C at 13000 rpm. The cytoplasmic fraction (middle phase) was transferred into a new tube and centrifuged again at 4 °C at 6000 rpm. Cell lysate was transferred into a new tube and protein quantified by means of Bradford assay.

2.2.3.2 SDS-polyacrylamide gel electrophoresis (SDS-PAGE)

10x Laemmli buffer: 250mM Tris, 2.5 M glycine, 0.1% SDS

2x SDS loading buffer: 100 mM Tris-HCl pH 6.8, 4% (w/v) SDS, 0.2% (w/v) bromophenol blue, 20% (v/v) glycerol, 200 mM dithiotheitol (DTT)

SDS polyacrylamide gel electrophoresis (Laemmli, 1970) was performed to separate proteins according to their molecular weight. Proteins were mixed with 2x loading buffer, denatured by boiling for 10 min at 95 °C and separated on a 10% SDS gel prepared according to standard protocols (Sambrook & Russel, 2001). Gel electrophoresis was performed in 1 x Laemmli buffer and a starting voltage of 150 V which was increased to 200 V when samples had migrated into the separating gel. As soon as the samples entered the separating gel the voltage was turned up to 200 V. To determine the molecular weight of the proteins, a standard protein marker was used (Page Ruler Plus Prestained Protein Ladder, Thermofisher).

2.2.3.3 Western blot

Transfer buffer: 2.9 g Glycine; 5.8 g Tris; 0.37 SDS; 200 ml Methanol (1 l)

TBS: 50 mM Tris, 150 mM NaCl, pH 7.6

TBST: 0.05 % Tween-20 in TBS

Blocking solution: 5% (w/v) dry, non-fat milk powder in TBST

Primary antibody: mouse Anti-myc (Sigma)

Proteins separated by SDS-PAGE were transferred onto a nitrocellulose membrane by semi-dry blotting for 1 h in transfer buffer at 13-15 V (Sambrook & Russel, 2001; Towbin *et al*., 1979). Afterwards, the membrane was blocked in blocking solution for 1 h at RT. Incubation with the primary antibody was carried out overnight at 4°C. The next day, the membrane was washed 3 times (10 min each) in blocking solution. Membrane was then incubated with the secondary antibody, coupled to a fluorescent IRdye (LI-COR) for 1 hr at RT. After, the membrane was washed three times (10 min each) with TBST at RT. Proteins were detected using the LI-COR Odyssey Infrared Imaging system was used.

2.2.4 *X. laevis* methods

2.2.4.1 Staging of *X. laevis* embryos

Classification of developmental stages were done according to Nieuwkoop and Faber (1967).

2.2.4.2 Priming of *X. laevis*

HCG: 1000 I.E./ml human chorionic gonadotrophin (hCG) (Ovogest, MSD animal health).

To stimulate egg laying the next day, 800 U human chorionic gonadotropin was injected subcutaneously into the dorsal lymph sac of the female frogs the day before (in the evening) and kept at 16 °C overnight. The frogs usually started egg-laying approximately 16 hours after hCG priming.

2.2.4.3 Isolation and preparation of the testes

5x MBS: 440 mM NaCl, 5 mM KCl, 4.1 mM $MgSO_4$, 12 mM $NaHCO_3$, 2.05 mM $CaCl_2$, 1.65 mM $Ca(NO_3)_2$, 50 mM HEPES, pH 7.8

Frog narcotic: 2.5% Tricane methanesulfonate (MS-222) in tap water, adjusted to neutral pH using Na_2HPO_4.

To obtain testis to fertilize eggs *in vitro*, male frogs were anesthetized 30 min in narcotic (1 g/l tricaine methanesulfonate, 0.1% Na_2HPO_4, pH 7) (Guénette *et al.*, 2013). The testes were isolated, washed in 1x MBS and stored at 4 °C in 1x MBS. For the fertilization of eggs, a piece of testis was minced in a small petri dish and mixed with 1X MBS to form a lysate. The testis lysate was then kept on ice.

2.2.4.4 *In vitro* fertilization of eggs

Primed female frogs were gently stroked on the back by the thumb to stimulate the release of eggs which were collected into a petri dish. The eggs were fertilized with a 1:10 dilution (with water as the diluent) of the testis-lysate. The volume of testis lysate used was dependent on the size of the batch of eggs as well as the freshness of isolated testis used. Usually, between 100 µl and 200 µl of testis lysate were used. The fertilized eggs were covered with 0.1x MBS after 20-30 min and incubated at 12.5 °C.

2.2.4.5 Culture of embryos and microinjections

Cysteine: 2% Cysteine-HCl in 0.1x MBS, pH 8

Injection buffer: 2% Ficoll in 1x MBS

To prepare fertilized eggs for injection, the jelly coat of the fertilized eggs was removed by treatment with 2% cysteine hydrochloride. This was done by covering the fertilized eggs with the cysteine solution in a beaker and gently swirling the contents. Dejellied

eggs were then washed three times with 0.1x MBS and cultivated in injection buffer at 12.5 °C until they reached the desired stage for injection. Needles for injection were prepared by pulling small glass capillaries (GB100F-8P, Science Products GmbH) with the needle puller PN-30 (Science Products GmbH). Injection mixes were backloaded into the injection needles with the help of microloader (Eppendorf) and then attached to microinjector PV 820 (H. Sauer) microinjector. The tip of the injection needle was cut open with the help of a pair of forceps and a 4 nl injection drop (adjusted with a micrometer scale) was injected animally into either one or both blastomeres of the two-cell stage embryo depending on the experimental approach. Injections were performed on a cooling plate at 12.5 °C. Injected embryos were kept in injection buffer for at least 30 min after which the injection buffer was exchanged for 0.1x MBS. Embryos were cultivated at 12.5 -14 °C until the desired developmental stage. For ectodermal explants, embryos were incubated at 12.5 °C on the day of injection to be further processed the following day.

2.2.4.6 Ectodermal explants (animal cap)

5x MBS: 440 mM NaCl, 5 mM KCl, 4.1 mM $MgSO_4$, 12 mM $NaHCO_3$, 2.05 mM $CaCl_2$, 1.65 mM $Ca(NO_3)_2$, 50 mM HEPES, pH 7.8

Agarose dish: 1 % agarose in 0.8x MBS

Blastula stage (8-9) embryos (both injected and un-injected controls) were transferred into an agarose-coated petri dish and the vitelline membranes removed using forceps. With the help of the gastromaster system (Xenotech Engineering, Bellville, USA), animal caps were isolated and transferred to a fresh agarose-coated petri dish containing 0.8x MBS. Animal caps were cultivated at 14°C until the equivalent of the desired developmental stage, determined by sibling control group, is reached. The caps (30-50) were collected in an Eppendorf tube, the buffer was carefully removed

and then snap-frozen in liquid nitrogen. The fixed caps were stored at -80 °C until needed.

2.2.4.7 Dexamethasone treatment

Through fusion of the protein of interest to the human glucocorticoid receptor, the protein of interest can be kept inactive and sequestered by heat shock proteins (Kolm & Sive, 1995). Fusion protein activity was induced in *X. laevis* by cultivating embryos or animal caps in 0.1X MBS or 0.8X MBS, respectively, containing 10 µM dexamethasone. Embryos were cultivated in the dark.

2.2.4.8 Whole mount in situ hybridization (WMISH)

The spatial and temporal expression patterns of endogenous transcripts were visualized by means of whole mount in situ hybridization (WMISH) which was performed based on (Harland, 1991; Hollemann *et al*., 1999; Nieber *et al*., 2009). The process utilizes Digoxygenin-11-UTP(Dig)-labeled anti-sense RNA probes and an alkaline phosphatase-coupled anti-Dig antibody for detection and visualization of the endogenous transcripts respectively. Unless indicated, all steps took place at room temperature under mild shaking.

2.2.4.8.1 Fixation and X-Gal staining of *lacZ* mRNA injected embryos

10x MEM: 1 M Mops; 20 mM EGTA; 10 mM $MgSO_4$; pH7.4 (stored in the dark at 4 ^oC)

10x PBS: 1.75 M NaCl; 1 M KCl; 65 mM Na_2HPO4; 18 mM KH_2PO_4; pH 7.4

$K_3Fe(CN)_6$: 0.5 M in H_2O (stored in the dark)

$K_4Fe(CN)_6$: 0.5 M in H_2O (stored in the dark)

MEMFA: 4% (v/v) formaldehyde (37%) in 1x MEM

X-Gal: 40 mg/ml 5-bromo-4-chloro-3-indolyl-b-D-galactopyranoside in Formamide (stored in the dark at -20 ^oC).

X-Gal staining solution: 1 mg/ml X-Gal; 5 mM $K_3Fe(CN)_6$; 5 mM $K_4Fe(CN)_6$; 2 mM $MgCl_2$ in 1x PBS

100% Ethanol

To identify the injected side of the embryo and analyze the distribution of the injected material, the co-injection of 75 pg *lacZ* mRNA was done. Embryos were collected in glass vials and fixed with MEMFA for 20 min followed by three washes with 1x PBS, each lasting for 10 min. For the visualization of the distribution of injected *lacZ* mRNA, X-Gal staining was performed (Hardcastle *et al*., 2000). The embryos were incubated in X-Gal staining solution in the dark until a desired intensity of staining was achieved. Embryos were then washed three times for 10 min each in 1x PBS to stop the staining reaction, refixed for 25 min in MEMFA and then washed three times for a total of 15 min with 100% ethanol. Finally, embryos were stored in 100% ethanol at -20 ^{o}C.

2.2.4.8.2 Fixation of uninjected embryos

Uninjected or staged embryos were fixed in glass vials with MEMFA for 1 hr, followed by three washes, lasting 5 min each, with 100% ethanol. Embryos were stored in 100% ethanol at -20 ^{o}C.

2.2.4.8.3 Rehydration

PTw: 0.1% tween-20 in 1x PBS

75% ethanol: 75% ethanol and 25% water

50% ethanol: 50% ethanol and 50% water

25% ethanol: 25% ethanol and 75% PTW

Using a series of solution with decreasing ethanol gradient (75%, 50%, 25%), embryos were rehydrated for 15 min (5 min per each ethanol concentration) and then washed four times (5 min each) with PTw.

2.2.4.8.4 Proteinase K treatment

PTw: 0.1% tween-20 in 1x PBS

Proteinase-K solution: 5 ug/ml Proteinase K (Merck) in PTw.

To allow better penetration of the antisense RNA probe, the embryos were treated with proteinase K. The embryos were incubated in 2 ml of PTw/protein-K solution for a period and temperature defined by the developmental stage:

stage	Time (min)	temperature
10 to 12	6	RT
14-16	10	RT
27-30	18	RT

2.2.4.8.5 Acetylation and refixation

Triethanolamine: 0.1 M (0.93 g in H_2O); pH 7.5

Acetic anhydride (Sigma)

PTw: 0.1% tween-20 in 1x PBS

PTw-FA: 4% formaldehyde (v/v) in PTw.

To stop the proteinase K treatment, embryos were washed two times (5 min per wash) with triethanolamine. To avoid unspecific interactions of the Dig-labeled antisense RNA probe, free amino-acid ends were blocked by acetylation. Embryos were treated with 25 µl acetic anhydride in 4 ml triethanolamine. Afterwards, the embryos were washed two times with PTw for a total of 10 min and fixed in PTw-FA for 20 min. The embryos were then washed 5 times (5 min per wash) with PTw.

2.2.4.8.6 Hybridization reaction

100x Denhardt's: 2% BSA; 2% Polyvinylpyrollidone (PVP); 2% Ficoll

20x SSC: 3 M NaCl; 0.3 M NaCitrate; pH 7.2-7.4

Hybridization Mix: 50% (v/v) formamide; 1 mg/ml Torula RNA (Sigma); 100 ug/ml heparin, 1x Denhardt's; 0.1% (v/v) Tween-20; 0.1% (v/v) CHAPs; 10 mM EDTA in 5x SSC

Antisense RNA probe: Dig-labeled antisense RNA probe in hybridization mix (stored at -20 ^{o}C)

Prior to the hybridization with the antisense RNA probe, embryos were incubated with 500 ul hybridization mix at 65 ^{o}C for 5 min and then 1 ml hybridization mix for 5 h at 65 ^{o}C. Hybridization with the antisense RNA probe (1 ml) occurred overnight at 65 ^{o}C.

2.2.4.8.7 Washing and RNase treatment

20x SSC: 3 M NaCl; 0.3 M NaCitrate; pH 7.2-7.4

RNase solution: 20 ug/ml RNase A and 10 U/ml RNase T1 (Fermentas) in 2x SSC

MAB: 100 mM Maleic acid; 150 mM NaCl; pH 7.5

The following morning, the antisense RNA probe was removed and stored at -20 ^{o}C and the embryos were washed three times with 2x SSC for 45 min at 65 ^{o}C. Excess (unhybridized) antisense RNA probe was removed by treating embryos with 2 ml RNase solution for 1 h at 37 ^{o}C. Embryos were washed once in 2x SSC for 10 min at RT and followed by twice (30 min each) in 0.2x SSC at 65 ^{o}C. Finally, the embryos were washed twice with MAB at RT for 30 min.

2.2.4.8.8 Antibody reaction

MAB: 100 mM maleic acid; 150 mM NaCl; pH 7.5

MAB/BMB: 2% BMB blocking reagent in 1x MAB

MAB/ BMB /HS: 20% heat-treated horse serum (HS) in MAB/BMB

MAB/ BMB /HS /AK: 1:5000 sheep-anti-Dig antibody link to alkaline phosphatase (AP) in MAB/BMB/HS (Sigma)

Prior to the antibody reaction, blocking steps were performed to decrease unspecific binding of the AP-linked anti-Dig antibody. These included incubation of the embryos for 20 min in MAB/BMB, and then MAB/BMB/HS for 40 min. For the detection of the hybridized antisense probe, the embryos were incubated with anti-Dig antibody containing MAB/BMB/HS solution (MAB/BMB/HS/AK) at 4 ^{o}C overnight.

2.2.4.8.9 Staining reaction

MAB: 100 mM maleic acid;150 mM NaCl; pH 7.5

APB: 100 mM Tris-HCl, pH 9.0; 50 mM $MgCl_2$; 100 mM NaCl; 0.1% Tween-20; pH 9.0

NBT: 100 mg/ml in 70% dimethylformamide (stored in the dark)

BCIP: 50 mg/ml in 100% dimethylformamide, stored in the dark

Staining solution: 80 µg (0.8 µl) NBT and 175 µg (3.5 µl) BCIP in 1 ml APB

The next day, embryos were extensively washed in MAB. The washing which lasted the entire day with intermittent refreshing of the MAB solution, was to minimize background due to the overnight incubation with the antibody. During the period of washing, the caps of the glass vials were changed. The embryos were afterwards washed twice (5 min each) in APB at 4 ^{o}C and then incubated with the staining solution in the dark at 4 ^{o}C. The staining reaction lasted till a desired staining intensity has been

achieved, typically between one and five days with intermittent refreshing of the staining solution. However, staining could proceed beyond a week for weaker probes.

2.2.4.8.10 Background removal and bleaching

20x SSC: 3 M NaCl;0.3 M NaCitrate; pH 7.2-7-5

MEMFA: 4% (v/v) formaldehyde (37%) in 1x MEM

Bleaching solution: 50% formamide and 1-2% H_2O_2 in 5x SSC

The staining reaction was stopped and background staining decreased by washing embryos in 100% methanol until the wash solution no longer became stained (remained clear). To remove the methanol, embryos were washed with decreasing concentration of methanol solution (75%, 50% and 25%) and then fixed in MEMFA for 30 min. To remove pigmentation for better visualization of the staining, the embryos were washed in 0.5x SSC for 5 min and incubated in bleaching solution. After depigmented, the embryos were washed twice with 0.5x SSC and stored in MEMFA for an indefinite period.

2.2.4.9 Sections

Gelatin/albumin: 4.44 mg/ml gelatin (Gelatin Sigma TypA G1890), 0.27 g/ml bovine serum albumin, 0.18 g/ml sucrose in PBS. The gelatin was dissolved by heating the solution to 60°C followed by the addition of albumin and sucrose and filtered with a 1.20 µm filter (Sartorius) and stored at -20°C.

Glutaraldehyde

Mowiol: 5 g Mowiol was dissolved in 20 ml 1X PBS by stirring overnight. 10 ml of glycerol was then added and the solution stirred again overnight. Undissolved Mowiol

was collected by centrifugation at 20,000 g for 30 min. The pH of the supernatant was adjusted to 7.0 with the help of pH strips and stored at -20°C.

Tailbud stage embryos analyzed by WMISH were embedded in gelatin/albumin crosslinked with glutaraldehyde (Hollemann *et al*., 1996). Sections (30 µm) were cut on a Leica VT1000M vibratome and mounted onto slides with Mowiol.

2.2.4.10 CRISPR/Cas system

The Clustered Regularly Interspaced Short Palindromic Repeat (CRISPR/Cas9) system has been successfully used as a gene modification tool in numerous organisms (Blitz *et al*., 2013; Nakayama *et al*., 2013; Sander & Joung, 2014; Wang *et al*., 2015; Zhang *et al*., 2014). Identified as a bacterial adaptive defense mechanism against virus and plasmid DNA (Fineran & Dy, 2014; Hsu *et al*., 2014; Terns & Terns, 2014), the system comprises an RNA-guided DNA endonuclease (Cas9) that causes double-strand breaks at the DNA target site. An imperfect repair mechanism by means of non-homologous end-joining (NHEJ) frequently induces insertion or deletion mutations (indels) (Waters *et al*., 2014).

2.2.4.10.1 sgRNA preparation

Zc3h12c gRNA was prepared according to Gagnon *et al*., (2014) with a few modifications. Briefly, the template for the transcription of the gRNA was generated in a 10 µl reaction by annealing 100 µM gene-specific oligonucleotide containing the SP6 promoter sequence (5′- ATTTAGGTGACACTATA-3′), a 20-base target site without the PAM, and a complementary region to 100 µM constant oligonucleotide encoding the reverse-complement of the tracrRNA tail. The following PCR conditions were applied: 95 ^{o}C (5 min) and cooled to 85 ^{o}C (-2 ^{o}C/sec) and then to 25 ^{o}C (-0.1 ^{o}C/sec) and finally

to 4 ºC. in a volume of 50 µl 1x annealing buffer. The T4 DNA polymerase (NEB) was used to fill in the ssDNA overhangs at 12 ºC for 20 min. Purification of the resulting *zc3h12c* gRNA template was done with the Invisorb® Fragment cleanup protocol according to the manufacturer´s instructions. DNA was ran on agarose gel to verify product size. The template was transcribed using the MEGAscript T7 kit (Thermo Scientific), DNase treated and precipitated with ammonium actetate/ethanol. The pellet was resuspended in 50 µl RNase-free water and concentration determined with Nanodrop. The *zc3h12c* gRNA was aliquoted and stored at -80 ºC.

2.2.4.10.2 Injection for mutation analysis

***zc3h12c* gRNA** (stored at – 80 ºC)

Cas9 protein stock: 1µg/µl (prepared from dilution of 50 µg stock powder with nuclease-free water), PNA Bio.

The *zc3h12c* gRNA stored at – 80 ºC was thaw on ice, heated at 70 ˚C for 2 mins and immediately chilled on ice to eliminate secondary structures. A ribonucleoprotein complex (RNP) of the Cas9 protein and *zc3h12c* gRNA was prepared by incubating the Cas9 protein and *zc3h12c* gRNA injection mix at 37 ˚C for 5 min. The RNP was then kept on ice and mixed with *MT-GFP* mRNA to enable the selection of injected embryos. The injection mix was kept on ice until the time of use. Injection of the RNP was done at the center of the animal hemisphere at the one-cell stage, 20-25 min post-fertilization. After injection, embryos were cultivated at room temperature (21-22 ˚C) and transferred from the high salt buffer with Ficoll to low salt buffer after stage 6.

2.2.4.10.3 Extraction of genomic DNA for mutation analysis

To identify the kind of mutations introduced into *zc3h12c* by the Cas9/gRNA system, genomic DNA was extracted using the DNeasy® Blood and Tissue Kit (QIAGEN)

according to the manufacturer's instructions. Briefly, collected embryos (one per tube) stored at -80 ^{o}C were thawed on ice. Cell lysis was performed by adding 180 µl buffer ATL and 20 µl proteinase K to the embryos, mixed by vortexing and incubated at 56 ^{o}C and1000 rpm until embryos were completely lysed. After, 200 µl Buffer AL was added and thoroughly mixed by vortexing, followed by 200 µl of 100% ethanol and thoroughly mixed by vortexing. Mixtures were pipetted into a DNeasy Mini column placed in a 2ml collection tube, and centrifuged at 7000 xg for 1 min. The collection tubes were then discarded and spin columns placed in new 2 ml collection tube. 500 µl of Buffer AW1 was added and centrifuged for 1 min at 7000 xg . Spin columns were again placed in new 2 ml collection tube and 500 µl Buffer AW2 was added and centrifuged at 17000 xg for 3 min. Finally, spin columns were transferred to a new 1.5ml microcentrifuge tube and DNA was eluted with 200 µl Buffer AE, incubated at room temperature for 1 min, and centrifuged at 7000 xg for 1 min. To increase the yield of genomic DNA, the flow through was again transferred onto the membrane and centrifuged at 7000 xg for 1 min. Genomic DNA were then stored at 4 ^{o}C.

2.2.4.10.4 Assessment of mutation

To assess the effect of the CRISPR/Cas9 knockdown, a region of the *zc3h12c* gene encompassing the region targeted by the gRNA was PCR-amplified with the primers, for: 5´-TGACATGTAGCAGCTTCATGG-3´ and rev: 5´-GGTCTTGTATAATCTCATTGCGC-3´. An amount (4 µl) of the crude PCR product was then subjected to fragment analysis. The remaining PCR product was purified, and1.2 µg sent for direct sequencing. To determine the type of mutations induced in *zc3h12c*, the purified product was further subjected to bacterial cloning and individual clones sequenced.

2.2.4.10.5 Cas9 injections for WMISH

To determine the effect of the Cas9 mutation on neuronal differentiation, embryos were injected unilaterally at the 2-cell stage and analyzed by WMISH for effects on neuronal differentiation. Preparation of injection mixes was done as described for the mutational analysis except that *lacZ* mRNA instead of *MT-GFP* mRNA was added to the RNP complex prior to injection.

2.2.5 Luciferase Reporter Assays

As an indirect approach to determine the molecular mechanism(s) by which Zc3h12c promotes neuronal differentiation and verify the regulation by Zc3h12c of some of the upregulated genes from the transcriptome analysis in the animal caps, embryos were injected with various luciferase reporter plasmids. Antisense morpholino oligonucleotides or mRNAs encoding the wildtype Zc3h12c or RNase deficient mutant, Zc3h12c.S^{D249N} were co-injected with the reporters depending on the experimental aim. To ensure the collection of only injected embryos, *MT-GFP* mRNA was co-injected. Embryos injected with mRNA encoding the inducible Zc3h12c constructs were treated with Dex. at stage 10.5. At the required developmental stage, embryos were collected in triplicates, consisting of 5-10 embryos per tube, snap frozen in liquid nitrogen and stored at -80 °C. Embryos were lysed with 50-100 µl 1x lysis buffer (10 µl per embryo) and the subsequent measurement of Renilla-Luciferase activity was performed on 10 µl lysate with the Dual Luciferase Assay Kit (1960), Promega according to the manufacturer's instructions. The Centro LB 960 Luminometer (Berthold Technologies) was used for the measurements. The resulting data was normalized to Renilla and presented as relative light units (RLU).

3 Results

3.1 Neurog2 positively regulates *zc3h12c* expression

The proneural transcription factor Neurog2 is sufficient to promote neuronal differentiation in pluripotent cells (Perron *et al*., 1999; Thoma *et al*., 2012). To identify the early transcriptional regulatory events induced by Neurog2 in such a system, we have previously characterized the transcriptome of *X. laevis* animal caps expressing Neurog2 (Heddrich, 2012). One gene of interest that was among the most highly upregulated transcripts was that encoding for the ribonuclease Zc3h12c. The *X. laevis* genome is tetraploid and the transcripts for both the L and S homeologs of *zc3h12c* were strongly induced by Neurog2 after 6 hr (*zc3h12c,* log2FC=3.1; *zc3h12c,* log2FC=3.0).

To verify the regulation of z*c3h12c* by Neurog2 in the *X. laevis* embryo, gain-of-function experiments were performed through microinjection of capped *in vitro* synthesized mRNA. A hormone-inducible version of Neurog2, comprising the ligand-binding domain of the glucocorticoid receptor (GR) fused to the Neurog2 coding sequence, was used to gain control over the onset of protein activity (Gammill & Sive, 1997; Perron *et al.*, 1999). *Neurog2-GR* mRNA (20 pg) was injected animally into one blastomere of 2-cell stage *X. laevis* embryos (Fig. 3.1A). In *X. laevis*, the first cleavage plane divides the left and right halves of the embryo (Klein, 1987). Thus, when mRNA is injected unilaterally at the two-cell stage, only one side of the embryo receives the injected material and the other side can serve as a control. *LacZ* mRNA (75 pg) was co-injected as a tracer, to determine the side of the embryo that has been injected and the distribution of the injected material (Detrick *et al*., 1990). At the gastrula stage (stage 10.5), Neurog2 activity was induced by the addition of dexamethasone (Dex) and the embryos cultured until neurula stage (stage 14). Whole mount in-situ

hybridization (WMISH) was used to evaluate the influence of Neurog2 on the expression of *zc3h12c* and the pan-neuronal marker *tubb2b*.

The expression of *tubb2b* at the open neural plate stage is restricted to three bilateral stripes on each side of the midline and in the trigeminal placodes (Chitnis *et al*., 1995). Consistent with previous findings (Ma *et al*., 1996), Neurog2 strongly induced neuronal differentiation as marked by the increased and ectopic expression of *tubb2b* (Fig. 3.1B). Neurog2 also induced the expression of *zc3h12c*, thus confirming the regulation of *zc3h12c* by Neurog2 observed in the RNAseq analysis (Fig. 3.1C).

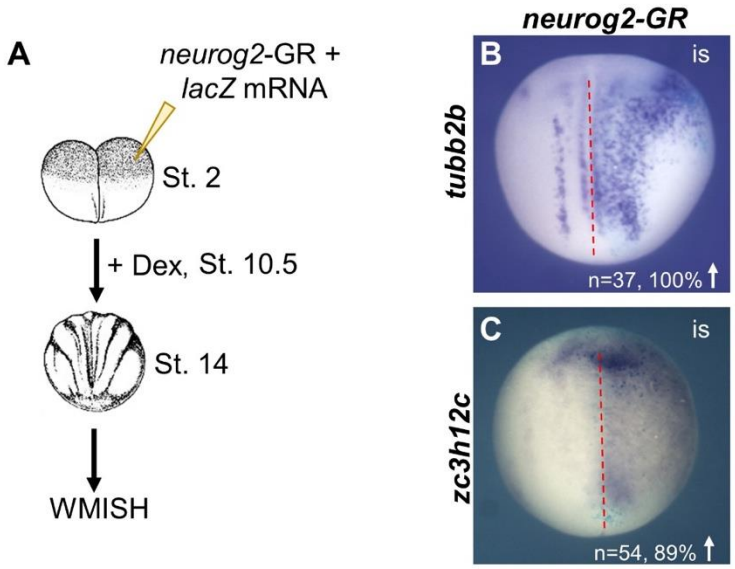

Figure 3.1 Zc3h12c is regulated by the proneural transcription factor Neurog2.

(**A**) Experimental procedure: *neurog2-GR* mRNA together with *lacZ* mRNA was injected animally into one blastomere of the two-cell stage embryos. Embryos were treated at stage 10.5 with Dex to induce Neurog2 activity. WMISH of *tubb2b* (**B**) and *zc3h12c* (**C**) in stage 14-injected embryos. The number of embryos with the shown phenotype are presented as a percentage of the total number of embryos (n) analyzed. Up pointing arrow represents an increase in expression of the probed marker. The injected side (is) is on the right and the red dashed line indicates the midline.

3.2 Zc3h12c localizes to the cytoplasm

The subcellular localization of Zc3h12c was evaluated to gain insight into the molecular function of Zc3h12c. As an antibody against the *X. laevis* Zc3h12c was not

commercially available, a construct was prepared in which the coding sequence of GFP was fused to the C-terminus of Zc3h12c. *Zc3h12c-GFP* mRNA (640 pg) was bilaterally injected at the 2-cell stage together with mRNA encoding the nuclear marker H2B-cherry (100 pg) (Fig. 3.2A). *MT-GFP* mRNA (200 pg) together with *H2B-cherry* mRNA (100 pg) was injected as control. At the blastula stage, animal caps were excised and analyzed by fluorescence microscopy. As shown in Fig. 3.2B and C, Zc3h12c was primarily localized in discrete punctuate cytoplasmic foci, while GFP was diffusely present in both the nucleus and cytoplasm. It should be noted that different concentrations of the injected mRNA were used in the experiment described in Fig. 3.2, higher concentrations of the *zc3h12c-GFP* mRNA were required to allow detection of the fusion protein.

Members of the Zc3h12c family possess an NYN/PIN domain, which functions as an RNase and a CCCH zinc finger domain for binding (Fu & Blackshear, 2017). Mutation of the conserved aspartic acid at position 141 to asparagine (D141N) within the ATP binding domain of Zc3h12a disrupts RNase activity, but not RNA binding activity (Iwasaki *et al*., 2011; Matsushita *et al*., 2009; Suzuki *et al.,* 2011). The NYN/PIN and zinc finger domains of Zc3h12a and Zc3h12c in both mouse and *X. laevis* are highly conserved, therefore, the corresponding mutation in Zc3h12c was introduced into the *X. laevis* Zc3h12c (Zc3h12c^{D249N}). As constructs bearing this mutation will be used in functional experiments, the subcellular localization of a GFP fusion was also evaluated. As shown in Figure 3.2D, Zc3h12c^{D249N}, the mutant localized similar to the wild-type GFP fusion protein in punctuate cytoplasmic foci. In summary, the presence of Zc3h12c in cytoplasmic foci suggests that it may be involved in modulating the stress response or mRNA degradation.

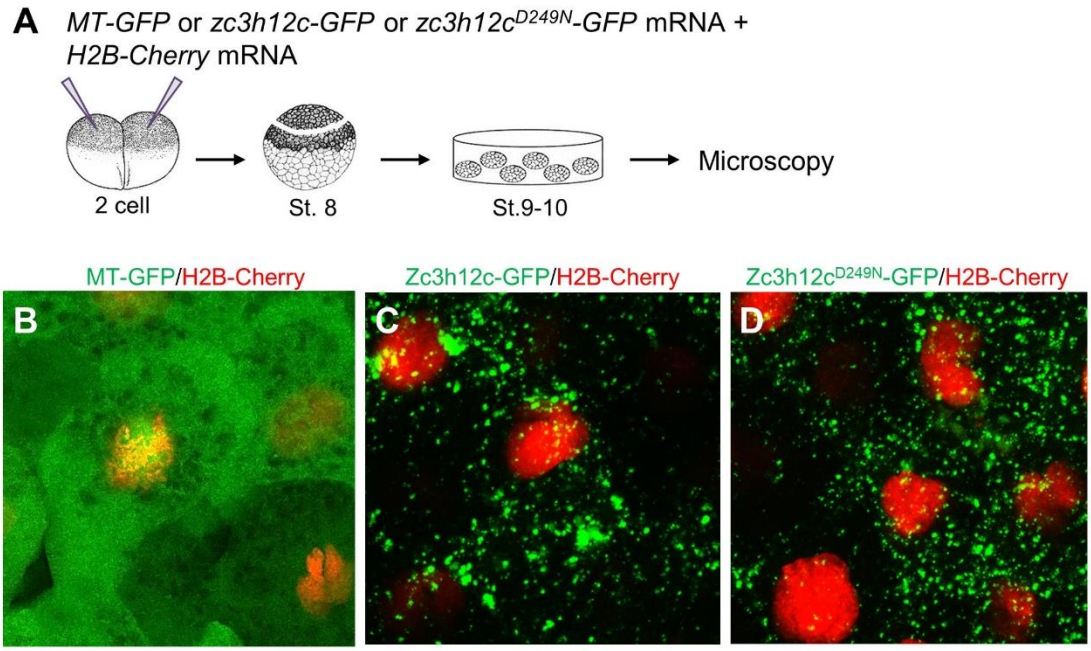

Figure 3.2 Subcellular localization of Zc3h12c.

(**A**) Scheme of the experimental procedure: 2-cell stage embryos were bilaterally injected with mRNA encoding MT-GFP (200) pg, Zc3h12c-GFP (640 pg) or Zc3h12c^{D249N}-GFP (640 pg) together with *H2B-cherry* mRNA (100 pg). At stage 8, animal caps were isolated and analyzed at the equivalent of stage 9-10. Confocal images showing the localization of (**B**) MT-GFP, (**C**) Zc3h12c-GFP, and (**D**) Zc3h12c^{D249N}-GFP (green) and the nuclei marker H2B-cherry (red) in animal caps.

3.3 *Zc3h12c* is expressed in the territories of primary neurogenesis

RNAseq expression data of *zc3h12c* available on Xenbase (Fortriede *et al*., 2020; Session *et al*., 2016) reveals a low-level expression of *zc3h12c* in the fertilized egg, which is maintained in early cleavage stages (Fig.3.3).

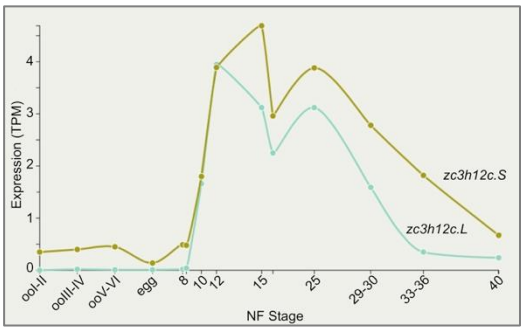

Figure 3.3 Temporal expression of *zc3h12c* during X. laevis development.

Shown is the expression in TPM determined by RNAseq of *zc3h12c* at various stages of development. The graph of expression was derived from data available from www.xenbase.org (Fortriede *et al*., 2020; Session *et al*., 2016).

At early gastrula stage 10 when neural induction begins, *zc3h12c* expression begins to increase steadily and peaks at stage 12 (*zc3h12c.L*) or stage 15 (*zc3h12c.S*). To gain further insight into the putative role of Zc3h12c during early development, the spatial and temporal expression of *zc3h12c* was evaluated by whole mount in-situ hybridization using staged embryos.

As shown in Figure 3.4, specific staining of *zc3h12c* transcripts was first detected in late gastrula stage 12.5 embryos in three bilateral stripes on each side of the dorsal midline (Fig. 3.4A). The medial, intermediate and lateral stripes prefigure the territories in which the motor, inter- and sensory primary neurons of the spinal cord are born (Chitnis *et al*., 1995; Hartenstein, 1989). At stage 14, transcripts of *zc3h12c* are also expressed anteriorly in the trigeminal placodes and in two arcs corresponding to the future ventral forebrain and midbrain as well as the anterior neural ridge (Fig. 3.4B and C). In stage 30 tailbud stage embryos, *zc3h12c* is expressed in the forebrain, midbrain, hindbrain, spinal cord and eyes (Fig. 3.4D). Taken together, the regulation and expression of *zc3h12c* strongly suggests a role for Zc3h12c in the developing nervous system.

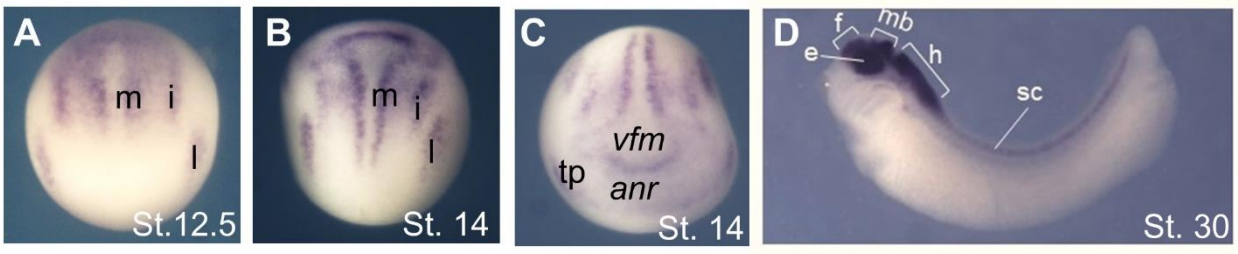

Figure 3.4 Expression of *zc3h12c* during neurogenesis.

WMISH against *zc3h12c* in staged *X. laevis* embryos: (**A**) St. 12.5, dorsal view; (**B**) Open neural plate St. 14, dorsal view; (**C**) St. 14, anterior view. (**D**) Tailbud St. 30, lateral view. m, i and l represent the medial, intermediate and lateral stripes of neurogenic regions respectively. tp: trigeminal placode; e: eye; f: forebrain; mb: midbrain; h: hindbrain; sc: spinal cord.

The timing and spatial expression of *zc3h12c* was compared to that of selected genes in the cascade of events leading to the formation of neurons including the bHLH proneural determination gene *neurog2* (Ma *et al*., 1996), the zinc finger transcription factor and Neurog2 direct target gene *myt1* (Bellefroid *et al*., 1996; Seo *et al*., 2007) as well as the pan-neuronal marker *tubb2b* (Moody *et al*., 1996; Oschwald *et al*., 1991). At mid-gastrula stages (St. 10.5), the expression of the neuronal determination gene *neurog2* can already be detected in three distinct domains on each side of the midline (Fig. 3.5A). These *neurog2* expression domains will give rise to the three domains of primary neurons in the posterior neural plate and clearly precedes the expression of the other marker genes (Fig. 3.5A-D). Transcripts of z*c3h12c* and *myt1* were first detected slightly later, at early gastrula stage (St. 11.5) (Fig. 3.5E-H). Within the open neural plate of stage 12.5 embryos, the expression of *neurog2*, *zc3h12c* and *myt1* are strongly expressed in the three stripes of primary neurogenesis, while the expression of *tubb2b* is just beginning to emerge in the medial stripe (Fig. 3.5I-L). At the neurula stage (stage 14), all markers are expressed in the three stripes of primary neurogenesis as well as the trigeminal placode (Fig. 3.5M-T). In the anterior neural plate, *zc3h12c* and *myt1* are also both found in the prospective ventral forebrain and midbrain, as well as the anterior neural ridge.

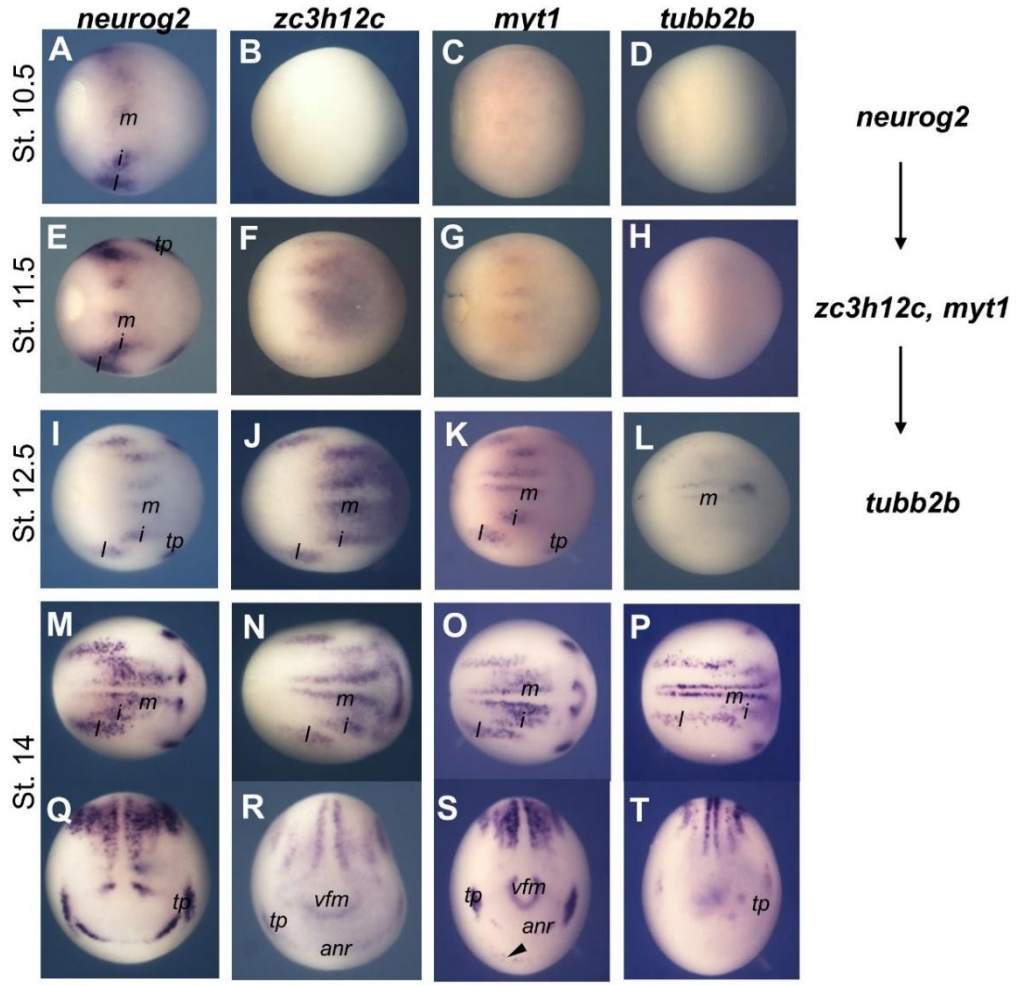

Figure 3.5 Comparative analysis of expression profiles of Zc3h12c, neurog2, myt1 and tubb2b.

WMISH of gastrula stage (St. 10.5 -12.5) embryos shown in dorsal view (**A-L**) and neurula stage (St. 14) embryos in dorsal (**M-P**) and anterior (**Q-T**) views. m, i and l represent the medial, intermediate and lateral stripes of neurogenic regions respectively. tp: trigeminal placode; vfm: future ventral forebrain and midbrain; anr: anterior neural ridge, arrowhead shows scattered cells in the anteroventral region of the embryo.

At the tailbud stage (stage 30), all markers are expressed throughout the CNS (Fig. 3.6A-D). Transverse sections from the level of the hindbrain revealed that similar to *myt1*, *zc3h12c* is expressed in the immediate zone, a region of active neuronal differentiation (Fig. 3.6F-G). In contrast, transcripts of *neurog2* are restricted to the inner, mitotically active ventricular zone, while *tubb2b* is expressed in the outermost differentiated layer (Fig. 3.6E and H).

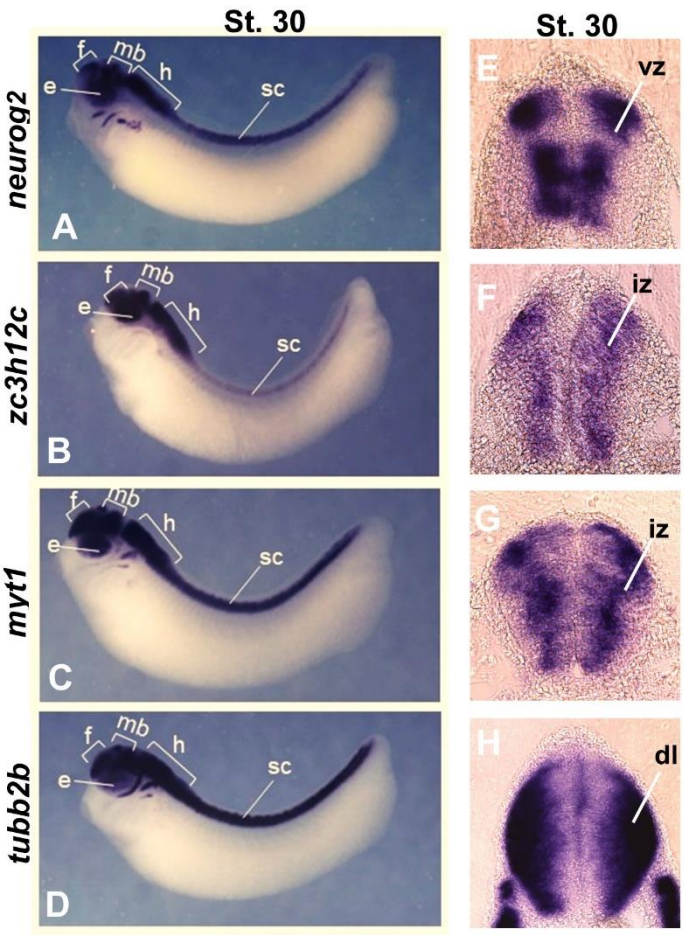

Figure 3.6 Expression profiles of neurog2, zc3h12c, myt1 and tubb2b in the tailbud embryo

WMISH of Stage 30 (St. 30) tailbud embryo in lateral view **(A-D)**. (**E-H**) Transversal section through the hindbrain of the stage 30 embryo. e: eye; f: forebrain; mb: midbrain; h: hindbrain; sc: spinal cord; vz: ventricular zone; iz: intermediate zone; dl: differentiated layer.

In collaboration with the Tuoc group (Neuroanatomie UMG), the expression of ZC3H12C in the developing mouse cortex was evaluated by IHC. As shown in Figure 3.7, in this system ZC3H12C is also a cytoplasm protein, with low expression in Pax6+/Sox2+/Tbr2+ cortical progenitors. ZC3H12C expression is high in HuCD+ cortical neurons and is strongest in the differentiating/immature neurons of the cortical intermediate zone. In summary, these results suggest that Zc3h12c may have a conserved function downstream of the proneural factors when neural precursors are differentiating.

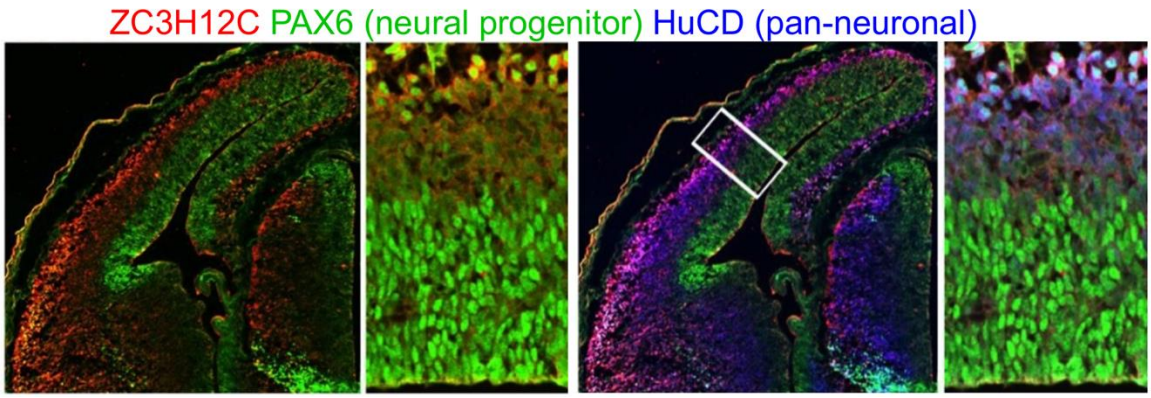

Figure 3.7 Expressioon analysis of ZC3H12C in the mouse cortex.

Shown is the immunohistochemistry for ZC3H12C (red), PAX6 (green) and HuCD (blue) at E12.5. The area delineated by the white box is shown at higher magnification. This experiment was performed by Dr. Huong Nguyen in the Institute of Neuroanatomy, UMG.

3.4 Zc3h12c positively regulates neurogenesis through its RNase activity

To evaluate if indeed Zc3h12c plays a role in neuronal differentiation, it would be useful to perform a gain of function study. However, it has been shown that Zc3h12a-mediated mRNA degradation in the context of inflammation is regulated post-translationally through phosphorylation and subsequent proteasomal degradation, as well as cleavage by the protease MALT1 (Uehata & Takeuchi, 2020). As Zc3h12c is also involved in the regulation of inflammation and functions as an RNase (Garg *et al*., 2021; Liu *et al*., 2021), it is probable that its expression also shows a high level of regulation so that the protein may not be very stable in a gain of function approach using mRNA injection. It is therefore essential to control that indeed the injected mRNA produces sufficient levels of protein. As there are no commercial antibodies available against the *X. laevis* Zc3h12c, Myc-tagged constructs of the wildtype Zc3h12c (MT-Zc3h12c) and Zc3h12c^{D249N} (MT-zc3h12c^{D249N}) were prepared to allow the assessment of protein expression *in vivo* by western blotting.

Therefore, *MT-zc3h12c* or *MT-zc3h12c^{D249N}* mRNA (1 ng) was injected bilaterally at the 2-cell stage together with *GFP-Flag* mRNA (100 pg) as tracer. *MT-GFP* mRNA

(200 pg)-injected embryos served as controls. At stage 11, ten GFP-positive embryos per condition were collected for protein extraction and western blot analysis using the anti-Myc Tag as primary antibody.

As indicated in Fig. 3.8A, both MT-Zc3h12c and MT-Zc3h12c^{D249N} proteins were detected in the cell lysates derived from the injected embryos. However, in addition to the protein band that corresponded to the expected size (~106 kDa), two additional bands of a higher and lower molecular weight were also detected (Fig. 3.8A). It is possible that this observation may be due to posttranslational modification or cleavage of the protein. Comparing the amount of Zc3h12c proteins detected (high amount of injected mRNA) with that of GFP (low amount of mRNA injected) suggests that the Zc3h12c proteins, as earlier proposed, may not be very stable.

Hence 500 pg of *MT-zc3h12c* mRNA together with 75 pg *lacZ* mRNA (as a tracer) were injected animally into one blastomere of the 2-cell stage embryos. The embryos were collected at the open neural plate stage (stage 14) and the expression of *tubb2b* determined by WMISH. As shown in Figure 3.8B, the overexpression of the wildtype Zc3h12c led to an increase in differentiated cells within the neurogenic stripes (increased *tubb2b* expression) at the injected side compared to the uninjected side. To determine if the positive effect of Zc3h12c on neurogenesis was dependent on its RNase activity, mRNA of the RNase deficient mutant, *MT-Zc3h12c^{D249N}* (500 pg) was also evaluated in the gain of function assay. In contrast to the wildtype *zc3h12c* mRNA, injection of mRNA encoding Zc3h12c^{D249N} resulted in a reduction of *tubb2b* expression on the injected side of the embryo (Fig. 38C and D).

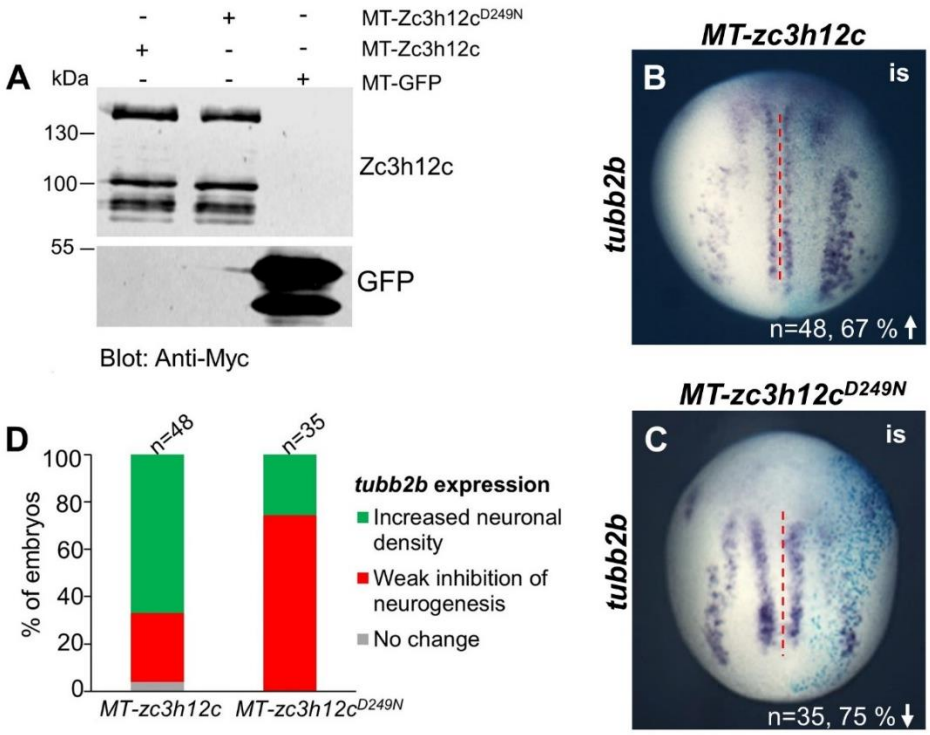

Figure 3.8 Zc3h12c promotes neuronal differentiation.

(A) Western blot analysis of the *in vivo* protein expression of MT-Z3h12c or MT-Zc3h12c^{D249N}. WMISH of stage 14 *MT-zc3h12c* (**B**) and *MT-zc3h12c^{D249N}* **(C)**-injected embryos. (**D**) Percentage of the total number of embryos showing the indicated *tubb2b* expression phenotypes.

The possibility that the Myc-tagged-Zc3h12c proteins may not be very stable, coupled with the weak WMISH phenotypes when injected at lower concentrations led to the preparation of hormone inducible constructs of the wildtype Zc3h12c (MT-Zc3h12c-GR) and Zc3h12c^{D249N} (MT-Zc3h12c^{D249N}-GR) (Fig 3.9A). GR fusion proteins have been shown in *X. laevis* to have increased stability compared to the native fusion proteins and produce more effective phenotypes (Kolm & Sive, 1995). Through the fusion of Zc3h12c to the GR domain, we could potentially increase protein stability as well as restrict its temporal activation to the desired stage of development. This would help to potentiate its effect within a narrow time frame and may therefore produce better phenotypes.

First, the expression of the MT-Z3h12c-GR fusion proteins *in vivo* was assessed by western blot analysis. *MT-zc3h12c-GR* or *MT-zc3h12c^{D249N}-GR* mRNA (2 ng) was

injected bilaterally at the 2-cell stage together with *GFP-Flag* mRNA (100 pg). *MT-GFP* mRNA (100 pg)-injected, as well as uninjected embryos served as controls. At stage 10.5, the embryos were divided and one batch was treated with Dex. Both groups of embryos (Dex-treated and untreated) were collected at stage 11 for protein extraction and western blot analysis using the anti-Myc Tag as the primary antibody. As indicated in Fig. 3.9B, both treated and untreated *MT-zc3h12c-GR or MT-zc3h12c^{D249N}-GR* mRNA-injected embryos produced proteins *in vivo*. However, the majority of protein produced were C-terminal truncations.

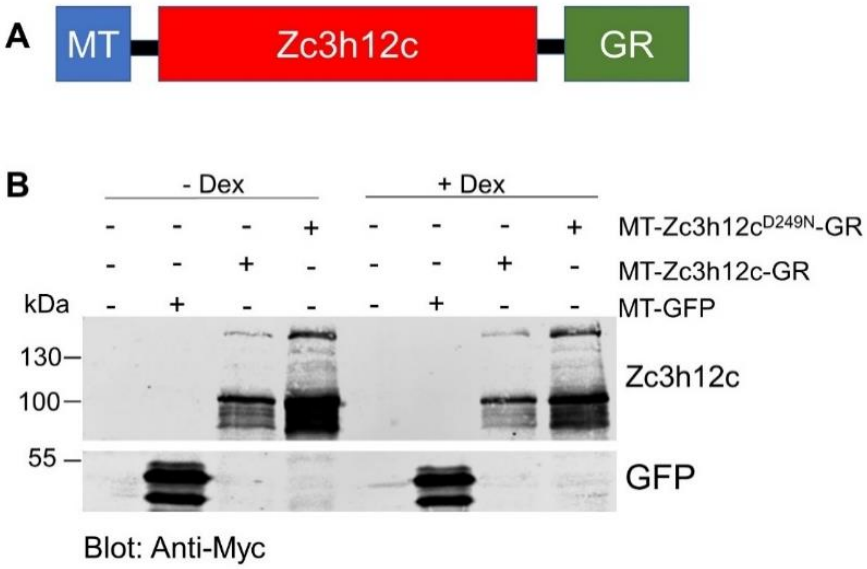

Figure 3.9 Fusion of GR domain to Zc3h12c increase amount of protein.

(A) Schematic diagram of inducible Zc3h12c construct**: (B)** Western blot analysis of MT-Zc3h12c-GR and MT-Zc3h12c^{D249N}-GR proteins on 10% SDS PAGE.

As multiple truncated products were produced from the injected mRNA, it was necessary to further confirm the functionality of the MT-Zc3h12c-GR fusion proteins *in vivo*. Target RNAs of Zc3h12c in *X. laevis* have not yet been identified, however, *IL6* mRNA has been shown to be destabilized by mammalian Zc3h12a and Zc3h12c (Garg *et al*., 2021; Kochan *et al*., 2015; Liu *et al*., 2021; Wawro *et al*., 2021). The effect of the Zc3h12c activity was therefore assessed using a luciferase reporter (pmiRGLO-IL6)

harboring the human *IL6* 3'UTR stem-loop structure required for Zc3h12c/Zc3h12a degradation (Kochan *et al*., 2015). The pmiRGLO-IL6 vector when injected into *X. laevis* embryos is expected to give rise to two transcripts, the Firefly luciferase transcript harboring the introduced *IL6 3'UTR* and the Renilla luciferase transcript that can be used for normalization. Both transcripts are under the control of the human phosphoglycerate kinase promoter allowing constitutive gene expression (Fig. 3.10A). If the MT-Zc3h12c-GR protein translated from the injected mRNA are functional, a decrease in the Firefly luciferase activity will be expected (Fig. 3.10B).

The pmiRGLO-IL6 vector (10 pg) was therefore injected alone or together with *MT-zc3h12c-GR* or *MT-zc3h12c*^{D249N}*-GR* mRNA (100 pg or 300 pg) animally into both blastomeres of the 2-cell stage embryos (Fig. 10C). To allow the collection of only injected embryos, *MT-GFP* mRNA (100 pg) was co-injected. Zc3h12c activity was induced at stage 10.5 by treatment of embryos with Dex. At open neural plate stage (stage 14), injected embryos were collected, cell lysates prepared and the dual luciferase assay performed.

Overexpression of the wildtype Zc3h12c resulted in a strong inhibition of the firefly luciferase reporter activity at both concentrations, whereas Zc3h12c^{D249N} did not significantly influence reporter activity (Fig. 3.10D). In addition, the firefly luciferase activity of the reporter without the IL6-3'UTR (pmirGLO) was not influenced by overexpression of the wild-type and mutant Zc3h12c constructs demonstrating specificity of the Zc3h12c RNase activity (Fig. 3.10E). In summary, these results provide evidence that the MT-Zc3h12c-GR construct is indeed active and can destabilize specific mRNAs, while the MT-Zc3h12c^{D249N}-GR is an RNase deficient mutant.

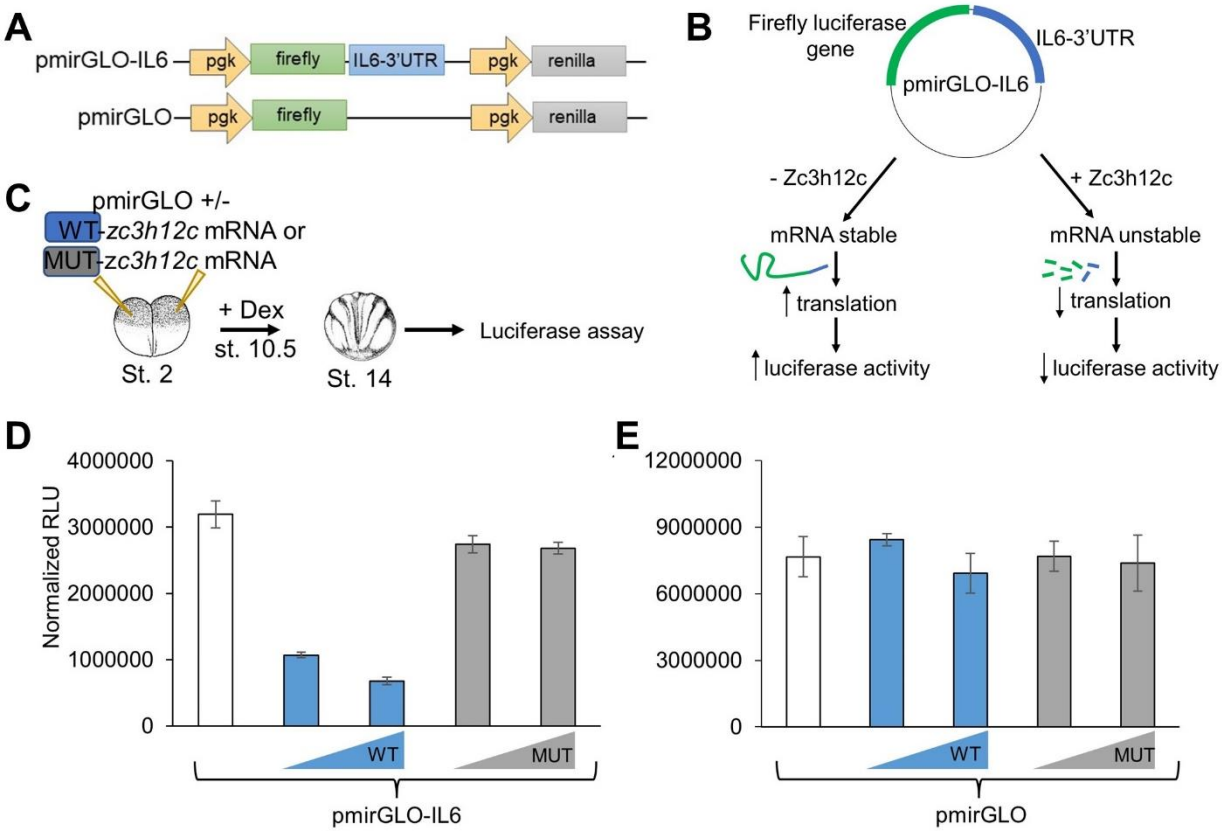

Figure 3.10 Inducible Zc3h12c constructs are functional.

(**A**) Schematic diagram of IL-6 -3'UTR (pmiRGLO-IL6) and control (pmirGLO) luciferase reporter constructs (**B**) Principle of luciferase assay as a readout for RNA destabilization (**B**) Scheme of experimental procedure. (**C**)The pmirGLO-IL6 or pmirGLO vector was injected together with *MT-zc3h12c-GR* (WT) or *MT-zc3h12c^{D249N}-GR* (MUT) bilaterally at the 2-cell stage. Embryos were collected at St. 14 for measurement of luciferase reporter activity. Normalized firefly luciferase activity of pmirGLO-IL6 (Luc-IL6-3'UTR) (**D**) and pmirGLO (Luc-empty) (**E**) measured as relative light units (RLU). Results were calculated from two independent biological replicates, consisting each of three independent measurements per condition. Error bars indicate the standard deviation of the population.

Having established that the MT-Zc3h12c-GR is functional, it was then tested in gain of function experiments in the embryo to determine the influence on neuronal differentiation. *MT-Zc3h12c-GR* or *MT-Zc3h12c^{D249N}-GR* mRNA (300 pg) together with 75 pg *lacZ* mRNA (as a tracer) were injected animally into one blastomere of the 2-cell stage embryo. Zc3h12c activity was induced at stage 10.5 and embryos were collected at stage 14 for the determination of *tubb2b* expression by WMISH.

As observed with the Myc-tagged constructs shown in Figure 3.8B and C, the overexpression of the wildtype MT-Zc3h12c-GR led to an increase in *tubb2b*

expression within the neurogenic stripes, while the MT-Zc3h12c^{D249N}-GR led to an inhibition (Fig. 3.11A and B). Altogether, these findings indicate that Zc3h12c functions in neuronal differentiation and that this positive regulation of neurogenesis by Zc3h12c is dependent on its RNase activity. Comparing the WMISH phenotypes of the inducible constructs to the Myc-tagged versions show that the former produces strong phenotypes at lower injection amounts than the latter (Figure 3.8D and C).

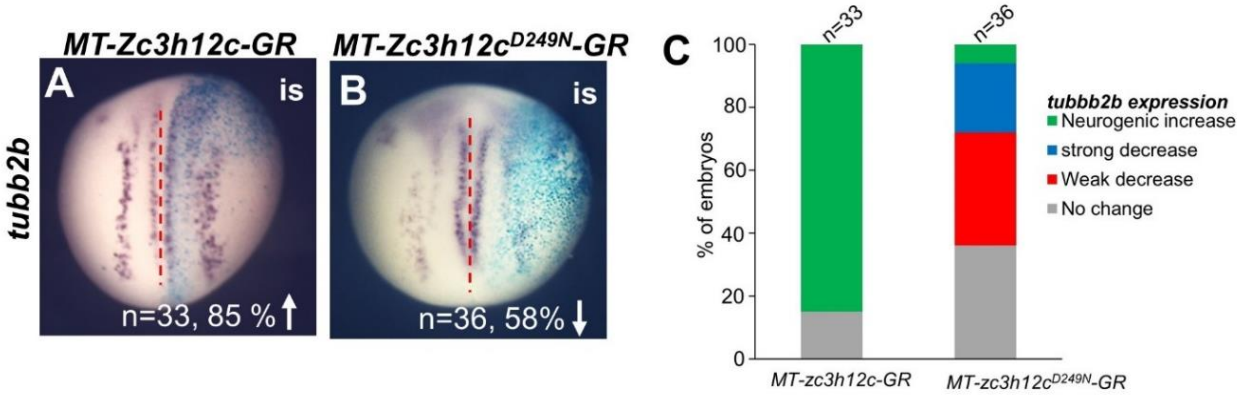

Figure 3.11 Zc3h12c constructs produce strong phenotype at low concentration.

WMISH against *tubb2b* in stage 14 embryos with unilateral overexpression of MT-Zc3h12c-GR (**A**) and MT-Zc3h12c^{D249N}-GR (**B**). (**C**) Column graph showing the percentage of injected embryos with various *tubb2b* expression phenotypes. is: injected side of embryo; n: total number of embryos; up and down pointing white arrows represent an increase and a decrease in *tubb2b* expression respectively. Red dashed line indicates the midline.

3.5 The CRISPR/Cas9/gRNA system effectively introduces mutations in *zc3h12c* in embryos

The Zc3h12c gain of function revealed its involvement in neuronal differentiation. To determine if *zc3h12c* has an essential role during neurogenesis, a loss of function approach using the CRISPR/Cas9 system was employed (Blitz *et al*., 2013; Wang *et al*., 2015). A single guide RNA (gRNA) was designed to target a region near the N-terminus of both *zc3h12c* homeologs (Fig. 3.12A). To evaluate the effect of the CRISPR/Cas9 system on the *zc3h12c* gene, the Cas9 protein (1 ng) was injected together with the *zc3h12c* gRNA (300 pg) and *MT-GFP* mRNA (100 pg) animally at the

one cell stage. Single injection of the Cas9 protein and the *zc3h12c* gRNA, as well as uninjected embryos, served as controls. At stage 14, GFP-positive embryos were individually collected, genomic extraction performed and a region of *zc3h12c* encompassing the target area PCR-amplified.

Fragment analysis of the crude PCR reaction revealed a single sharp peak for the control embryos (control uninjected embryos, Cas9 alone or zc3h12c gRNA alone). In *X. laevis*, injection of Cas9/gRNA, even at the one-cell stage, results in mosaic F0 indels (Aslan *et al.*, 2017). Correspondingly, the Cas9 protein and *zc3h12c* gRNA-injected samples exhibited a broad peak around 375 bp, as well as several flanking peaks indicating the formation of multiple distinct indels. (Fig. 3.12B). Applying the Direct Sequencing of PCR amplicon method (DSP assay) (Nakayama *et al*., 2013) to the purified PCR products, showed that the amplicons of the controls (uninjected embryo, Cas9 alone and *zc3h12c* alone gRNA-injected samples) were unmodified, while that of the Cas9/*zc3h12c* gRNA-injected embryo presented with a mixture of base-calling peaks in the area targeted by *zc3h12c* gRNA (Fig. 3.12C).

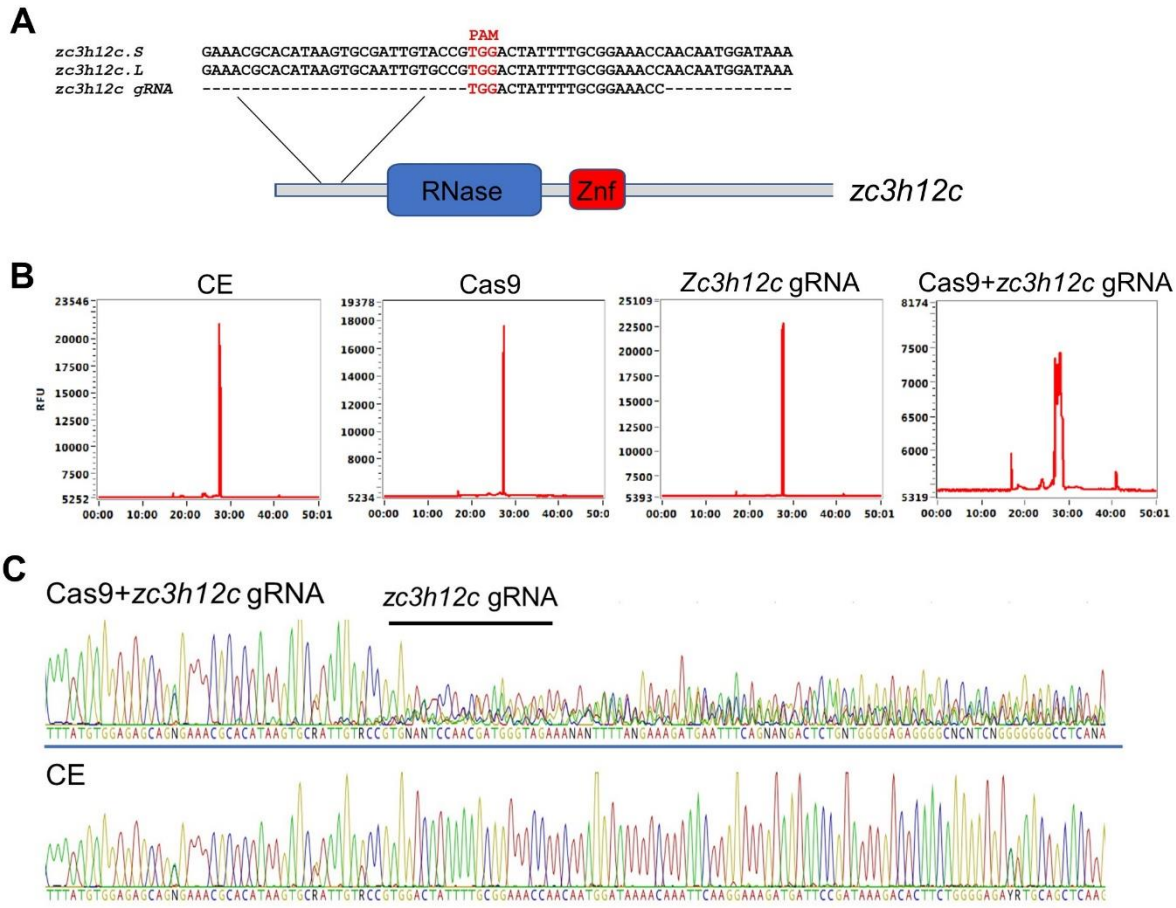

Figure 3.12 CRISPR/Cas9 system introduces mosaic mutation in *zc3h12c*.

(A) Schematic diagram of *zc3h12c* showing the target region of the designed gRNA. **(B)** Fragment analysis of crude PCR product showing representative results for two individual embryos each of the controls (uninjected embryo, Cas9, and *zc3h12c* gRNA-injected samples) and five embryos for Cas9 and *zc3h12c* gRNA-injected embryos **(C)** DSP assay shows representative results of all control samples (n=6) and Cas9/*zc3h12c* gRNA-injected samples (n=5).

To identify the specific mutation(s) introduced into *zc3h12c*, the purified PCR amplicon from one uninjected control embryo and two Cas9/*zc3h12c* gRNA-injected embryos were further subcloned and individual clones subjected to sequencing. The sequencing results revealed that the CRISPR/Cas9 system effectively introduced diverse (mosaic) mutations in both homeologs of *zc3h12c* (Fig. 3.13). Of the total number of clones sequenced (n=22), 59% (n=13) were from *zc3h12c.L* and 41% (n=9) from *zc3h12c.S*. 85% (11/13) of the indels in *zc3h12c.L* were not in multiples of three and would be expected to result in frameshift mutations. Out of the nine *zc3h12c.S* sequences, 44% could also result in frameshift mutation. In summary, 73% of the 22

samples sequenced could result in frameshift mutations suggesting that the Cas9/gRNA may be used to knockdown Zc3h12c function.

Figure 3.13 Specific mutations induced by the CRISPR/Cas9 system in *zc3h12c*.

Sequence alignment of individual clones (n=22) from a representative sequenced Cas9/zc3h12c gRNA-injected embryo (n=2) shows mosaic F0 indels. Red coloured fonts show the target site of the gRNA in *zc3h12c*. Dash lines indicate deletions whereas blue fonts represent insertions. The number of times each phenotype (wildtype, deletion, insertion) was present is indicated at the right side. ***** shows discontinuous sequence.

Reproducing the experiment in the 2-cell stage embryo (injection into both blastomeres) also revealed by the DPS assay, unmodified *zc3h12c* in control samples and a mixture of base-calling peaks in the targeted sequence in Cas9 and *zc3h12c* gRNA-injected embryo (data not shown). This suggests that the injection of Cas9 together with *zc3h12c* gRNA in 2-cell stage embryos would produce mosaic frameshift mutations in *zc3h12c* and can be used to evaluate the effect of Zc3h12c loss of function by WMISH with the uninjected side being a control.

The effect on neurogenesis of the CRISPR/Cas9 knockdown of *zc3h12c* was therefore

analyzed in stage 15 embryos by WMISH against *tubb2b*. Cas9 protein (1 ng) together with *zc3h12c* gRNA (300 pg) was injected into one blastomere of the 2-cell stage embryo. Embryos injected only with Cas9 protein, *zc3h12c* gRNA or *lacZ* mRNA served as controls. Embryos were cultivated until the stage 15 and analyzed by WMISH. The results indicate that the Cas9/gRNA-mediated knockdown of Zc3h12c had no influence on neuronal differentiation, as there was no difference in *tubb2b* expression on the injected side compared to the uninjected side (Fig. 3.14A). Additionally, there was no change in *tubb2b* expression between the controls and the crispants (Fig. 3.14A and B). This result suggest that the mosaic mutations produced by the Cas9/*zc3h12c* gRNA knockdown was not penetrant enough to produce a phenotype.

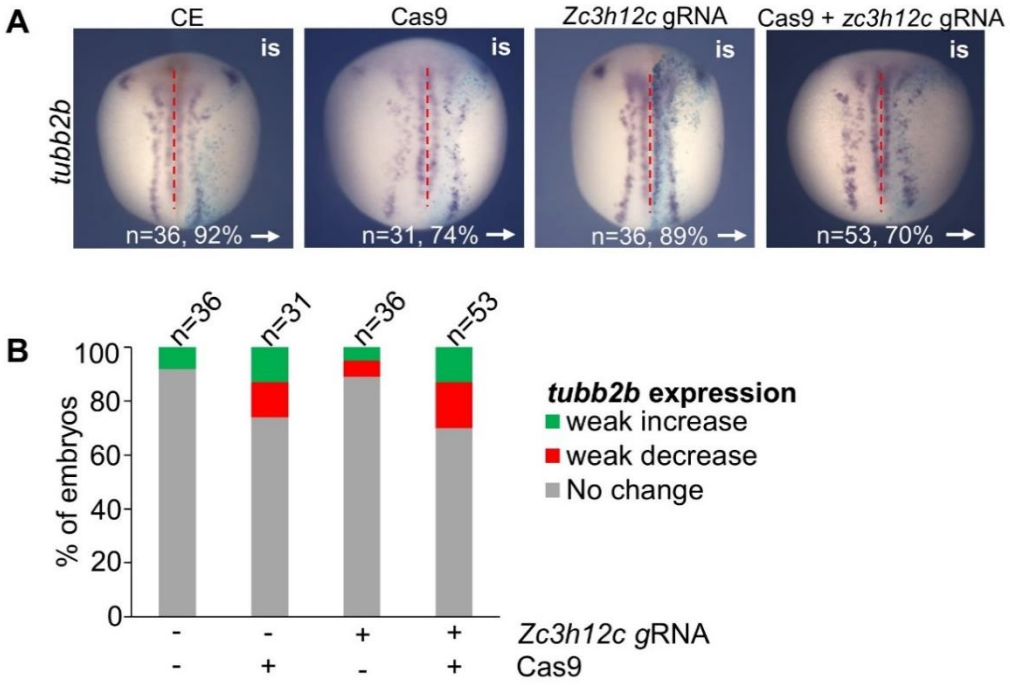

Figure 3.14 Mosaic CPISPR/Cas9 mutations do not provide penetrant loss of Zc3h12c function phenotypic in embryos.

(A) WMISH of stage 15 uninjected embryos or embryos with unilateral expression of the indicated CRISPR component(s). Right pointing arrow indicates no change in *tubb2b* expression and n represents the total number of embryos injected. The number of embryos showing the exhibited phenotype are shown as a percentage of the total number of embryos injected. Red dashed line shows the midline; 'is' represent the injected side of the embryo (**B**) Statistical presentation of WMISH results.

3.6 Zc3h12c is required for neuronal differentiation

Due to the lack of a penetrant phenotype of the CRISPR/Cas9 system in the embryo, which may be due to the mosaicism in F0 embryos, gene knockdown with antisense morpholino oligonucleotides (MO) was alternatively used to study the loss of function effect of Zc3h12c on neurogenesis. Morpholinos are nucleotides with modified backbone that bind to short sequences of pre-mRNAs or mRNAs and alter their splicing or block translation (Summerton & Weller, 1997). Due to the tetraploid nature of the *X. laevis* genome, two morpholino oligonucleotides, against the *zc3h12c* homeologs *zc3h12c.L* and *zc3h12c.S* were designed to bind the junction between the second exon and intron (Fig. 3.15A).

To test the functionality of each morpholino, the *zc3h12c.L*-MO or the *zc3h12c.S*-MO (10 ng) were bilaterally injected at the 2-cell stage together with *GFP* mRNA (100 pg), which insured the collection of injected embryos. *GFP* mRNA alone-injected embryos served as a control. At gastrula stage (stage 14), four GFP-positive embryos were collected per condition and total RNA isolated. Semiquantitative RT-PCR was performed using primers spanning the region of interest and the PCR amplicon subjected to fragment analysis.

The gel image from the fragment analysis revealed a slightly larger product size for the MO-injected amplicons (Fig. 3.15B). The amplicons were further subcloned and individual colonies subjected to sequencing. Alignment of the sequenced products with the *X. laevis* genome revealed altered splicing of *zc3h12c* in sequences derived from both *zc3h12c.L*-MO (68%, n=22) and *Zc3h12c.S*-MO (35%, n=26)-injected embryo compared to the uninjected control (100% correctly spliced, n=21) (Fig. 3.15C and D). Both MOs resulted in the partial retention of the second intron. Varying lengths of intron retention were observed (27-552 nt), but all resulted in the introduction of a stop codon

in the *zc3h12c* transcript at the beginning of the RNase domain (Fig. 3.15C and D). Shown in Figure 3.15C is the sequence of the 27-nt intron retention. Additionally, both MOs altered the splicing of both *zc3h12c.L* and *zc3h12c.S* (Fig. 3.15D) indicating cross-reactivity of the MOs as both differed in only three nucleotides (Fig. 3.15A). Thus, the injection of either MO should be able to induce a knockdown of Zc3h12c in the early *X. laevis* embryo.

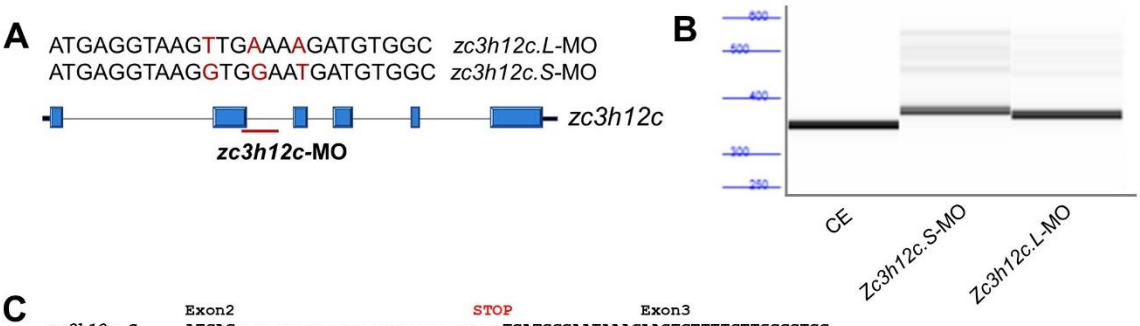

C

```
                Exon2                       STOP            Exon3
zc3h12c.S       ATGAG--------------------------TCATGGCAATAAAGAAGTCTTTTCTTGCCGTGG
zc3h12c.L       ATGAG--------------------------TCATGGGAATAAAGAAGTCTTTTCTTGCCGTGG

CE              ATGAG--------------------------TCATGGCAATAAAGAAGTCTTTTCTTGCCGTGG spliced (zc3h12c.S)
Zc3h12c.L-MO    ATGAGGTAAGTTGAAAAGATGTGGCATCTCATTCATGGGAATAAAGAAGTCTTTTCTTGCCGTGG 27 nt insert (zc3h12c.L)
Zc3h12c.S-MO    ATGAGGTAAGTTGAAAAGATGTGGCATCTCATTCATGGCAATAAAGAAGTCTTTTCTTGCCGTGG 27 nt insert (zc3h12c.L)
```

D

Experiment/Injection	Total sequences	Type and number of sequences with particular phenotype			
		Correctly spliced		Intron retention	
		Zc3h12c.L	*Zc3h12c.S*	*Zc3h12c.L*	*Zc3h12c.S*
CE	21	10	11	-	-
***Zc3h12c.L*-MO**	22	2	5	13 (27 nt)	1(67 nt) 1(156 nt)
***Zc3h12c.S*-MO**	26	7	10	6 (27 nt)	1 (140) 1 (551) 1 (552 nt)

Figure 3.15 *Zc3h12c*-MOs altered splicing of the *zc3h12c* gene.

(**A**) Sequence of the morpholinos designed to knockdown Zc3h12c. Nucleotides differing between the *zc3h12c* homeolog MOs are indicated in red. The *zc3h12c*-MOs bind the boundary between the second exon and second intron. (**B**) Gel image of PCR amplicons from control and *zc3h12c*-MO-injected stage 14 embryos subjected to fragment analysis. (**C**) Alignment of selected sequenced products with *zc3h12c* shows retention of the second intron (yellow) and the introduction of a stop codon (red). (**D**) Summarized data of the sequencing results.

The *zc3h12c.L*-MO or *zc3h12c.S*-MO (10 ng) was injected into one animal blastomere of 2-cell stage embryos together with *lacZ* mRNA (75 pg). A standard control morpholino (Moulton, 2006) (Co-MO, 10 ng) that targets the human β-globin and has no known target in the *X. laevis* genome was injected as control. WMISH was performed on open neural plate stage 14 embryos against the pan-neuronal marker *tubb2b*. The knockdown of Zc3h12c in the embryos by both MOs inhibited the expression of *tubb2b* (*zc3h12c.L*-MO: 100%; *zc3h12c.S*-MO: 100%) (Fig. 3.16A). To evaluate if the inhibition of the neuronal marker was due to the loss of neural progenitor cells, the expression of *sox2* was evaluated. As shown in Fig. 3.16A, knockdown of Zc3h12c had no influence on *sox2* expression (*zc3h12c.L*-MO: 93%; *zc3h12c.L*-MO: 92%) (Fig. 3.16A). The Co-MO did not influence the expression of either *tubb2b* or *sox2* demonstrating specificity of the *zc3h12c*-MOs (Fig. 3.16A). These findings indicate that Zc3h12c is essential for neuronal differentiation and suggest a role for Zc3h12c downstream of Neurog2 after generation of the neural progenitor cells.

To confirm that the loss of neurons in the Zc3h12c morphant embryos was due to the knockdown of Zc3h12c, a rescue experiment was performed. The *zc3h12c.S*-MO (10 ng) was injected alone or in combination with *MT-zc3h12c*-GR mRNA (300 pg) together with *lacZ* mRNA (75 pg) animally into one blastomere of the two-cell stage embryo. The injection of *lacZ* mRNA (75 pg) alone or together with *MT-zc3h12c*-GR mRNA (300 pg) served as controls. All embryos were treated with Dex at stage 10.5 to induce Zc3h12c activity and were collected at stage 14 for WMISH against *tubb2b*. The co-expression of the wildtype Zc3h12c partially rescued the loss of differentiated neurons caused by the knockdown of *zc3h12c* by the *zc3h12c.S*-MO (Fig. 3.16B and C), suggesting that the loss of Zc3h12c activity could at least partly account for the loss of neurons in Zc3h12c morphant embryos.

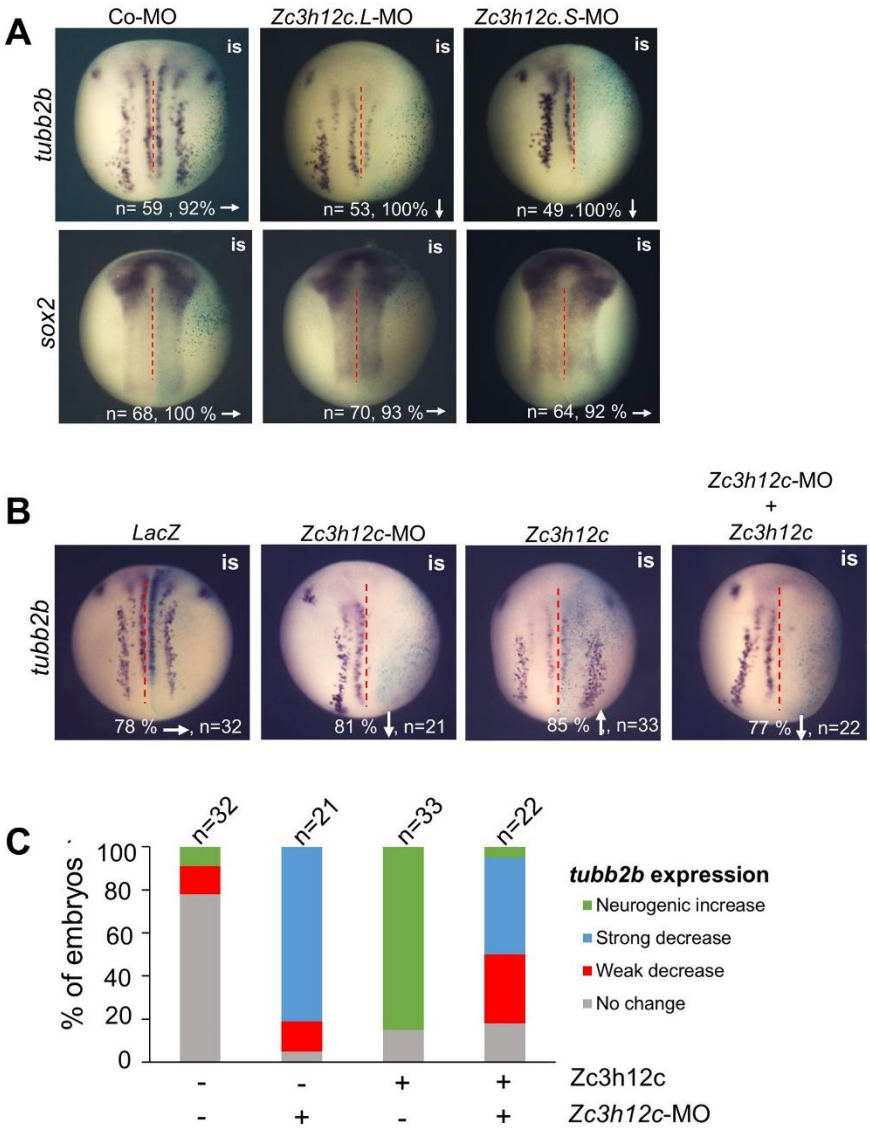

Figure 3.16 Zc3h12c is essential for neuronal differentiation.

(**A**) WMISH analysis of stage 14 embryos injected with the indicated MOs. (**B-C**) Rescue experiment. Up, down and right pointing arrows indicate an increase, a decrease or no change respectively in the expression of indicated marker on the injected compared to uninjected side. Red dashed line indicates the midline. is represent the injected sides of the embryo.

3.7 Knockdown of Zc3h12c markedly inhibits Neurog2-induced neuronal differentiation

Since this study has confirmed the regulation of *zc3h12c* by Neurog2, we further examined the effect of Zc3h12c knockdown on Neurog2-induced neuronal differentiation. *Neurog2* mRNA (20 pg) in the presence or absence of the *zc3h12c.S*-MO (10 ng) as well as the MO alone, was injected animally into one blastomere of the 2-cell stage embryo. At stage 14, embryos were collected for analysis by WMISH against *tubb2b*. Consistent with previous results, Neurog2 and the *zc3h12c.S*-MO strongly induced and inhibited, respectively, *tubb2b* expression. Moreover, the *zc3h12c.S*-MO strongly reduced the induction of *tubb2b* expression by Neurog2 (Fig. 3.17A and B). These results further support the requirement of Zc3h12c during neuronal differentiation and together with the upregulation of *zc3h12c* by Neurog2, suggest that Zc3h12c has an essential function downstream of Neurog2.

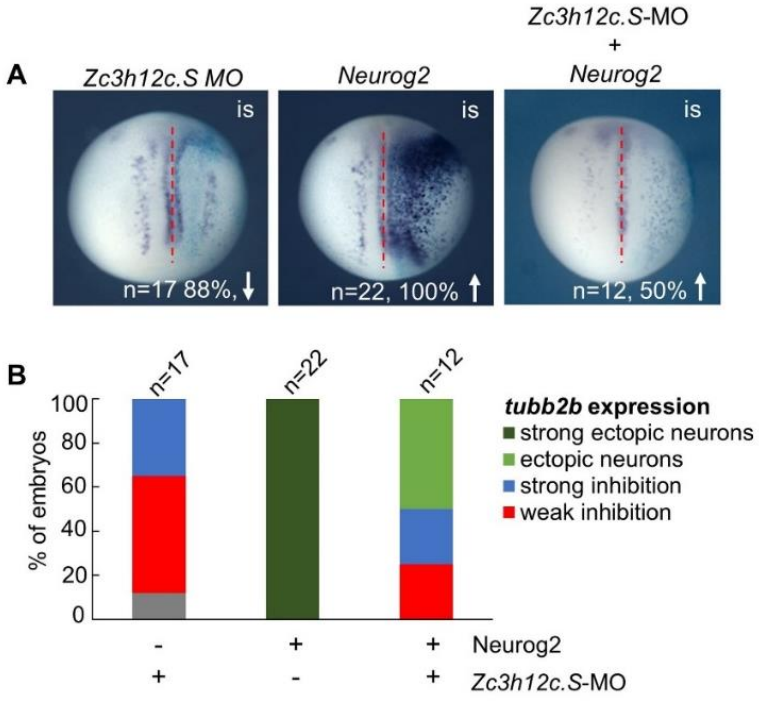

Figure 3.17 Zc3h12c is essential for Neurog2-induced neuronal differentiation.

(A-B) WMISH against *tubb2b* in St.14 embryos with unilateral overexpression of Neurog2 and/or *zc3h12c*-MO as indicated. Embryos injected with the *zc3h12c*-MO or *neurog2* alone served as controls. *LacZ* mRNA was co-injected as tracer. Up and down pointing arrows indicate an increase and a decrease respectively in the expression of indicated marker on the injected compared to uninjected side. Red dashed lines indicate the midline, is represents the injected side of the embryo.

3.8 Transcriptome analysis of *zc3h12c* morphant Neurog2-neuronalized animal caps

The observation that the RNase-deficient mutant Zc3h12c^{D249N} inhibits neurogenesis, while the wild-type Zc3h12c but not the mutant promotes neurogenesis, suggests that the loss of Zc3h12c function during neurogenesis is dependent on its RNase activity. Therefore, the inhibition of neurons by Zc3h12c knockdown could be due to an increase in the activity of a negative regulator whose mRNA would under normal circumstances be degraded by Zc3h12c. Moreover, to gain further insight into the essential role of Zc3h12c during neurogenesis it is of interest to determine the genes influenced by Zc3h12c knockdown. A Zc3h12c knockdown approach coupled with RNAseq analysis was performed to address these aims.

To restrict the analysis to neuronal-related transcriptional changes, animal caps (ACs), which are pluripotent embryonic cells derived from blastula stage ectoderm, were directed to undergo neuronal differentiation using a hormone-inducible Neurog2 (Fig. 3.18A). ACs were injected with *neurog2-GR* mRNA (20 pg) together with the *zc3h12c.S*-MO or a Co-MO (10 ng). At the equivalent of stage 10.5, which is slightly after the onset of zygotic *zc3h12c* expression, the activity of Neurog2 was induced by the addition of dexamethasone. At the equivalent of open neural plate stage (stage 14), total RNA was isolated and first analyzed by semi-quantitative RT-PCR. Uninjected ACs treated with Dex served as a control. Consistent with previous WMISH analysis in the embryo, the *zc3h12c.S*-MO, but not the Co-MO, markedly inhibited Neurog2-induced induction of the neuronal differentiation marker *tubb2b* (Fig. 3.18B).

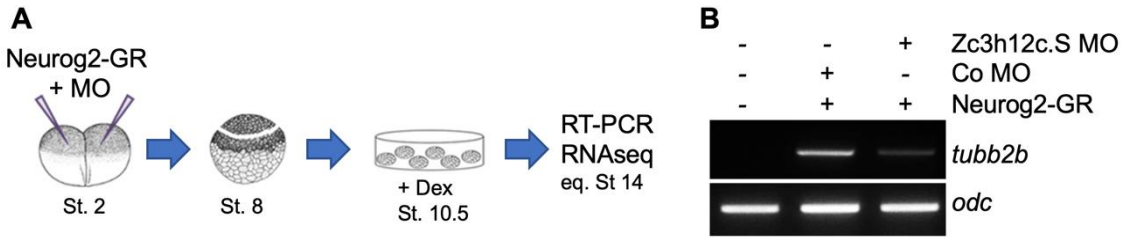

Figure 3.18 Transcriptome analysis of *zc3h12c* morphant neuronalized animal caps.

(A) Scheme of experimental approach. **(B)** RT-PCR results showing *tubb2b* expression in *zc3h12c*-MO-injected neuronalized caps in comparison with their Co MO-injected counterparts.

This experiment was then analyzed by RNAseq analysis with the aims of allowing the unbiased characterization of early Neurog2 downstream genes and the elucidation of those genes whose expression are dependent on the presence of Zc3h12c. Moreover, transcripts that are upregulated by the *zc3h12c.S*-MO are putative target RNAs, which would have otherwise been degraded.

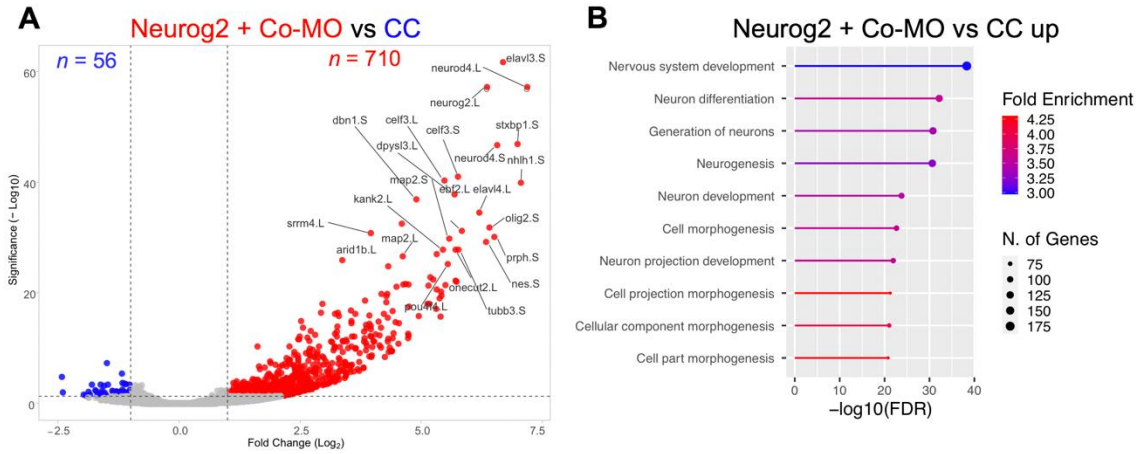

Figure 3.19 Neurog2-Co-MO directed neuronal differentiation in ACs.

(A) Volcano plot of gene expression of control and *neurog2-GR* injected ACs. Differentially expressed genes (DEGs) with an adjusted p-value of <0.05 and a log2 fold--change ≥ 1 are indicated in red (Neurog2-upregulated) and blue (Neurog2-down regulated). Volcano plots were created using VolcaNoseR (https://huygens.science.uva.nl/VolcaNoseR/) (Goedhart & Luijsterburg 2020). **(B)** Gene ontology analysis `plots depicting the most significant terms of Neurog2-upregulated DEGs. Gene ontology enrichment analysis plots were created using ShinyGo v0.75 (http://bioinformatics.sdstate.edu/go/) (Ge *et al*., 2020).

Three biological replicates were used for the RNAseq analysis and a minimum two-fold change (log2FC1) and a false discovery rate (FDR) of ≤0.05 was used to identify

significant differentially expressed genes (DEGs). A total of 766 DEGs were identified in ACs expressing Neurog2 together with the Co-MO compared to uninjected controls (Fig. 3.19A). The majority of the DEGs were upregulated (710 genes) while only 56 genes were down regulated (Appendix 1 and 2). Gene Ontology (GO) analysis of the upregulated DEGs was performed and the most significant biological processes terms identified are shown in Fig. 3.19B. Consistent with the known proneural activity of Neurog2, the most significantly enriched terms included, nervous system development, neuron differentiation and neuron projection development (Appendix 6.3).

Among the upregulated genes (Fig. 3.20) are those known to be involved the early

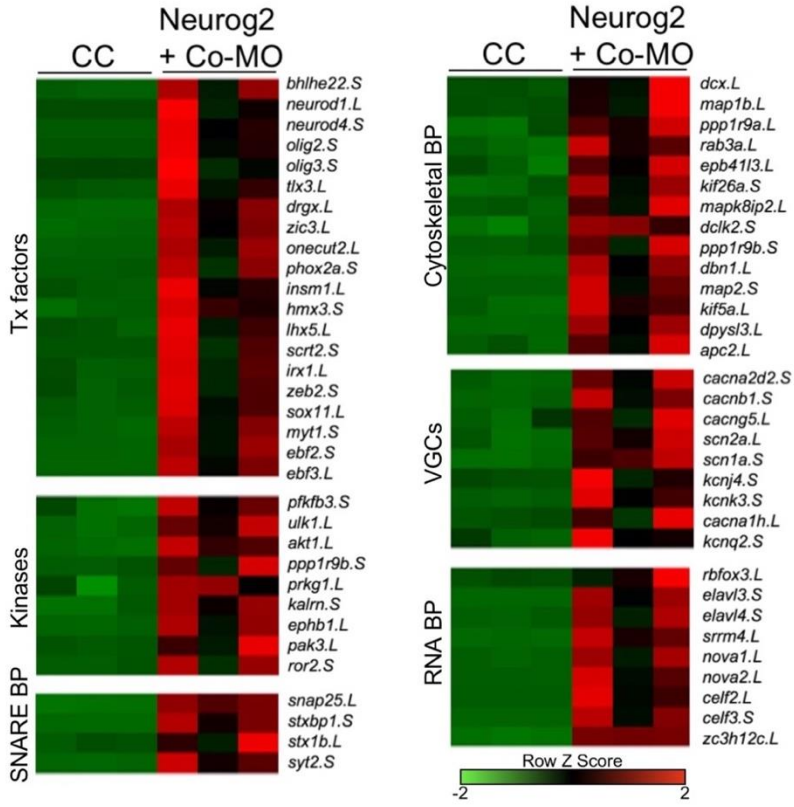

Figure 3.20 Heat map of selected neuronal genes upregulated by Neurog2.

Each column represents a biological replicate. Genes are grouped by their molecular functions. The colour ranging from green to red indicated low to high relative gene expression levels. Heat maps were generated using ShinyGO (http://shinyheatmap.com) (Khomtchouk *et al*., 2017).

events of vertebrate neuronal differentiation, maturation and function including transcription factors (*bhlhe22, neurod1, neurod4, olig2, olig3, tlx3, drgx, zic3, onecut2, phox2a, insm1, hmx3, lhx5, scrt2, irx1, zeb2, sox11, myt1, ebf2, ebf3*), kinases (*pfkfb3, ulk1, akt1, ppp1r9b, prkg1, kalrn, ephb1, pak3, ror2*), snare binding proteins (*snap25, stxbp1, stx1b, syt2*), cytoskeletal binding proteins (*dcx, map1b, ppp1r9a, rab3a, epb41l3, kif26a, mapk8ip2, dclk2, ppp1r9b, dbn1, map2, kif5a, dpysl3, apc2),* and genes involved in voltage gated channel activity (*cacna2d2, cacnb1, cacng5, scn2a, scn1a, kcnj4, kcnq3, cacna1h, kcnq2).* In addition, several mRNA binding proteins were upregulated including *zc3h12c* and known regulators of neurogenesis (*rbfox3, elavl3, elavl4, srrm4, nova1, nova2, celf2, celf3*). The results demonstrate that under the experimental conditions used, the ACs are indeed programmed to undergo neuronal differentiation when expressing Neurog2 together with the Co-MO.

In ACs expressing Neurog2 together with the *zc3h12c.S*-MO, significantly more DEGs were identified than observed in the presence of the Co-MO. In comparison to control caps, a total of 2119 genes were upregulated and 1867 downregulated in Neurog2 together with the *zc3h12c.S*-MO ACs (Fig. 3.21A) (Appendix 6.4 and 5). The top significantly enriched GO biological process terms of the upregulated genes were similar to that observed with the Co-MO and included nervous system development, neurogenesis and neuron projection development (Fig. 3.21B) (Appendix 6.6).

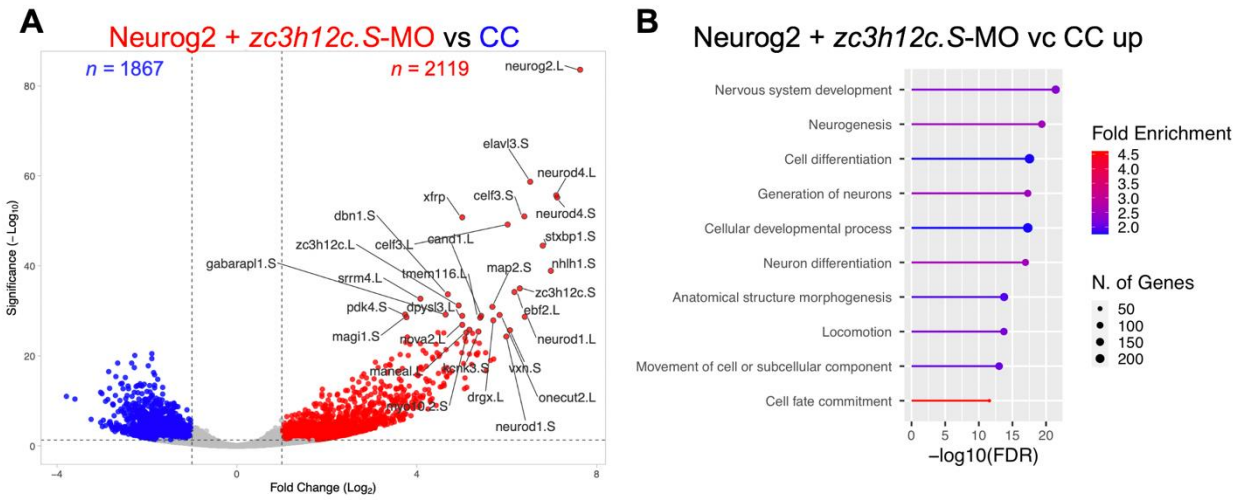

Figure 3.21 Neurog2-zc3h12c-MO differentially expressed genes.

(**A**) Volcano plot comparing gene expression of neurog2-GR mRNA together with Zc3h12c.S-MO injected ACs versus control ACs (CC). Differentially expressed genes (DEGs) with an adjusted p-value of <0.05 and a log2 fold-change ≥ 1. Neurog2/*zc3h12c.S*-MO upregulated DEGs are in red, down regulated DEGs in blue. Volcano plots were created using VolcaNoseR (https://huygens.science.uva.nl/VolcaNoseR/) (Goedhart & Luijsterburg 2020). (**B**) Gene ontology analysis plots depicting the most significant terms of Neurog2/*zc3h12c.S*-MO-upregulated DEGs. Gene ontology enrichment analysis plots were created using ShinyGo v0.75 (http://bioinformatics.sdstate.edu/go/) (Ge *et al*., 2020).

As demonstrated by the semi-quantitative RT-PCR (Fig. 3.18B), neuronal differentiation as assessed by *tubb2b* expression was only inhibited but not abolished, so it is not unexpected that genes involved in the development and function of the nervous system were still significantly enriched. As shown in the Venn diagram (Fig. 3. 22A), the majority of Neurog2/Co-MO-upregulated genes were still upregulated in the presence of the *zc3h12c*-MO. To better evaluate the influence of Zc3h12c knockdown on neuronal differentiation, a direct comparison of Neurog2 expressing ACs injected with the Co-MO or *zc3h12c*-MO was performed. A total of 2227 DEGs were identified in the presence of the *zc3h12c*-MO compared to the control MO, with 1040 genes being down regulated and 1187 genes being upregulated (Fig. 3.22B) (Appendix 6.7 and 8).

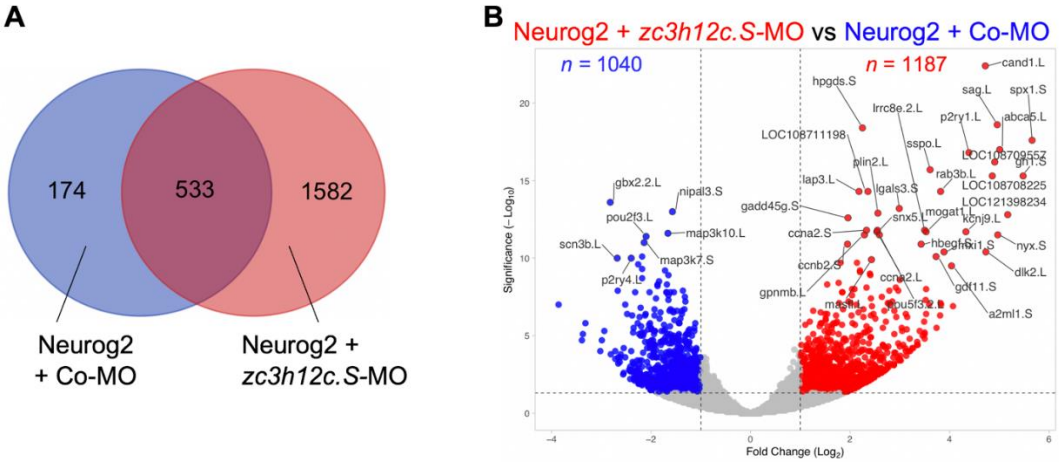

Figure 3.22 Neurog_Co-MO and Neurog2-zc3h12c-MO ACs share several upregulated genes.

(**A**) Venn diagram comparing the upregulated DEGs for Neurog2 together with the Co-MO or the zc3h12c.S-MO compared to control caps. Venn diagrams created http://bioinformatics.psb.ugent.be/webtools/Venn/. (**B**) Volcano plot comparing gene expression of *neurog2-GR* mRNA injected ACs with *zc3h12c.S*-MO injected ACs versus control ACs (CC). Differentially expressed genes (DEGs) with an adjusted p-value of <0.05 and a log2 fold-change ≥ 1. Neurog2/*zc3h12c.S*-MO upregulated DEGs are in red, downregulated DEGs in blue. Volcano plots were created using VolcaNoseR (https://huygens.science.uva.nl/VolcaNoseR/) (Goedhart & Luijsterburg 2020).

3.9 Zc3h12c-dependant Neurog2 downstream genes

To determine which Neurog2 downstream genes were affected by the knockdown of Zc3h12c, we compared the upregulated DEGs from Neurog2/Co-MO compared to control caps with the up and downregulated DEGs from the comparison of Neurog2 together with the *zc3h12c.S*-MO and Neurog2/Co-MO. As shown in the Venn diagram (Fig. 3.23A), only a small subset of Neurog2 downstream genes (78 genes) was significantly altered by the Zc3h12c knockdown. GO analysis demonstrated that they are indeed involved in neuron differentiation and neuron projection development/morphogenesis (Fig. 3.23B) (Appendix 9). Zc3h12c-dependant Neurog2 downstream genes included *tubb2b, ncam1, map1b, amigo1, olig2 and snap25* (Appendix 10). Absent from this category were genes known to be involved in the early events of neuronal differentiation such as *cba2t2, myt1, ebf2*, and *ebf3*. Thirty-seven

Neurog2-downstream genes were actually more robustly activated when Zc3h12c was knocked down including *zc3h12c*, which may be indicative of a negative autoregulation (Appendix 6.10).

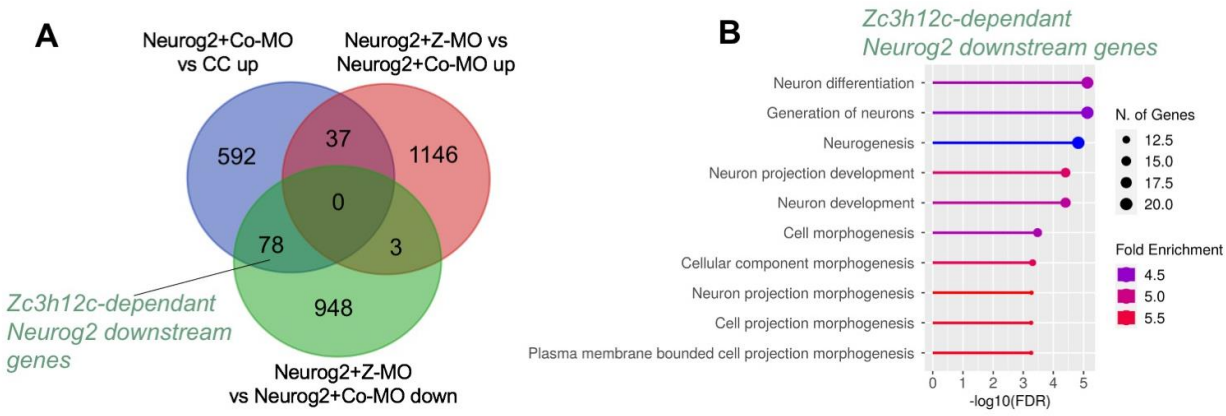

Figure 3.23 Knockdown of Zc3h12c affects only a subset of Neurog-induced downstream genes.

(**A**) Venn diagram comparing the DEGs obtained from RNAseq analysis. DEGs were defined as having an adjusted p-value of <0.05 and a log2 fold-change ≥ 1. Neurog2/Co-MO versus control caps upregulated DEGs are in blue. Neurog2/zch12c.S-MO versus Neurog2/Co-MO upregulated DEGs are in red, downregulated DEGs in green. Venn diagram was created using http://bioinformatics.psb.ugent.be/webtools/Venn/. (**B**) Gene ontology analysis plots depicting the most significant terms of the 78 Zc3h12c-dependant Neurog2 downstream genes. Gene ontology enrichment analysis plots were created using ShinyGo v0.75 (http://bioinformatics.sdstate.edu/go/) (Ge *et al*., 2020).

3.10 Inhibition of Notch signaling does not rescue Zc3h12c knockdown phenotype

We further investigated the genes that are specifically upregulated in the presence of Neurog2 and the *zch312c.S*-MO. Neurog2 activates Notch signaling, which limits the number of neural progenitors that undergo neuronal differentiation via lateral inhibition, thereby giving rise to the characteristic salt and pepper pattern of primary neurogenesis (Chitnis *et al*., 1995; Ma *et al*., 1996). The Hes family of bHLH proteins are intracellular mediators of the Notch pathway and are correspondingly induced by Neurog2 (Wettstein *et al*., 1997). In the RNAseq analysis, several *hes* genes (*hes6.1S, hes5.10L*, *hes5.10S*, *hes5.5L*, *hes5.7L*, *hes5.4L*, *hes5.1L*, *hes5.6L*, *hes5.8L*, *hes5.7S*,

hes5.9L, *hes5.2L*, *hes7.1L*, *hes2.L*, *hes6.2S*) as expected were upregulated by Neurog2 (Fig. 3.24). Interestingly the upregulation of most of the *hes* genes was significantly stronger in the presence of the *zc3h12c.S*-MO.

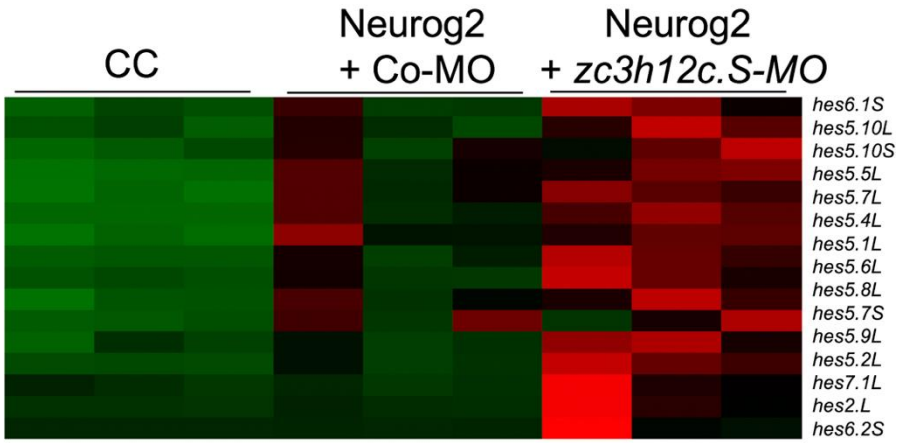

Figure 3.24 Heat map hes genes upregulated by Neurog2 upon Zc3h12c Knockdown.

Each column represents a biological replicate. Genes are grouped by their molecular functions. The colour ranging from green to red indicated low to high relative gene expression levels. Heat maps were generated using ShinyGO (http://shinyheatmap.com) (Khomtchouk *et al*., 2017*).*

As shown in this study, the overexpression of the wildtype Zc3h12c resulted in an increase in differentiated neurons (*tubb2b* expression) within the neurogenic stripes, a phenotype similar to the inhibition of Notch by the DN-Rbpj (Wettstein *et al*., 1997). The overexpression of the Zc3h12c^{D249N} also led to a decrease in differentiated neurons *(tubb2b* expression), similar to the activation of Notch by the NICD (Chitnis *et al*., 1995). An important question therefore arises as to whether Zc3h12c modulates Notch signaling. Is the inhibition of neuronal differentiation by the z*c3h12c.S*-MO or Zc3h12c^{D249N} the result of an increase in Notch signaling and the Zc3h12c-induced increase in neuronal differentiation the result of inhibition of Notch activity?

To answer this question, a possible rescue of the loss of differentiated neurons in Zc3h12c morphant embryos was attempted. The z*c3h12c.S*-MO (10 ng) together with the *DN-rbpj* mRNA (500 pg) was injected into one blastomere of the 2-cell stage

embryos. The injection of z*c3h12c.S*-MO or *DN-rbpj* mRNA alone served as controls. Embryos were collected at stage 14 and the influence on *tubb2b* evaluated by WMISH. If the above assumption that Zc3h12c regulates Notch activity holds true, it would be expected that the inhibition of neurons by the z*c3h12c.S*-MO (increased Notch signaling), would be rescued by the co-expression of the DN-Rbpj (decreased Notch signaling). However, embryos injected with both z*c3h12c.S*-MO and the *DN-rbpj* mRNA presented with a strong inhibition of neurogenesis (total loss of *tubb2b* expression) on the injected side similar to their z*c3h12c.S*-MO-injected counterparts (Fig. 3.25A and B). This finding reveals that the inhibition of neuronal differentiation upon Zc3h12c knockdown is not only due to an increase in Notch signaling.

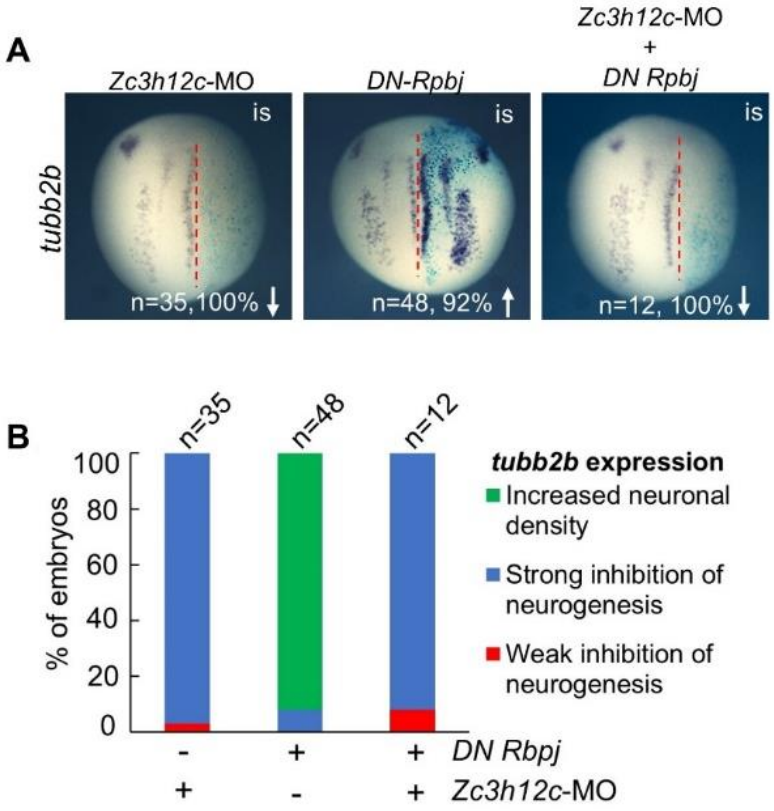

Figure 3.25 Zc3h12c activity is not regulated by Notch signaling.

(**A**) WMISH analysis of an attempted rescue experiment. Dashed red line indicates the midline, is represent the injected side of the embryo. (**B**) Statistical presentation of the percentage of embryos of the different conditions with the indicated tubb2b expression. Up and down pointing arrows indicate an increase and a decrease respectively in the expression of indicated marker on the injected compared to uninjected side.

GO analysis of the 1187 genes upregulated in Neurog2/*zc3h12c.S*-MO compared to Neurog2/Co-MO injected animal caps was performed. As shown in Figure 3.26, the most significantly enriched terms for the upregulated genes were those related to the cell cycle (Appendix 6.11). Among the regulators of cell cycle progression that were upregulated were several of cyclin genes including *ccna2, ccnb1, ccnb1.2, ccnb2, ccnb3, ccne1* and c*cne2*.

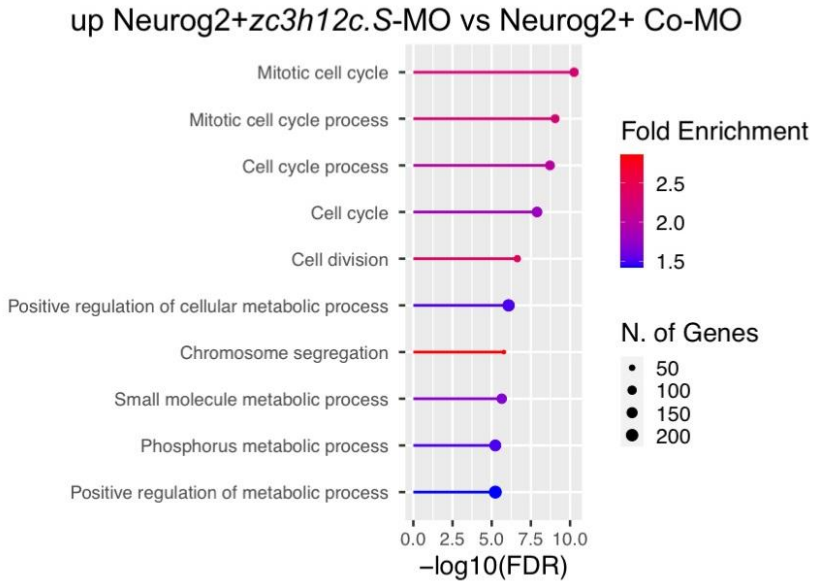

Figure 3.26 Loss of Zc3h12c activity upregulates cell cycle genes in neuronalized ACs.

Gene ontology analysis plots depicting the most significant terms of the upregulated DEGs in animal caps expressing Neurog2/*zc3h12c.S*-MO versus Neurog2/Co-Mo. Gene ontology enrichment analysis plots were created using ShinyGo v0.75 (http://bioinformatics.sdstate.edu/go/) (Ge *et al*., 2020).

As only a subset of Neurog2-induced genes was influenced by Zc3h12c knockdown (Fig. 3.23), a selected number of neuronal genes involved in the early events of vertebrate neuronal differentiation, maturation and function shown in Figure 3.20 together with selected cyclins were further analyzed. A heatmap analysis was performed using hierarchical clustering giving rise to three clusters of DEGs (Fig. 3.27).

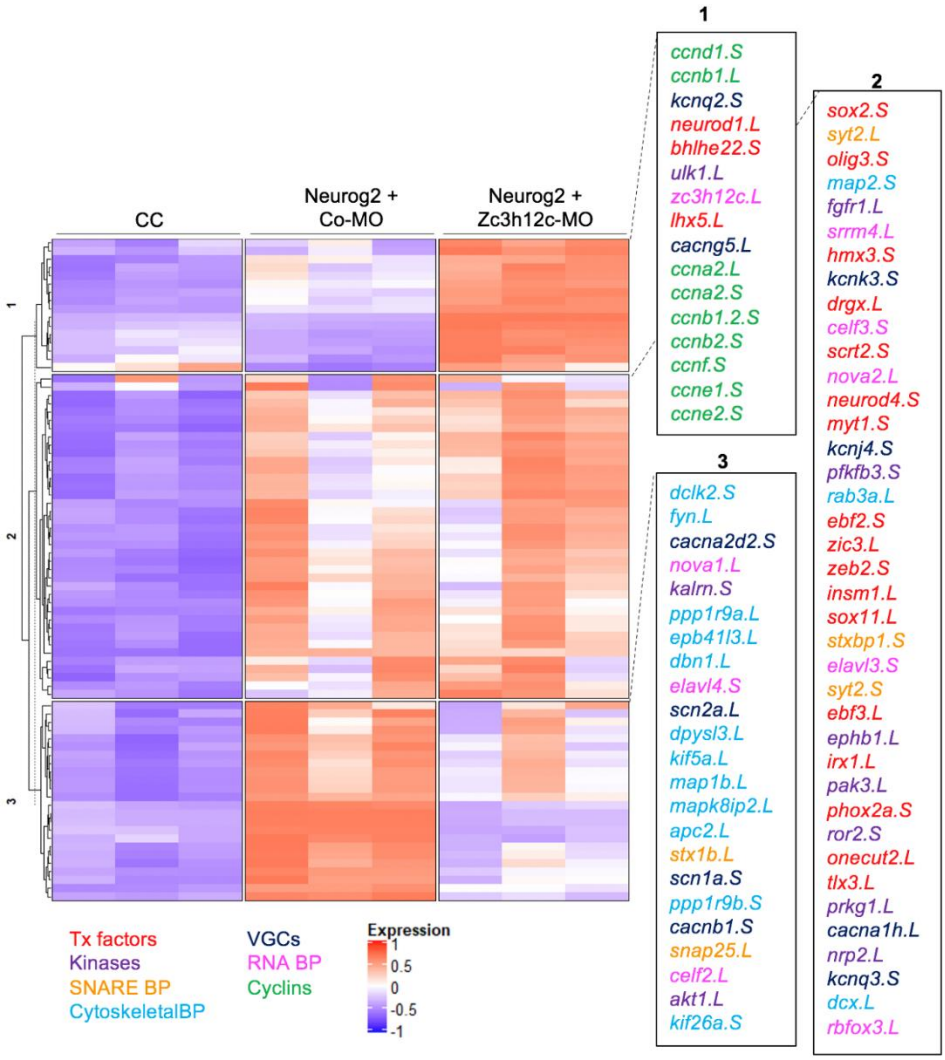

Figure 3.27 Zc3h12c regulates cell cycle exit and terminal differentiation.

(A) Heatmap comparing selected DEGs from the RNAseq analysis. Heatmap was kindly prepared by Dr. S. Richts (Institute für Molekularebiologie, UMG) and was created in R (R Core Team 2020) using the ComplexHeatmap package (Gu *et al.*, 2016). Hierarchical clustering was applied by use of the hclust function using default settings. Normalization was performed for each biological replicate individually to overcome a potential batch effect. Cyclin genes are in green and the genes encoding proteins involved in neuronal differentiation, maturation and function are colored as follows: transcription factors (red), kinases (purple), SNARE binding proteins (orange), cytoskeletal binding proteins (light blue), voltage-gated ion channels (dark blue) and RNA binding proteins (pink).

The first cluster represents genes that were selectively upregulated by Neurog2 in the presence of the *zc3h12c*-MO. This cluster contained all the cyclins analyzed and several early neuronal transcription factors, as well as *zc3h12c.* The second cluster contains DEGs strongly upregulated by Neurog2 in the presence of the CO-MO or the *zc3h12c.S*-MO, thus, their activation by Neurog2 is independent of

Zch12c activity. Included in this cluster were the rest of the analyzed transcription factors and most of the RNA binding proteins. The third cluster contained genes whose induction by Neurog2 was strongly reduced upon Zc3h12c knockdown. These genes include almost all of the cytoskeletal binding proteins evaluated and several SNARE binding proteins and voltage-gated ion channel genes. This analysis strong supports the notion that Zc3h12c acts downstream of Neurog2 to insure late aspects of neuronal differentiation and maturation. Absent Zc3h12c, terminal differentiation may be impaired through the upregulation of the Notch pathway and inhibition of cell cycle exit.

4 Discussion

4.1 Summary

In this thesis, the role of the RNase Zc3h12c as a novel regulator of early neural development in *X. laevis* has been investigated. Zc3h12c is induced by Neurog2 and plays an essential role in neurogenesis downstream of Neurog2. The overexpression of Zc3h12c promotes neuronal differentiation and this activity is dependent on functional RNase activity. The knockdown of Zc3h12c inhibited neuronal differentiation and increased cell cycle regulators including several cyclins. The knockdown of Zc3h12c also led to an increase in Notch target genes suggesting Zc3h12c may inhibit this pathway. As the knockdown phenotype could not be rescued through Notch inhibition, the role of Zc3h12c during neurogenesis may be also related to cell cycle. Zc3h12c localized as granule-like structures in the cytoplasm of ectodermal explants and may be involved in RNA turnover. Since the neurogenic role of Zc3h12c is dependent on its RNase activity, Zc3h12c may regulate neurogenesis by regulating the turnover of transcripts that are positive regulators of cell cycle progression.

4.2 Zc3h12c functions downstream of Neurog2 in the neurogenic cascade

The proneural factor, Neurog2 induces neural differentiation in both *X. laevis* ectodermal explants and embryos (Perron *et al*., 1999; Ma *et al*., 1996). During primary neurogenesis, the activation of Neurog2-induced neuronal program within a progenitor cell activates downstream genes such as *myt1* (Bellefroid *et al*., 1996), *ebf2* (Dubois *et al*., 1998) and *neurod1* (Lee *et al*. 1995) in a cascade of events leading to the terminal differentiation of the cell. Additionally, Neurog2 also activates the expression

of *dll1* (Ma *et al*., 1996) which mediates the lateral inhibitory pathway via Notch signaling and limits neuronal differentiation to a subset of neural progenitors.

In *X. laevis* embryos, the overexpression of Neurog2 results in the ectopic differentiation of both neural and nonneuronal ectodermal cells as shown by the expression of *tubb2b* (Ma *et al*., 1996).

In this study, the overexpression of Neurog2 induced the ectopic expression of *tubb2b* as well as *zc3h12c* in the *X. laevis* embryo. WMISH of staged embryos showed that the expression of *neurog2* transcripts preceded that of z*c3h12c* and *myt1,* both of which also preceded the neuronal marker *tubb2b.* The expression of *neurog2*, *zc3h12c* and *myt1* anticipated the formation of primary neurons in a spatiotemporal manner. Both the induction of *zc3h12c* by Neurog2 as well as its temporal and spatial expression patterns are therefore consistent with a neurogenic role. Within the neural tube, *neurog2* expression was found in the highly mitotic cells of the ventricular zone, while *zc3h12c*, similar to *myt1*, was restricted to the intermediate zone, where cells are undergoing differentiation. *Tubb2b* in contrast, was expressed in the outer differentiated layer. As the different domains of expression correlate with the progression of differentiation (Bellefroid *et al*., 1996), the presence of *zc3h12c* transcripts in the intermediate zone shows that Zc3h12c acts downstream of Neurog2 in the cascade of events leading to differentiation similar to Myt1 (Bellefroid *et al*., 1996). In collaboration with the Tuoc group, we could show that in the E12.5 mouse, ZC3H12C was high in the differentiating neurons of the cortical intermediate zone suggesting a conserved function downstream of the proneural factors.

4.3 Zc3h12c localizes to cytoplasmic granules

Zc3h12c belongs to the Zc3h12 family characterized structurally by the presence of an RNase domain and a CCCH zinc finger domain. Members of the Zc3h12 family have been shown to modulate inflammation by regulating the expression of transcripts of pro-inflammatory cytokines in an RNase-dependent fashion (Fu & Blackshear, 2017).

As the environment within which a protein operates provide cues of protein function, we determined the subcellular localization of Zc3h12c. Zc3h12c-GFP localized as distinct granule-like structures in the cytoplasm. Whereas this pattern of Zc3h12c localization agrees with the study in murine macrophages by von Gamm *et al.* (2019), it contrasts with the findings of Wawro *et al.* (2021) in U251-MG cells, which found a diffused cytoplasmic localization of Zc3h12c. In the murine macrophages, Zc3h12c showed an endosomal localization by localizing partially with the autophagosome marker LC3B and completely with endocytosed Dextran Texas Red conjugates, showing a localization to phagosomes (von Gamm *et al*., 2019). Zc3h12c also colocalized with the early endosomal marker Rab7 and Rab 11 (von Gamm *et al*., 2019).

Zc3h12a, Zc3h12b and Zc3h12d have all been reported to show cytoplasmic granule-like localization (Wawro *et al*., 2019; Suzuki *et al.,* 2011; Mino *et al.,* 2015; von Gamm *et al*., 2019; Huang *et al*., 2015). Zc3h12a has been shown to localize to the endoplasmic reticulum (Mino *et al.,* 2015) and GW-bodies (Huang *et al*., 2015; Suzuki *et al.,* 2011). Zc3h12a, co-localized with Calnexin, a type I membrane protein of the endoplasmic reticulum (ER) in NIH 3T3 cells, but not with disulfide isomerase (PDI), a protein found within the ER (Mino *et al.,* 2015). Zc3h12a partly co-localised to GW182 or Dcp1a, with a higher colocalization frequency for GW182 (Suzuki *et al*., 2011) and colocalized with Zc3h12d in GW182 and Argonaute 2 (Ago2) (Huang *et al*., 2015).

Mino *et al.* (2015) found that Zc3h12a bind translationally active mRNAs and degrade them with the help of the helicase UPF1, similar to nonsense-mediated mRNA decay. The localization of Zc3h12a to the endoplasmic reticulum suggests an association with the mRNA translational machinery and therefore supports this mechanism of Zc3h12a function. GW-bodies are also associated with mRNA turnover (Jakymiw *et al*., 2007) and agree with the function of Zc3h12a in mRNA degradation. The phagocytic localization of Zc3h12c in murine and the endoplasmic reticulum or GW-body localization of Zc3h12a are all supportive of a role for Zc3h12c members in RNA degradation.

It has been reported that CCCH zinc finger proteins shuttle between different cellular compartments (nucleus to cytoplasm), and RNA compartments (polysomes, stress granules and P-bodies) in their function in RNA metabolism (Fu & Blackshear, 2017). Both TTP and Roquin, known CCCH zinc finger domain proteins with functions in the regulation of inflammation, localize to both SGs and PBs under different conditions (Fu & Blackshear, 2017). Zc3h12 members may also exhibit context specific localization depending on the different cellular conditions. For instance, Zc3h12d has been reported to show a context-dependent localization in peripheral blood mononuclear cells derived from mice (Tomita *et al.*, 2021). In mice without tumors, Zc3h12d localized to the cell surface in contrast to an intracellular localization in mice with tumors.

4.4 Zc3h12c is essential for neurogenesis.

In *X. laevis*, primary neurogenesis produces scattered neurons that become organised in three longitudinal domains, medial, intermediate and lateral on either side of the dorsal midline (Hartenstein, 1989; Chitnis *et al.,* 1995). Through loss and gain of function approaches, a positive regulation of Zc3h12c on neuronal differentiation was

established. Overexpression of a wildtype Zc3h12c in *X. laevis* embryos resulted in an increase in post-mitotic neurons within the open neural plate neurogenic stripes, while an RNase deficient mutant inhibited neurogenesis. Zc3h12 members contain four aspartic acid residues in their PIN domain that chelates Mg^{2+}. Mutating a single aspartic acid residue is sufficient to abolish RNase activity (Matsushita *et al.,* 2009; Wawro *et al.,* 2017). Therefore, the inhibition of differentiation by the RNase deficient Zc3h12c mutant suggests the neurogenic activity of Zc3h12c is dependent on its RNase activity.

A knockdown of Zc3h12c with a splicing MO similarly inhibited normal neurogenesis in the embryo, as well as Neurog2-induced neuronal differentiation. This reveals an essential role for Zc3h12c in neurogenesis and provides further support that Zc3h12c acts downstream of Neurog2 within the neurogenic cascade. The loss of neuronal differentiation by the *zc3h12c*-MO could be partially rescued by the co-expression of the wildtype Zc3h12c suggesting that the inhibition of Zc3h12c could partly account for the inhibition of neurons. However, the inability to obtain a full rescue may be that an optimal dosage of Zch12c is required.

During primary neurogenesis, the number of neural progenitors within the induced neuroectoderm that undergo differentiation is restricted by the Notch pathway through lateral inhibition (Kageyama *et al*., 2008). Activating Notch signaling, for instance, through the overexpression of a constitutively active NICD decreases neuronal differentiation (Chitnis *et al.,* 1995), while inhibiting Notch by the overexpression of a dominant negative Rbpj increases neuronal differentiation within the territories of primary neurogenesis (Wettstein *et al*., 1997).

The finding that the neurogenic function of Zc3h12c requires RNase activity raises an important question as to which RNAs are targets of Zc3h12c-mediated degradation. The increase in differentiation within the neurogenic stripes by the Zc3h12c gain of function phenotype is similar to when Notch signaling is inhibited (Wettstein *et al*., 1997), while the RNase-deficient mutant phenotype parallels that of an increase in Notch signaling (Chitnis *et al*., 1995). The knockdown of Zc3h12c also strongly inhibited neurogenesis. This raised the intriguing possibility that Zc3h12c may target mRNAs associated with the Notch pathway allowing the neuronally fated cells to escape lateral inhibition and undergo terminal differentiation.

Upon ligand activation, the intracellular domain of the Notch receptor (Notch-ICD) is released and interacts with the DNA binding protein Rbpj allowing activation of target genes including those of the *hes* family (Kageyama *et al*., 2008). The Hes family of bHLH repressor proteins are intracellular effectors of the Notch pathway and act by repressing target gene expression including those involved in neuronal differentiation (Kageyama *et al*., 2008). The transcriptome analysis of Zc3h12c morphant Neurog2-neuronalized animal caps compared to their Co-MO injected counterparts, revealed the upregulation of several *hes* genes indicating an increase in Notch signaling upon Zc3h12c knockdown. It was therefore tested if the *zc3h12c*-MO loss of neuronal differentiation could be rescued through blocking of the Notch pathway by a DNA-binding mutant version of Rbpj (DN-Rbpj), which inhibits Notch-mediated gene induction (Wettstein *et al.,*1997). However, the DN-Rbpj could not rescue the Zc3h12c morphant phenotype suggesting that an increase in Notch signaling does not solely account for the inhibition of neuronal differentiation in the morphant embryos.

4.5 Zc3h12c may influence cell cycle exit during neurogenesis

Differentiation of neuronal progenitor cells is usually linked to terminal mitosis and cell cycle exit (Ohnuma & Harris, 2003). The neurogenic process involves an interplay between proliferation and differentiation, with a reciprocal regulation existing between cell cycle progression and differentiation: regulators of the cell cycle regulate determination and vice versa (Ohnuma & Harris, 2003). In *X. laevis,* factors such as Foxg1 and Rax maintain active cell division through inhibition of the Cip/Kip cyclin-dependent kinase inhibitor. Cdknx inhibits neuronal differentiation in the anterior region of the early neurula embryo (Hardcastle & Papalopulu, 2000). On the contrary, several genes expressed in the regions of primary neurogenesis, such as *cdknx, p21 activated kinase 3 (pak3)* and *gadd45g* support neuronal differentiation by inducing cell cycle arrest (de la Calle-Mustienes *et al*., 2002; Souopgui *et al*., 2002; Vernon *et al*., 2003). In addition to promoting differentiation, Neurog2 also induces *pak3* and *gadd45g*, coupling the process of neurogenesis with cell cycle exit (Souopgui *et al*., 2002; de la Calle-Mustienes *et al.,* 2002).

To gain insight into the molecular mechanism by which Zc3h12c promotes neuronal differentiation, it is important to identify which step of the neurogenic pathway it regulates and the target genes that may be involved. The transcriptome analysis of the Zc3h12c morphant caps induced to undergo differentiation by Neurog2 overexpression reveal that genes involved in the early events of neurogenesis such as *myt1* (Bellefroid *et al*., 1996), *ebf2* (Dubois *et al*., 1998) *dll1* (Ma *et al*., 1996) and *numbl* (Nieber *et al*., 2013) were not altered by the Zc3h12c loss of function. Instead, genes that are involved in late aspects of neuronal differentiation, maturation and function such as *tubb2b* (Chitnis *et al*., 1995), *l1cam* (Linneberg *et al*., 2019), *snap25* (Pozzi *et al*., 2019), *amigo* (Zhao *et al.,* 2014) were decreased. However, the Zc3h12c loss of

function particularly upregulated genes mostly related to the cell cycle including several cyclins such as *ccna2, ccnb1, ccnb1.2, ccnb2, ccnb3, ccne1* and c*cne2*.

Interestingly, the Zc3h12c loss of function also upregulated *zc3h12c* expression, suggesting a possible mechanism of Zc3h12c autoregulation. Indeed, Zc3h12c has been reported to significantly reduced the levels of a reporter gene habouring the 3'UTR of its mRNA, although the degradation efficiency was lower than the extent of degradation achieved by Zc3h12a (Wawro *et al*., 2021). In addition, Zc3h12a is also involved in the self-regulation of its own transcripts in a manner involving its RNase activity (Wawro *et al.,* 2016). Therefore, autoregulation may be a mechanism by which members of the Zc3h12c family regulate the expression of their own transcripts.

The upregulation of cell cycle genes by the Zc3h12c loss of function suggests a positive effect on cell cycle and indicated a possible regulation of the cell cycle by Zc3h12c. Could it be that the knockdown of Zc3h12c releases its inhibitory effects on positive regulators of the cell cycle hence increasing their mRNA stability? If this assumption holds true, then transcripts of such targets will be expected to be downregulated by Neurog2.

It has been reported that in chick embryos, the activation of Neurog2 drives cell cycle exit of neuronal precursors by rapidly repressing indirectly, a subset of cyclins acting at the G1 and S phases of the cell cycle including *ccnd1*, *ccne1/2* and *ccna2* (Lacomme *et al*., 2012). Expectedly, a search through the results of the transcriptome analysis found that the transcripts of *ccnd1*, *ccne1/2* and *ccna2* were downregulated by Neurog2, but increased in the presence of the *zc3h12c*-MO. These results support a potential role for Zc3h12c in the regulation of the cell cycle in the context of neuronal development. Interestingly a high *zc3h12c* expression was associated with a low-risk prognostic signature of colorectal cancer (Li *et al*., 2021). Other members of the

Zc3h12 family have been reported to have inhibitory roles in cell proliferation by inhibiting the cell cycle. The overexpression of Zc3h12a, for instance, inhibited the proliferation of Caki-1 cells through the downregulation of transcripts coding for DDB1 E3 ligase and an increase in both the transcript and protein level of $p21^{Cip1}$ (Lichawska-Cieslar *et al*., 2018). Zc3h12b overexpression also inhibited proliferation by stalling the cell cycle in the G2 phase in an RNase dependent manner (Wawro *et al.,* 2019). Furthermore, the overexpression of Zc3h12d inhibited G1 to S phase progression in a mouse pro-B cell line, Ba/F3, and a human leukemia cell line, Jurkat, by suppressing the phosphorylation of retinoblastoma protein (Minagawa *et al*., 2009).

In this study, the loss of neuronal differentiation by the Zc3h12c knockdown was not due to the loss of neural progenitors. Therefore, it is possible that the inhibition of neuronal differentiation by the knockdown of Zc3h12c is due to the dysregulation of the cell cycle exit of neural progenitor cells in addition to an increase in Notch signaling. The inability of the progenitor cells to exit the cell cycle, prevents their differentiation. Progenitor cells thus induced to undergo differentiation by Neurog2 remain in the cell cycle in the absence of Zc3h12c regulation. This fits well with our finding that Zc3h12c acts downstream of Neurog2 in the neurogenic pathway.

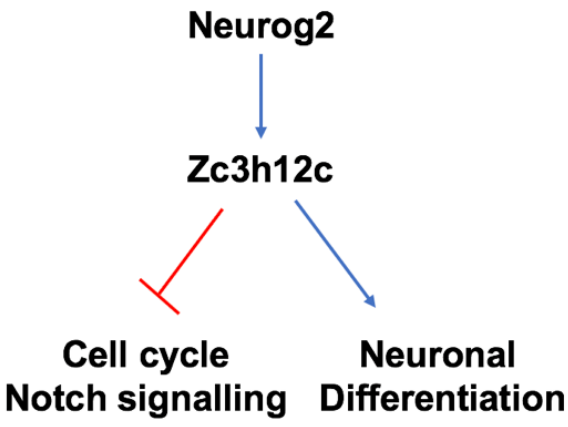

We therefore propose a mechanism whereby Zc3h12c is induced by Neurog2 and promotes neuronal differentiation by inhibiting cyclins (probably *ccnd1*, *ccne1/2* and *ccna2*) in an RNase-dependent manner.

It will therefore be of interest in the future to evaluate the effect on neuronal differentiation of Zc3h12 regulation on the cell cycle as well as to identify direct binding targets of Zc3h12c. This would put in a better context the molecular mechanism by which Zc3h12c functions and may have implications not only in the context of neural development but in diseases such as colorectal cancer in which low *zc3h12c* expression is a poor prognostic indicator (Li *et al.,* 2021).

5 References

Anantharaman, V., & Aravind, L. (2006). The NYN domains: Novel predicted RNAses with a PIN domain-like fold. *RNA Biology*, *3*(1), 18–27. https://doi.org/10.4161/rna.3.1.2548.

Anders, S., & Huber, W. (2010). Differential expression analysis for sequence count data. *Genome Biology*, *11*(10), R106. https://doi.org/10.1186/gb-2010-11-10-r106.

Ankö, M.-L., & Neugebauer, K. M. (2012). RNA-protein interactions in vivo: Global gets specific. *Trends in Biochemical Sciences*, *37*(7), 255–262. https://doi.org/10.1016/j.tibs.2012.02.005.

Andrews, S. (2019). FastQC: A quality control tool for high throughput sequence data. https://www.bioinformatics.babraham.ac.uk/projects/fastqc/.

Aslan, Y., Tadjuidje, E., Zorn, A. M., & Cha, S.-W. (2017). High-efficiency non-mosaic CRISPR-mediated knock-in and indel mutation in F0 Xenopus. *Development*, *144*(15), 2852–2858. https://doi.org/10.1242/dev.152967.

Baker, N. E., & Brown, N. L. (2018). All in the family: Proneural bHLH genes and neuronal diversity. *Development*, *145*(9). https://doi.org/10.1242/dev.159426.

Beatus, P., & Lendahl, U. (1998). Notch and neurogenesis. *Journal of Neuroscience Research*, *54*(2), 125–136. https://doi.org/10.1002/(SICI)1097-4547(19981015)54:2<125:AID-JNR1>3.0.CO;2-G

Behrens, G., Winzen, R., Rehage, N., Dörrie, A., Barsch, M., Hoffmann, A., Hackermüller, J., Tiedje, C., Heissmeyer, V., & Holtmann, H. (2018). A translational silencing function of MCPIP1/Regnase-1 specified by the target site context. *Nucleic Acids Research*, *46*(8), 4256–4270. https://doi.org/10.1093/nar/gky106

Bellefroid, E. J., Kobbe, A., Gruss, P., Pieler, T, Gurdon, J. B., & Papalopulu, N (1998). Xiro3 encodes a Xenopus homolog of the Drosophila Iroquois genes and functions in neural specification. *The EMBO Journal*, *17*(1), 191–203. https://doi.org/10.1093/emboj/17.1.191.

Bellefroid, E. J., Bourguignon, C., Hollemann, T., Ma, Q., Anderson, D. J., Kintner, C., & Pieler, T. (1996). X-MyT1, a Xenopus C2HC-type zinc finger protein with a regulatory function in neuronal differentiation. *Cell*, *87*(7), 1191–1202. https://doi.org/10.1016/s0092-8674(00)81815-2

Bertrand, N., Castro, D. S., & Guillemot, F. (2002). Proneural genes and the specification of neural cell types. *Nature Reviews. Neuroscience*, *3*(7), 517–530. https://doi.org/10.1038/nrn874

Bian, S., & Sun, T. (2011). Functions of noncoding RNAs in neural development and neurological diseases. *Molecular Neurobiology*, *44*(3), 359–373. https://doi.org/10.1007/s12035-011-8211-3

Blitz, I. L., Biesinger, J., Xie, X., & Cho, K. W. Y. (2013). Biallelic genome modification in F0 Xenopus tropicalis embryos using the CRISPR/Cas system. *Genesis (New York, N.Y. 2000)*, *51*(12), 827–834. https://doi.org/10.1002/dvg.22719

Borchers, A., & Pieler, T. (2010). Programming pluripotent precursor cells derived from Xenopus embryos to generate specific tissues and organs. *Genes*, *1*(3), 413–426. https://doi.org/10.3390/genes1030413

Borodinsky, L. N. (2017). Xenopus laevis as a model organism for the study of spinal cord formation, development, function and regeneration. *Frontiers in Neural Circuits*, *11*, 90. https://doi.org/10.3389/fncir.2017.00090

Boy, S., Souopgui, J., Amato, M. A., Wegnez, M., Pieler, T., & Perron, M. (2004). Xseb4r, a novel RNA-binding protein involved in retinal cell differentiation downstream of bHLH proneural genes. *Development*, *131*(4), 851–862. https://doi.org/10.1242/dev.00983

Bray, S. J. (2006). Notch signalling: A simple pathway becomes complex. *Nature Reviews. Molecular Cell Biology*, *7*(9), 678–689. https://doi.org/10.1038/nrm2009.

Brinegar, A. E., & Cooper, T. A. (2016). Roles for RNA-binding proteins in development and disease. *Brain Research*, *1647*, 1–8. https://doi.org/10.1016/j.brainres.2016.02.050

Brümmer, A., Kishore, S., Subasic, D., Hengartner, M., & Zavolan, M. (2013). Modeling the binding specificity of the RNA-binding protein GLD-1 suggests a function of coding region-located sites in translational repression. *RNA*, *19*(10), 1317–1326. https://doi.org/10.1261/rna.037531.112

Cau, E., Gradwohl, G., Casarosa, S., Kageyama, R., & Guillemot, F. (2000). Hes genes regulate sequential stages of neurogenesis in the olfactory epithelium. *Development*, *127*(11), 2323-2332. https://doi.org/10.1242/dev.127.11.2323

Chitnis, A., Henrique, D., Lewis, J., Ish-Horowicz, D., & Kintner, C. (1995). Primary neurogenesis in Xenopus embryos regulated by a homologue of the Drosophila neurogenic gene Delta. *Nature*, *375*(6534), 761–766. https://doi.org/10.1038/375761a0

Chitnis, A., & Kintner, C. (1996). Sensitivity of proneural genes to lateral inhibition affects the pattern of primary neurons in Xenopus embryos. *Development*, *122*(7), 2295–2301. https://doi.org/10.1242/dev.122.7.2295

Cooper, T. A., Wan, L., & Dreyfuss, G. (2009). RNA and disease. *Cell*, *136*(4), 777-793. https://doi.org/10.1016/j.cell.2009.02.011

Dai, W., Li, W., Hoque, M., Li, Z., Tian, B., & Makeyev, E. V. (2015). A post-transcriptional mechanism pacing expression of neural genes with precursor cell differentiation status. *Nature Communications*, *6*, 7576. https://doi.org/10.1038/ncomms8576

DeBoer, E. M., Kraushar, M. L., Hart, R. P., & Rasin, M. R. (2013). Post-transcriptional regulatory elements and spatiotemporal specification of neocortical

stem cells and projection neurons. *Neuroscience*, *248*, 499–528. https://doi.org/10.1016/j.neuroscience.2013.05.042.

de la Calle-Mustienes, E., Glavic, A., Modolell, J., & Gómez-Skarmeta, J. L. (2002). Xiro homeoproteins coordinate cell cycle exit and primary neuron formation by upregulating neuronal-fate repressors and downregulating the cell-cycle inhibitor XGadd45-γ. *Mechanisms of Development*, *119*(1), 69–80. https://doi.org/10.1016/s0925-4773(02)00296-4

Detrick, R., Dickey, D., & Kintner, C. R. (1990). The effects of N-cadherin misexpression on morphogenesis in Xenopus embryos. *Neuron*, *4*(4), 493–506. https://doi.org/10.1016/0896-6273(90)90108-r.

Dichmann, D. S., Fletcher, R. B., & Harland, R. M. (2008). Expression cloning in Xenopus identifies RNA-binding proteins as regulators of embryogenesis and Rbmx as necessary for neural and muscle development. *Developmental Dynamics*, *237*(7), 1755–1766. https://doi.org/10.1002/dvdy.21590.

Dobin, A., Davis, C. A., Schlesinger, F., Drenkow, J., Zaleski, C., Jha, S., Batut, P., Chaisson, M., & Gingeras, T. R. (2013). Star: Ultrafast universal RNA-seq aligner. *Bioinformatics*, *29*(1), 15–21. https://doi.org/10.1093/bioinformatics/bts635.

Doyle, M., & Kiebler, M. A. (2012). A zipcode unzipped. *Genes & Development*, *26*(2), 110–113. https://doi.org/10.1101/gad.184945.111.

Droz, S. T., & McLaughlin, K. A. (2017). Use of Xenopus frogs to study renal development/repair. *Results and Problems in Cell Differentiation*, *60*, 77–107. https://doi.org/10.1007/978-3-319-51436-9_4.

Dubey, A., & Saint-Jeannet, J. P. (2017). Modeling human craniofacial disorders in Xenopus. *Current Pathobiology Reports*, *5*(1), 79–92. https://doi.org/10.1007/s40139-017-0128-8

Dubois, L., Bally-Cuif, L., Crozatier, M., Moreau, J., Paquereau, L., & Vincent, A. (1998). XCoe2, a transcription factor of the Col/Olf-1/EBF family involved in the specification of primary neurons in Xenopus. *Current Biology*, *8*(4), 199–209. https://doi.org/10.1016/S0960-9822(98)70084-3

Exner, C. R. T., & Willsey, H. R. (2021). Xenopus leads the way: Frogs as a pioneering model to understand the human brain. *Genesis*, *59*(1-2), e23405. https://doi.org/10.1002/dvg.23405

Fan, L. W., & Pang, Y. (2017). Dysregulation of neurogenesis by neuroinflammation: Key differences in neurodevelopmental and neurological disorders. *Neural Regeneration Research*, *12*(3), 366–371. https://doi.org/10.4103/1673-5374.202926

Fineran, P. C., & Dy, R. L. (2014). Gene regulation by engineered CRISPR-Cas systems. *Current Opinion in Microbiology*, *18*, 83–89. https://doi.org/10.1016/j.mib.2014.02.007

Fortriede, J. D., Pells, T. J., Chu, S., Chaturvedi, P., Wang, D., Fisher, M. E., James-Zorn, C., Wang, Y., Nenni, M. J., Burns, K. A., Lotay, V. S., Ponferrada, V. G., Karimi, K., Zorn, A. M., & Vize, P. D. (2020). Xenbase: Deep integration of GEO &

SRA RNA-seq and ChIP-seq data in a model organism database. *Nucleic Acids Research*, *48*(D1), D776-D782. https://doi.org/10.1093/nar/gkz933

Fu, M., & Blackshear, P. J. (2017). RNA-binding proteins in immune regulation: A focus on CCCH zinc finger proteins. *Nature Reviews. Immunology*, *17*(2), 130–143. https://doi.org/10.1038/nri.2016.129

Gagnon, J. A., Valen, E., Thyme, S. B., Huang, P., Akhmetova, L., Ahkmetova, L., Pauli, A., Montague, T. G., Zimmerman, S., Richter, C., & Schier, A. F. (2014). Efficient mutagenesis by Cas9 protein-mediated oligonucleotide insertion and large-scale assessment of single-guide RNAs. *PloS One*, *9*(5), e98186. https://doi.org/10.1371/journal.pone.0098186

Gammill, L. S., & Sive, H. (1997). Identification of otx2 target genes and restrictions in ectodermal competence during Xenopus cement gland formation. *Development*, *124*(2), 471–481. https://doi.org/10.1242/dev.124.2.471

Gao, J., Chen, Y., Wu, K. C., Liu, J., Zhao, Y. Q., Pan, Y. L., Du, R., Zheng, G.R., Xiong, Y. M., Xu, H. L., & Fan, D.M. (2010). Runx3 directly interacts with intracellular domain of Notch1 and suppresses Notch signaling in hepatocellular carcinoma cells. *Experimental Cell Research*, *316*(2), 149–157. https://doi.org/10.1016/j.yexcr.2009.09.025

Garg, A. V., Amatya, N., Chen, K., Cruz, J. A., Grover, P., Whibley, N., Conti, H. R., Hernandez Mir, G., Sirakova, T., Childs, E. C., Smithgall, T. E., Biswas, P. S., Kolls, J. K., McGeachy, M. J., Kolattukudy, P. E., & Gaffen, S. L. (2015). MCPIP1 endoribonuclease activity negatively regulates interleukin-17-mediated signaling and inflammation. *Immunity*, *43*(3), 475–487. https://doi.org/10.1016/j.immuni.2015.07.021.

Garg, A., Roske, Y., Yamada, S., Uehata, T., Takeuchi, O., & Udo Heinemann, U. (2021). PIN and CCCH Zn-finger domains coordinate RNA targeting in ZC3H12 family endoribonucleases. *Nucleic Acids Research*, *49*(9), 5369-5381. https://doi.org/10.1093/nar/gkab316

Ge, S. X., Jung, D., & Yao, R. (2020). Shinygo: A graphical gene-set enrichment tool for animals and plants. *Bioinformatics*, *36*(8), 2628–2629. https://doi.org/10.1093/bioinformatics/btz931

Glisovic, T., Bachorik, J. L., Yong, J., & Dreyfuss, G. (2008). RNA-binding proteins and post-transcriptional gene regulation. *FEBS Letters*, *582*(14), 1977–1986. https://doi.org/10.1016/j.febslet.2008.03.004.

Goedhart, J., & Luijsterburg, M. S. (2020). Volcanoser is a web app for creating, exploring, labeling and sharing volcano plots. *Scientific Reports*, *10*(1), 20560. https://doi.org/10.1038/s41598-020-76603-3

Gómez-Skarmeta, J. L., Glavic, A., de la Calle-Mustienes, E., Modolell, J., & Mayor, R. (1998). Xiro, a Xenopus homolog of the Drosophila Iroquois complex genes, controls development at the neural plate. *The EMBO Journal*, *17*(1), 181–190. https://doi.org/10.1093/emboj/17.1.181.

Green, J. (1999). The animal cap assay. *Methods in Molecular Biology*, *127*, 1–13. https://doi.org/10.1385/1-59259-678-9:1.

Gu, Z., Eils, R., & Schlesner, M. (2016). Complex heatmaps reveal patterns and correlations in multidimensional genomic data. *Bioinformatics (Oxford, England)*, *32*(18), 2847–2849. https://doi.org/10.1093/bioinformatics/btw313

Guénette, S. A., Giroux, M.-C., & Vachon, P. (2013). Pain perception and anaesthesia in research frogs. *Experimental Animals*, *62*(2), 87–92. https://doi.org/10.1538/expanim.62.87

Guillemot, F. (2007). Cell fate specification in the mammalian telencephalon. *Progress in Neurobiology*, *83*(1), 37–52. https://doi.org/10.1016/j.pneurobio.2007.02.009

Habacher, C., & Ciosk, R. (2017). Zc3h12a/Mcpip1/Regnase-1-related endonucleases: An evolutionary perspective on molecular mechanisms and biological functions. *BioEssays : News and Reviews in Molecular, Cellular and Developmental Biology*, *39*(9). https://doi.org/10.1002/bies.201700051

Habacher, C., Guo, Y., Venz, R., Kumari, P., Neagu, A., Gaidatzis, D., Harvald, E. B., Færgeman, N. J., Gut, H., & Ciosk, R. (2016). Ribonuclease-mediated control of body fat. *Developmental Cell*, *39(*3), 359-369. https://doi.org/10.1016/j.devcel.2016.09.018

Han, J., Kim, H. J., Schafer, S. T., Paquola, A., Clemenson, G. D., Toda, T., Oh, J., Pankonin, A. R., Lee, B. S., Johnston, S. T., Sarkar, A., Denli, A. M., & Gage, F. H. (2016). Functional implications of miR-19 in the migration of newborn neurons in the adult Brain. *Neuron*, *91*(1), 79-89. https://doi.org/10.1016/j.neuron.2016.05.034.

Han, J., Lee, Y., Yeom, K.-H., Kim, Y.-K., Jin, H., & Kim, V. N. (2004). The Drosha-DGCR8 complex in primary microRNA processing. *Genes & Development*, *18*(24), 3016–3027. https://doi.org/10.1101/gad.1262504

Hardcastle, Z., Chalmers, A. D., & Papalopulu, L. (2000). FGF-8 stimulates neuronal differentiation through FGFR-4a and interferes with mesoderm induction in Xenopus embryos. *Current biology*, *10*(23), 1511-1514. doi: 10.1016/s0960-9822(00)00825-3

Hardcastle, Z., & Papalopulu, N. (2000). Distinct effects of XBF-1 in regulating the cell cycle inhibitor p27(XIC1) and imparting a neural fate. *Development (Cambridge, England)*, *127*(6), 1303–1314. https://doi.org/10.1242/dev.127.6.1303

Harland, R. M. (1991). In situ hybridization: an improved whole-mount method for Xenopus embryos. *Methods in Cell Biology*, 36, 685-965. https://doi.org/ 10.1016/s0091-679x(08)60307-6

Hartenstein, V. (1989). Early neurogenesis in xenopus: The spatio-temporal pattern of proliferation and cell lineages in the embryonic spinal cord. *Neuron*, *3*(4), 399–411. https://doi.org/10.1016/0896-6273(89)90200-6

Hedderich, M. (2012). "Doctoral Thesis: Molecular characterization of Ptf1a activity during Xenopus embryogenesis."

Hentze, M. W., Castello, A., Schwarzl, T., & Preiss, T. (2018). A brave new world of RNA-binding proteins. *Nature Reviews. Molecular Cell Biology*, *19*(5), 327–341. https://doi.org/10.1038/nrm.2017.130

Hollemann, T., Panitz, F., & Pieler, T. (1999). In situ hybridization techniques with Xenopus embryos. In: Richter, J. D. (ed) A comparative methods approach to the study of oocytes and embryos. Oxford University Press, Oxford, pp 279-290.

Hollemann, T., Schuh, R., Pieler, T. & Stick, R. (1996). Xenopus Xsal-1, a vertebrate homolog of the region specific homeotic gene spalt of Drosophila. *Mechanisms of development*, *55*(1), 19-32. https://doi.org/ 10.1016/0925-4773(95)00485-8

Hollemann, T., Chen, Y., Grunz, H. and Pieler, T. (1998) Regionalized metabolic activity establishes boundaries of retinoic acid signalling. EMBO J. 17, 7361-7372.

Hsu, P. D., Lander, E. S., & Zhang, F. (2014). Development and applications of CRISPR-Cas9 for genome engineering. *Cell*, *157*(6), 1262–1278. https://doi.org/10.1016/j.cell.2014.05.010

Huang, S., Liu, S., Fu, J. J., Wang, T. T., Yao, X., Kumar, A., Liu, G., & Fu, M. (2015). Monocyte chemotactic protein-induced protein 1 and 4 form a complex but act independently in regulation of interleukin-6 mRNA degradation. *The Journal of Biological Chemistry*, *290*, 20782–20792. https://doi.org/10.1074/jbc.M114.635870

Iwasaki, H., Takeuchi, O., Teraguchi, S., Matsushita, K., Uehata, T., Kuniyoshi, K., Satoh, T., Saitoh, T., Matsushita, M., Standley, D. M., & Akira, S. (2011). The IκB kinase complex regulates the stability of cytokine-encoding mRNA induced by TLR-IL-1R by controlling degradation of regnase-1. *Nature Immunology*, *12*(12), 1167–1175. https://doi.org/10.1038/ni.2137

Jakymiw, A., Pauley, K. M., Li, S., Ikeda, K., Lian, S., Eystathioy, T., Satoh, M., Fritzler, M. J., & Chan, E. K. L. (2007). The role of GW/P-bodies in RNA processing and silencing. *Journal of Cell Science*, *120*(Pt 8), 1317–1323. https://doi.org/10.1242/jcs.03429

Jiang, H., Lv, X., Lei, X., Yang, Y., Yang, X., & Jiao, J. (2016). Immune regulator MCPIP1 modulates TET expression during early neocortical development. *Stem Cell Reports*, *7*(3), 439–453. https://doi.org/10.1016/j.stemcr.2016.07.011

Kageyama, R., & Nakanishi, S. (1997). Helix-loop-helix factors in growth and differentiation of the vertebrate nervous system. *Current Opinion in Genetics & Development*, *7*(5), 659–665. https://doi.org/10.1016/s0959-437x(97)80014-7

Kageyama, R., Ohtsuka, T., Shimojo, H., & Imayoshi, I. (2008). Dynamic Notch signaling in neural progenitor cells and a revised view of lateral inhibition. *Nature Neuroscience*, *11*(11), 1247–1251. https://doi.org/10.1038/nn.2208

Kanemitsu, Y., Fujitani, M., Fujita, Y., Zhang, S., Su, Y.-Q., Kawahara, Y., & Yamashita, T. (2017). The RNA-binding protein MARF1 promotes cortical neurogenesis through its RNase activity domain. *Scientific Reports*, *7*(1), 1155. https://doi.org/10.1038/s41598-017-01317-y

Kashef, J., Köhler, A., Kuriyama, S., Alfandari, D., Mayor, R., & Wedlich. D. (2009). Cadherin-11 regulates protrusive activity in Xenopus cranial neural crest cells upstream of Trio and the small GTPases. *Genes and Development*, *23*(12),1393-1398. https://doi.org/10.1101/gad.519409.

Kasza, A., Wyrzykowska, P., Horwacik, I., Tymoszuk, P., Mizgalska, D., Palmer, K., Rokita, H., Sharrocks, A. D., & Jura, J. (2010). Transcription factors Elk-1 and SRF are engaged in IL1-dependent regulation of ZC3H12A expression. *BMC Molecular Biology*, *11*, 14. https://doi.org/10.1186/1471-2199-11-14

Kelaini, S., Chan, C., Cornelius, V. A., & Margariti, A. (2021). RNA-binding proteins hold key roles in function, dysfunction, and disease. *Biology, 10*(5), 366. https://doi.org/10.3390/biology10050366

Khomtchouk, B. B., Hennessy, J. R., & Wahlestedt, C. (2017). Shinyheatmap: Ultra fast low memory heatmap web interface for big data genomics. *PloS One*, *12*(5), e0176334. https://doi.org/10.1371/journal.pone.0176334

Kiyota, T. & Kinoshita, T. (2002) Cysteine-rich region of X-Serrate-1 is required for activation of Notch signaling in Xenopus primary neurogenesis. *International Journal of Developmental Biology*, *46*, 1057 - 1060

Klein, S. L. (1987). The first cleavage furrow demarcates the dorsal-ventral axis in Xenopus embryos. *Developmental Biology*, *120*(1), 299–304. https://doi.org/10.1016/0012-1606(87)90127-8

Knuckles, P., Vogt, M. A., Lugert, S., Milo, M., Chong, M. M. W., Hautbergue, G. M., Wilson, S. A., Littman, D. R., & Taylor, V. (2012). Drosha regulates neurogenesis by controlling neurogenin 2 expression independent of microRNAs. *Nature Neuroscience*, *15*(7), 962–969. https://doi.org/10.1038/nn.3139

Kochan, J., Wawro, M., & Kasza, A. (2016). IF-combined smRNA FISH reveals interaction of MCPIP1 protein with IER3 mRNA. *Biology open*, *5*(7), 889–898. https://doi.org/10.1242/bio.018010

Kochan, J., Wawro, M., & Kasza, A. (2015). Simultaneous detection of mRNA and protein in single cells using immunofluorescence-combined single-molecule RNA FISH. *BioTechniques*, *59*(4), 209-12, 214, 216 passim. https://doi.org/10.2144/000114340

Kolm, P. J., & Sive, H. L. (1995). Efficient hormone-inducible protein function in Xenopus laevis. *Developmental Biology*, *171*(1), 267–272. https://doi.org/10.1006/dbio.1995.1279

Kroll, K. L., Salic, A. N., Evans, L. M., & Kirschner, M. W. (1998). Geminin, a neuralizing molecule that demarcates the future neural plate at the onset of gastrulation. *Development (Cambridge, England)*, *125*(16), 3247–3258. https://doi.org/10.1242/dev.125.16.3247

Lacomme, M., Liaubet, L., Pituello, F., & Bel-Vialar, S. (2012). Neurog2 drives cell cycle exit of neuronal precursors by specifically repressing a subset of cyclins acting

at the G1 and S phases of the cell cycle. *Molecular and Cellular Biology*, *32*(13), 2596–2607. https://doi.org/10.1128/MCB.06745-11

Laemmli, U. K. (1970). Cleavage of structural proteins during the assembly of the head of bacteriophage T4. *Nature*, *227*(5259), 680–685. https://doi.org/10.1038/227680a0.

Lang, M. F., & Shi, Y. (2012). Dynamic Roles of microRNAs in Neurogenesis. *Frontiers in Neuroscience*, *6*, 71. https://doi.org/10.3389/fnins.2012.00071.

Lara-Pezzi, E., Desco, M., Gatto, A., & Gómez-Gaviro, M. V. (2017). Neurogenesis: Regulation by Alternative Splicing and Related Posttranscriptional Processes. *The Neuroscientist, 23*(5), 466–477. https://doi.org/10.1177/1073858416678604

Lee, J. E. (1997). NeuroD and neurogenesis. *Developmental Neuroscience*, *19*(1), 27–32. https://doi.org/10.1159/000111182

Lee, J. E., Hollenberg, S. M., Snider, L., Turner, D. L., Lipnick, N., & Weintraub, H. (1995). Conversion of Xenopus ectoderm into neurons by NeuroD, a basic helix-loop-helix protein. *Science (New York, N.Y.)*, *268*(5212), 836–844. https://doi.org/10.1126/science.7754368

Lee-Liu, D., Méndez-Olivos, E. E., Muñoz, R., & Larraín, J. (2017). The African clawed frog Xenopus laevis: A model organism to study regeneration of the central nervous system. *Neuroscience Letters*, *652*, 82–93. https://doi.org/10.1016/j.neulet.2016.09.054

Letunic, I., Doerks, T. & Bork, P. (2009). SMART 6: recent updates and new developments. *Nucleic Acids Research*, 37(1), D229–D232. https://doi.org/10.1093/nar/gkn808

Li, T., Hui, W., Halike, H., & Gao, F. (2021). RNA Binding Protein-based model for prognostic prediction of colorectal cancer. *Technology in Cancer Research & Treatment*. https://doi.org/10.1177/15330338211019504

Li, M., Cao, W., Liu, H., Zhang, W., Liu, X., Cai, Z., Guo, J., Wang, X., Hui, Z., Zhang, H., Wang, J., & Wang, L. (2012). Mcpip1 down-regulates IL-2 expression through an ARE-independent pathway. *PloS One*, *7*(11), e49841. https://doi.org/10.1371/journal.pone.0049841

Liang, J., Saad, Y., Lei, T., Wang, J., Qi, D., Yang, Q., Kolattukudy, P. E., & Fu, M. (2010). Mcp-induced protein 1 deubiquitinates TRAF proteins and negatively regulates JNK and NF-kappaB signaling. *The Journal of Experimental Medicine*, *207*(13), 2959–2973. https://doi.org/10.1084/jem.20092641

Liang, J., Wang, J., Azfer, A., Song, W., Tromp, G., Kolattukudy, P. E., & Fu, M. (2008). A novel CCCH-zinc finger protein family regulates proinflammatory activation of macrophages. *The Journal of Biological Chemistry*, *283*(10), 6337–6346. https://doi.org/10.1074/jbc.M707861200

Liao, Y., Smyth, G. K., & Shi, W. (2013). “featureCounts: an efficient general purpose program for assigning sequence reads to genomic features.” *Bioinformatics*, *30*(7), 923-930. https://doi.org/10.1093/bioinformatics/btt656.

Lichawska-Cieslar, A., Pietrzycka, R., Ligeza, J., Kulecka, M., Paziewska, A., Kalita, A., Dolicka, D. D., Wilamowski, M., Miekus, K., Ostrowski, J., Mikula, M., & Jura, J. (2018). RNA sequencing reveals widespread transcriptome changes in a renal carcinoma cell line. *Oncotarget*, *9*(9), 8597–8613. https://doi.org/10.18632/oncotarget.24269

Lin, R.-J., Chien, H.-L., Lin, S.-Y., Chang, B.-L., Yu, H.-P., Tang, W.-C., & Lin, Y.-L. (2013). Mcpip1 ribonuclease exhibits broad-spectrum antiviral effects through viral RNA binding and degradation. *Nucleic Acids Research*, *41*(5), 3314–3326. https://doi.org/10.1093/nar/gkt019

Linneberg, C., Toft, C. L. F., Kjaer-Sorensen, K., & Laursen, L. S. (2019). L1cam-mediated developmental processes of the nervous system are differentially regulated by proteolytic processing. *Scientific Reports*, *9*(1), 3716. https://doi.org/10.1038/s41598-019-39884-x

Liu, B., Huang, J., Ashraf, A., Rahaman, O., Lou, J., Wang, L., Cai, P., Wen, J., Anwaar, S., Liu, X., Ni, H., Ganguly, D., Zhao, J., & Yang, C. Y. (2021). The RNase MCPIP3 promotes skin inflammation by orchestrating myeloid cytokine response. *Nature Communications*, *12*(1), 4105. https://doi.org/10.1038/s41467-021-24352-w

Louvi, A., & Artavanis-Tsakonas, S. (2006) Notch signalling in vertebrate neural development. *Nature Reviews. Neuroscience* 7, 93–102 (2006). https://doi.org/10.1038/nrn1847

Lukong, K. E., Chang, K., Khandjian, E. W., & Richard, S. (2008). RNA-binding proteins in human genetic disease. *Trends in Genetics*, *24*(8), 416–425. https://doi.org/10.1016/j.tig.2008.05.004

Lunde, B. M., Moore, C., & Varani, G. (2007). Rna-binding proteins: Modular design for efficient function. *Nature Reviews. Molecular Cell Biology*, *8*(6), 479–490. https://doi.org/10.1038/nrm2178.

Luo, Y., Shan, G., Guo, W., Smrt, R. D., Johnson, E. B., Li, X., Pfeiffer, R. L., Szulwach, K. E., Duan, R., Barkho, B. Z., Li, W., Liu, C., Jin, P., & Zhao, X. (2010). Fragile X mental retardation protein regulates proliferation and differentiation of adult neural stem/progenitor cells. *PLoS Genetics*, *6*(4), e1000898. https://doi.org/10.1371/journal.pgen.1000898

Ma, Q., Kintner, C., & Anderson, D. J. (1996). Identification of neurogenin, a Vertebrate Neuronal Determination Gene. *Cell*, *87*(1), 43–52. https://doi.org/10.1016/S0092-8674(00)81321-5

Mancilla, A., & Mayor, R. (1996). Neural crest formation in Xenopus laevis: Mechanisms of Xslug induction. *Developmental Biology*, *177*(2), 580-589. https://doi.org/10.1006/dbio.1996.0187

Mao, R., Yang, R., Chen, X., Harhaj, E. W., Wang, X., & Fan, Y. (2017). Regnase-1, a rapid response ribonuclease regulating inflammation and stress responses. *Cellular & Molecular Immunology*, *14*(5), 412–422. https://doi.org/10.1038/cmi.2016.70

Massari, M. E., & Murre, C. (2000). Helix-loop-helix proteins: Regulators of transcription in eucaryotic organisms. *Molecular and Cellular Biology*, *20*(2), 429–440. https://doi.org/10.1128/MCB.20.2.429-440.2000

Masserdotti, G., Gascón, S., & Götz, M. (2016). Direct neuronal reprogramming: Learning from and for development. *Development*, *143*(14), 2494–2510. https://doi.org/10.1242/dev.092163.

Matsushita, K., Takeuchi, O., Standley, D. M., Kumagai, Y., Kawagoe, T., Miyake, T., Satoh, T., Kato, H., Tsujimura, T., Nakamura, H., & Akira, S. (2009). Zc3h12a is an RNase essential for controlling immune responses by regulating mRNA decay. *Nature*, *458*(7242), 1185–1190. https://doi.org/10.1038/nature07924

Meredith, A., & Johnson, J. E. (2000). Negative autoregulation of Mash1 expression in CNS development. *Developmental Biology*, *222*(2), 336–346. https://doi.org/10.1006/dbio.2000.9697

Mimoto, M. S., & Christian, J. L. (2011). Manipulation of gene function in Xenopus laevis. *Methods in Molecular Biology*, *770*, 55–75. https://doi.org/10.1007/978-1-61779-210-6_3

Minagawa, K., Katayama, Y., Nishikawa, S., Yamamoto, K., Sada, A., Okamura, A., Shimoyama, M., & Matsui, T. (2009). Inhibition of G1 to S phase progression by a novel zinc finger protein P58(TFL) at P-bodies. *Molecular Cancer Research*, *7*(6), 880–889. https://doi.org/10.1158/1541-7786.MCR-08-0511

Mino, T., Murakawa, Y., Fukao, A., Vandenbon, A., Wessels, H.-H., Ori, D., Uehata, T., Tartey, S., Akira, S., Suzuki, Y., Vinuesa, C. G., Ohler, U., Standley, D. M., Landthaler, M., Fujiwara, T., & Takeuchi, O. (2015). Regnase-1 and Roquin Regulate a Common Element in Inflammatory mRNAs by Spatiotemporally Distinct Mechanisms. *Cell*, *161*(5), 1058–1073. https://doi.org/10.1016/j.cell.2015.04.029

Mizuseki, K., Kishi, M., Matsui, M., Nakanishi, S., & Sasai, Y. (1998a). Xenopus Zic-related-1 and Sox-2, two factors induced by chordin, have distinct activities in the initiation of neural induction. *Development*, *125*(4), 579–587. https://doi.org/10.1242/dev.125.4.579

Mizuseki, K., Kishi, M., Shiota, K., Nakanishi, S., & Sasai, Y. (1998b). SoxD: An essential mediator of induction of anterior neural tissues in Xenopus embryos. *Neuron*, *21*(1), 77–85. https://doi.org/10.1016/S0896-6273(00)80516-4

Moody, S. A. (1987). Fates of the blastomeres of the 32-cell-stage Xenopus embryo. *Developmental Biology*, *122*(2), 300–319. https://doi.org/10.1016/0012-1606(87)90296-x

Moody, S. A., & Je, H. S. (2002). Neural induction, neural fate stabilization, and neural stem cells. *The Scientific World Journal*, *2*, 1147–1166. https://doi.org/10.1100/tsw.2002.217

Moody, S. A., Miller, V., Spanos, A., & Frankfurter, A. (1996). Developmental expression of a neuron-specific beta-tubulin in frog (Xenopus laevis): A marker for growing axons during the embryonic period. *The Journal of Comparative Neurology*, *364*(2), 219–230. https://doi.org/10.1002/(SICI)1096-9861(19960108)364:2<219::AID-CNE3>3.0.CO;2-8

Moulton, J. D. (2006). Using morpholinos to control gene expression. *Current Protocols in Nucleic Acid Chemistry*, *27*(1), 4301–43024. https://doi.10.1002/0471142700.nc0430s27

Mullis, K., Faloona, F., Scharf, S., Saiki, R. K., Horn, G., Erlich, H. (1986) Specific enzymatic amplication of DNA in vitro: the polymerase chain reaction. *Cold Spring Harbor Symposium on Quantitative Biology*, 51, 263–273.

Nakata, K., Nagai, T., Aruga, J., & Mikoshiba, K. (1997). Xenopus Zic3, a primary regulator both in neural and neural crest development. *Proceedings of the National Academy of Sciences of the United States of America*, *94*(22), 11980–11985. https://doi.org/10.1073/pnas.94.22.11980

Nakata, K., Nagai, T., Aruga, J., & Mikoshiba, K. (1998). Xenopus Zic family and its role in neural and neural crest development. *Mechanisms of Development*, *75*(1-2), 43–51. https://doi.org/10.1016/s0925-4773(98)00073-2

Nakayama, T., Fish, M. B., Fisher, M., Oomen-Hajagos, J., Thomsen, G. H., & Grainger, R. M. (2013). Simple and efficient CRISPR/Cas9-mediated targeted mutagenesis in Xenopus tropicalis. *Genesis*, *51*(12), 835–843. https://doi.org/10.1002/dvg.22720

Nguyen, T. A., Jo, M. H., Choi, Y. G., Park, J., Kwon, S. C., Hohng, S., Kim, V. N., & Woo, J. S. (2015). Functional anatomy of the human microprocessor. *Cell*, *161*(6), 1374–1387. https://doi.org/10.1016/j.cell.2015.05.010

Nieber, F., Hedderich, M., Jahn, O., Pieler, T., & Henningfeld, K. A. (2013). Numbl is essential for Xenopus primary neurogenesis. *BMC Developmental Biology*, *13*, 36. https://doi.org/10.1186/1471-213X-13-36

Nieber, F., Pieler, T., & Henningfeld, K. A. (2009). Comparative expression analysis of the neurogenins in Xenopus tropicalis and Xenopus laevis. *Developmental Dynamics*, *238*(2), 451–458. https://doi.org/10.1002/dvdy.21845

Nieuwkoop, P.D. and Faber, J. (1967) Normal Table of Xenopus laevis (Daudin). 2nd ed. North-Holland Publishing Company, Amsterdam.

Nussbacher, J. K., Tabet, R., Yeo, G. W., & Lagier-Tourenne, C. (2019). Disruption of RNA metabolism in neurological diseases and emerging therapeutic interventions. *Neuron*, *102*(2), 294–320. https://doi.org/10.1016/j.neuron.2019.03.014

Ohnuma, S., & Harris, W. A. (2003). Neurogenesis and the cell cycle. *Neuron*, *40*(2), 199–208. https://doi.org/10.1016/S0896-6273(03)00632-9

Oschwald, R., Richter, K., Grunz, H. (1991). Localization of a nervous system-specific class II beta-tubulin gene in Xenopus laevis embryos by whole-mount in situ hybridization. *International Journal of Developmental Biology*, *35*(4), 399-405. PMID: 1801865

Perron, M., Opdecamp, K., Butler, K., Harris, W. A., & Bellefroid, E. J. (1999). X-ngnr-1 and Xath3 promote ectopic expression of sensory neuron markers in the neurula ectoderm and have distinct inducing properties in the retina. *Proceedings of the National Academy of Sciences of the United States of America*, *96*(26), 14996–15001. https://doi.org/10.1073/pnas.96.26.14996

Pilaz, L.J., & Silver, D. L. (2015). Post-transcriptional regulation in corticogenesis: How RNA-binding proteins help build the brain. *Wiley Interdisciplinary Reviews. RNA*, *6*(5), 501–515. https://doi.org/10.1002/wrna.1289.

Pozzi, D., Corradini, I., & Matteoli, M. (2019). The Control of Neuronal Calcium Homeostasis by SNAP-25 and its Impact on Neurotransmitter Release. *Neuroscience*, *420*, 72–78. https://doi.org/10.1016/j.neuroscience.2018.11.009

Pozzoli, O., Bosetti, A., Croci, L., Consalez, G. G., & Vetter, M. L. (2001). Xebf3 is a regulator of neuronal differentiation during primary neurogenesis in Xenopus. *Developmental Biology*, *233*(2), 495–512. https://doi.org/10.1006/dbio.2001.0230

R Core Team (2020). R: A language and environment for statistical computing. R Foundation for Statistical Computing, Vienna, Austria. https://www.r-project.org/

Ramos, A. D., Andersen, R. E., Liu, S. J., Nowakowski, T. J., Hong, S. J., Gertz, C. C., Ryan D. Salinas, R. D., Zarabi, H., Kriegstein, A. R & Lim, D. A. (2015). The long noncoding RNA Pnky regulates neuronal differentiation of embryonic and postnatal neural stem cells. *Cell Stem Cell, 16*(4), 439-447. https://doi.org/10.1016/j.stem.2015.02.007.

Raj, B., O'Hanlon, D., Vessey, J. P., Pan, Q., Ray, D., Buckley, N. J., Miller, F. D., & Blencowe, B. J. (2011). Cross-regulation between an alternative splicing activator and a transcription repressor controls neurogenesis. *Molecular Cell*, *43*(5), 843–850. https://doi.org/10.1016/j.molcel.2011.08.014

Rogers, C. D., Moody, S. A., & Casey, E. S. (2009). Neural induction and factors that stabilize a neural fate. *Birth Defects Research. Part C, Embryo Today : Reviews*, *87*(3), 249–262. https://doi.org/10.1002/bdrc.20157.

Saffary, R., & Xie, Z. (2011). FMRP regulates the transition from radial glial cells to intermediate progenitor cells during neocortical development. *The Journal of Neuroscience*, *31*(4), 1427–1439. https://doi.org/10.1523/JNEUROSCI.4854-10.2011

Saiki, R. K., Scharf, S., Faloona, F., Mullis, K. B., Horn, G. T., Erlich, H. A., & Norman Arnheim, N. (1985). Enzymatic amplification of β-Globin genomic sequences and restriction site analysis for diagnosis of sickle cell anemia. *Science*, *230*(4732), 1350-1354. https://doi.org/10.1126/science.2999980

Sambrook, J. and Russell, D.W. (2001) Molecular Cloning: A Laboratory Manual. 3rd Edition, Vol. 1, Cold Spring Harbor Laboratory Press, New York.

Sander, J. D., & Joung, J. K. (2014). CRISPR-Cas systems for editing, regulating and targeting genomes. *Nature Biotechnology, 32*(4), 347-355. https://doi.org/10.1038/nbt.2842

Sanduja, S., Blanco, F. F., Young, L. E., Kaza, V., & Dixon, D. A. (2012). The role of tristetraprolin in cancer and inflammation. *Frontiers in Bioscience (Landmark edition)*, *17*(1), 174–188. https://doi.org/10.2741/3920

Sasai, Y. (1998). Identifying the missing links: genes that connect neural induction and primary neurogenesis in vertebrate embryos. *Neuron*, *21*(3), 455-458.

Schlosser, G. (2002). Development and evolution of lateral line placodes in amphibians. - II. Evolutionary diversification. *Zoology*, *105*(3), 177–193. https://doi.org/10.1078/0944-2006-00062.

Schneider, M. L., Turner, D. L., & Vetter, M. L. (2001). Notch signaling can inhibit Xath5 function in the neural plate and developing retina. *Molecular and Cellular Neurosciences*, *18*(5), 458–472. https://doi.org/10.1006/mcne.2001.1040.

Seo, S., Lim, J.-W., Yellajoshyula, D., Chang, L.-W., & Kroll, K. L. (2007). Neurogenin and NeuroD direct transcriptional targets and their regulatory enhancers. *The EMBO Journal*, *26*(24), 5093–5108. https://doi.org/10.1038/sj.emboj.7601923

Session, A. M., Uno, Y., Kwon, T., Chapman, J. A., Toyoda, A., Takahashi, S., Fukui, A., Hikosaka, A., Suzuki, A., Kondo, M., van Heeringen, S. J., Quigley, I., Heinz, S., Ogino, H., Ochi, H., Hellsten, U., Lyons, J. B., Simakov, O., Putnam, N., . . . Rokhsar, D. S. (2016). Genome evolution in the allotetraploid frog Xenopus laevis. *Nature*, *538*(7625), 336–343. https://doi.org/10.1038/nature19840

Sharp, P. A., Sugden, B., & Sambrook, J. (1973): Detection of two restriction endonuclease activities in Haemophilus parainfluenzae using analytical agarose--ethidium bromide electrophoresis. In *Biochemistry* 12 (16), pp. 3055–3063. https://doi.org/10.1021/bi00740a018.

Sharpe, C. R. (1990). Regional neural induction in Xenopus laevis. *BioEssays : News and Reviews in Molecular, Cellular and Developmental Biology*, *12*(12), 591–596. https://doi.org/10.1002/bies.950121206

Sommer, L., Ma, Q., & Anderson, D. J. (1996). Neurogenins, a novel family of atonal-related bHLH transcription factors, are putative mammalian neuronal determination genes that reveal progenitor cell heterogeneity in the developing CNS and PNS. *Molecular and Cellular Neurosciences*, *8*(4), 221–241. https://doi.org/10.1006/mcne.1996.0060.

Souopgui, J., Sölter, M., & Pieler, T. (2002). Xpak3 promotes cell cycle withdrawal during primary neurogenesis in Xenopus laevis. *The EMBO Journal*, *21*(23), 6429–6439. https://doi.org/10.1093/emboj/cdf644.

Suk, F. M., Chang, C. C., Lin, R. J., Lin, S. Y., Chen, Y. T., & Liang, Y. C. (2018). MCPIP3 as a potential metastasis suppressor gene in human colorectal cancer. *International Journal of Molecular Sciences*, *19*(5). https://doi.org/10.3390/ijms19051350

Sullivan, S. A., Akers, L., & Moody, S. A. (2001). Foxd5a, a Xenopus winged helix gene, maintains an immature neural ectoderm via transcriptional repression that is dependent on the C-terminal domain. *Developmental Biology*, *232*(2), 439–457. https://doi.org/10.1006/dbio.2001.0191

Summerton, J., & Weller, D. (1997). Morpholino antisense oligomers: Design, preparation, and properties. *Antisense & Nucleic Acid Drug Development*, *7*(3), 187–195. https://doi.org/10.1089/oli.1.1997.7.187

Suzuki, H. I., Arase, M., Matsuyama, H., Choi, Y. L., Ueno, T., Mano, H., Sugimoto, K., & Miyazono, K. (2011). Mcpip1 ribonuclease antagonizes dicer and terminates microRNA biogenesis through precursor microRNA degradation. *Molecular Cell*, *44*(3), 424–436. https://doi.org/10.1016/j.molcel.2011.09.012

Takebayashi, K., Takahashi, S., Yokota, C., Tsuda, H., Nakanishi, S., Asashima, M., & Kageyama, R. (1997). Conversion of ectoderm into a neural fate by ATH-3, a vertebrate basic helix-loop-helix gene homologous to Drosophila proneural gene atonal. *The EMBO Journal*, *16*(2), 384–395. https://doi.org/10.1093/emboj/16.2.384

Tanaka, H., Arima, Y., Kamimura, D., Tanaka, Y., Takahashi, N., Uehata, T., Maeda, K., Satoh, T., Murakami, M., & Akira, S. (2019). Phosphorylation-dependent Regnase-1 release from endoplasmic reticulum is critical in IL-17 response. *The Journal of Experimental Medicine*, *216*(6), 1431–1449. https://doi.org/10.1084/jem.20181078

Terns, R. M., & Terns, M. P. (2014). Crispr-based technologies: Prokaryotic defense weapons repurposed. *Trends in Genetics*, *30*(3), 111–118. https://doi.org/10.1016/j.tig.2014.01.003

Thoma, E. C., Wischmeyer, E., Offen, N., Maurus, K., Sirén, A.-L., Schartl, M., & Wagner, T. U. (2012). Ectopic expression of neurogenin 2 alone is sufficient to induce differentiation of embryonic stem cells into mature neurons. *PloS One*, *7*(6), e38651. https://doi.org/10.1371/journal.pone.0038651

Thuret, R., Auger, H., & Papalopulu, N. (2015). Analysis of neural progenitors from embryogenesis to juvenile adult in Xenopus laevis reveals biphasic neurogenesis and continuous lengthening of the cell cycle. *Biology Open*, *4*(12), 1772–1781. https://doi.org/10.1242/bio.013391

Tomita, T., Kato, M., Mishima, T., Matsunaga, Y., Sanjo, H., Ito, K. I., Minagawa, K., Matsui, T., Oikawa, H., Takahashi, S., Takao, T., Iwai, N., Mino, T., Takeuchi, O., Maru, Y., & Hiratsuka, S. (2021). Extracellular mRNA transported to the nucleus exerts translation-independent function. *Nature Communications*, *12*(1), 3655. https://doi.org/10.1038/s41467-021-23969-1

Towbin, H., Staehelin, T., & Gordon. J. (1979). Electrophoretic transfer of proteins from polyacrylamide gels to nitrocellulose sheets: procedure and some applications.

Proceedings of the National Academy of Science of the United States of America, 76(9), 4350-4354. https://doi.org/10.1073/pnas.76.9.4350

Tsoi, L. C., Spain, S. L., Knight, J., Ellinghaus, E., Stuart, P. E., Capon, F., Ding, J., Li, Y., Tejasvi, T., Gudjonsson, J. E., Kang, H. M., Allen, M. H., McManus, R., Novelli, G., Samuelsson, L., Schalkwijk, J., Ståhle, M., Burden, A. D., Smith, C. H., . . . Trembath, R. C. (2012). Identification of 15 new psoriasis susceptibility loci highlights the role of innate immunity. *Nature Genetics*, *44*(12), 1341–1348. https://doi.org/10.1038/ng.2467.

Uehata, T., & Akira, S. (2013). mRNA degradation by the endoribonuclease Regnase-1/ZC3H12a/MCPIP-1. *Biochimica Et Biophysica Acta*, *1829*(6-7), 708–713. https://doi.org/10.1016/j.bbagrm.2013.03.001

Uehata, T., & Takeuchi, O. (2020). RNA recognition and immunity-Innate Immune Sensing and Its Posttranscriptional Regulation Mechanisms. *Cells*, *9*(7). https://doi.org/10.3390/cells9071701.

Vernon, A. E., Devine, C., & Philpott, A. (2003). The cdk inhibitor p27Xic1 is required for differentiation of primary neurones in Xenopus. *Development*, *130*(1), 85-92. https://doi.org/10.1242/dev.00193

Vessey, J. P., Amadei, G., Burns, S. E., Kiebler, M. A., Kaplan, D. R., & Miller, F. D. (2012). An asymmetrically localized Staufen2-dependent RNA complex regulates maintenance of mammalian neural stem cells. *Cell Stem Cell*, *11*(4), 517–528. https://doi.org/10.1016/j.stem.2012.06.010.

von Gamm, M. von, Schaub, A., Jones, A. N., Wolf, C., Behrens, G., Lichti, J., Essig, K., Macht, A., Pircher, J., Ehrlich, A., Davari, K., Chauhan, D., Busch, B., Wurst, W., Feederle, R., Feuchtinger, A., Tschöp, M. H., Friedel, C. C., Hauck, S. M., . . . Glasmacher, E. (2019). Immune homeostasis and regulation of the interferon pathway require myeloid-derived Regnase-3. *The Journal of Experimental Medicine*, *216*(7), 1700–1723. https://doi.org/10.1084/jem.20181762.

Wang, F., Shi, Z., Cui, Y., Guo, X., Shi, Y. B., & Chen, Y. (2015). Targeted gene disruption in Xenopus laevis using CRISPR/Cas9. *Cell & Bioscience*, *5*, 15. https://doi.org/10.1186/s13578-015-0006-1

Waters, C. A., Strande, N. T., Pryor, J. M., Strom, C. N., Mieczkowski, P., Burkhalter, M. D., Oh, S., Qaqish, B. F., Moore, D. T., Hendrickson, E. A., & Ramsden, D. A. (2014). The fidelity of the ligation step determines how ends are resolved during nonhomologous end joining. *Nature Communications*, *5*, 4286. https://doi.org/10.1038/ncomms5286

Wawro, M., Kochan, J., & Kasza, A. (2016). The perplexities of the ZC3H12A self-mRNA regulation. *Acta Biochimica Polonica*, *63*(3), 411–415. https://doi.org/10.18388/abp.2016_1325

Wawro, M., Kochan, J., Krzanik, S., Jura, J., & Kasza, A. (2017). Intact NYN/PIN-Like Domain is Crucial for the Degradation of Inflammation-Related Transcripts by

ZC3H12D. *Journal of Cellular Biochemistry*, *118*(3), 487–498. https://doi.org/10.1002/jcb.25665

Wawro, M., Kochan, J., Sowinska, W., Solecka, A., Wawro, K., Morytko, A., Kwiecinska, P., Grygier, B., Kwitniewski, M., Fu, M., Cichy, J., & Kasza, A. (2021). Molecular Mechanisms of ZC3H12C/Reg-3 Biological Activity and Its Involvement in Psoriasis Pathology. *International Journal of Molecular Sciences*, *22*(14). https://doi.org/10.3390/ijms22147311.

Wawro, M., Wawro, K., Kochan, J., Solecka, A., Sowinska, W., Lichawska-Cieslar, A., Jura, J., & Kasza, A. (2019). Zc3h12b/mcpip2, a new active member of the ZC3H12 family. *RNA (New York, N.Y.)*, *25*(7), 840–856. https://doi.org/10.1261/rna.071381.119

Wettstein, D. A., Turner, D. L., & Kintner, C. (1997). The Xenopus homolog of Drosophila Suppressor of Hairless mediates Notch signaling during primary neurogenesis. *Development*, *124*(3), 693–702. https://doi.org/10.1242/dev.124.3.693

Wullimann, M. F., Rink, E., Vernier, P., & Schlosser, G. (2005). Secondary neurogenesis in the brain of the African clawed frog, Xenopus laevis, as revealed by PCNA, Delta-1, Neurogenin-related-1, and NeuroD expression. *The Journal of Comparative Neurology*, *489*(3), 387–402. https://doi.org/10.1002/cne.20634.

Xia, Y. J., Zhao, S. H., & Mao, B. Y. (2012). Involvement of XZFP36L1, an RNA-binding protein, in Xenopus neural development. *Dongwuxue Yanjiu*, 33(E5-6), E82-8. https://doi.org/10.3724/SP.J.1141.2012.E05-06E82

Yao, H., Ma, R., Yang, L., Hu, G., Chen, X., Duan, M., Kook, Y., Niu, F., Liao, K., Fu, M., Hu, G., Kolattukudy, P., & Buch, S. (2014). MiR-9 promotes microglial activation by targeting MCPIP1. *Nature communications*, *5*, 4386. https://doi.org/10.1038/ncomms5386

Yokogawa, M., Tsushima, T., Noda, N. N., Kumeta, H., Enokizono, Y., Yamashita, K., Standley, D. M., Takeuchi, O., Akira, S., & Inagaki, F. (2016). Structural basis for the regulation of enzymatic activity of Regnase-1 by domain-domain interactions. *Scientific Reports*, *6*, 22324. https://doi.org/10.1038/srep22324

Yoshinaga, M., & Takeuchi, O. (2019). RNA binding proteins in the control of autoimmune diseases. *Immunological Medicine*, *42*(2), 53–64. https://doi.org/10.1080/25785826.2019.1655192

Zahr, S. K., Kaplan, D. R., & Miller, F. D. (2019). Translating neural stem cells to neurons in the mammalian brain. *Cell Death and Differentiation*, *26*(12), 2495–2512. https://doi.org/10.1038/s41418-019-0411-9

Zhang, F., Wen, Y., & Guo, X. (2014). Crispr/cas9 for genome editing: Progress, implications and challenges. *Human Molecular Genetics*, *23*(R1), R40-6. https://doi.org/10.1093/hmg/ddu125

Zhao, X., Kuja-Panula, J., Sundvik, M., Chen, Y.-C., Aho, V., Peltola, M. A., Porkka-Heiskanen, T., Panula, P., & Rauvala, H. (2014). Amigo adhesion protein regulates

development of neural circuits in zebrafish brain. *The Journal of Biological Chemistry*, *289*(29), 19958–19975. https://doi.org/10.1074/jbc.M113.545582

Zhou, H., Mangelsdorf, M., Liu, J., Zhu, L., & Wu, J. Y. (2014). RNA-binding proteins in neurological diseases. *Science China Life Sciences*, *57*(4), 432–444. https://doi.org/10.1007/s11427-014-4647-9

6 Appendices

Appendix 6.1 Top 210 upregulated DEGs: Neurog2 + Co-MO vs CC

Neurog2 + Co-MO vs CC		
gene	log2FC	padj
neurod4.L	7.19	5.98E-58
nhlh1.S	7.06	1.39E-40
stxbp1.S	6.99	1.14E-47
elavl3.S	6.69	1.81E-62
neurod4.S	6.57	1.97E-47
prph.S	6.51	7.92E-31
olig2.S	6.41	1.63E-32
neurog2.L	6.36	5.76E-58
nes.S	6.34	6.05E-30
ebf2.L	6.20	2.84E-35
elavl4.L	5.84	6.91E-32
tubb3.S	5.77	1.64E-28
celf3.S	5.76	9.01E-42
tubb2b.S	5.73	1.09E-22
onecut2.L	5.71	1.64E-28
tubb3.L	5.71	6.20E-23
dpysl3.L	5.69	1.53E-38
map2.S	5.58	1.51E-30
pou4f4.L	5.55	6.48E-26
ebf2.S	5.50	4.24E-22
celf3.L	5.48	4.90E-41
kank2.L	5.45	1.62E-28
nhlh1.L	5.42	3.36E-20
neurod1.L	5.41	6.91E-21
igfbpl1.S	5.40	1.88E-16
sipa1.L	5.38	1.11E-19
syt2.S	5.32	9.56E-28
MGC53786	5.32	2.54E-21
tespa1.S	5.31	8.90E-18
pou4f1.L	5.25	4.35E-23
drgx.L	5.19	1.51E-23
scrt2.S	5.17	1.06E-18
shd.L	5.15	4.69E-22
vxn.S	5.13	9.96E-19
rasef.S	4.95	1.56E-16
dbn1.S	4.90	1.17E-37
st18.L	4.75	2.94E-18
ebf3.L	4.74	5.59E-13
myo10.2.S	4.74	3.07E-22
LOC121401564	4.73	2.66E-13
olig2.L	4.73	1.63E-12
slc43a2.S	4.68	2.60E-22
onecut1.L	4.63	3.07E-22
map2.L	4.62	2.43E-27
dbn1.L	4.60	3.16E-33
prdm14.L	4.54	2.99E-15
hes5.2.S	4.53	1.42E-11
faxc.L	4.49	7.83E-22
chga.L	4.47	2.04E-15
tm116.S	4.43	2.12E-13
kcnk3.S	4.41	1.81E-17
paqr9.L	4.41	1.54E-12
dpysl4.L	4.40	2.90E-10
igfbpl1.L	4.39	3.75E-10
sv2b.S	4.37	3.42E-10
cd276.S	4.35	8.82E-11
st6galnac6.L	4.33	4.83E-10
snap25.L	4.32	1.49E-25
tlx3.L	4.32	2.23E-12
des.1.L	4.31	2.82E-16
frmpd1.L	4.31	6.70E-12
ncam1.S	4.30	1.73E-20
ncam1.L	4.28	4.48E-19
nova2.L	4.28	4.09E-20
mllt11.S	4.25	3.93E-09
hecw1.L	4.23	6.04E-17
cacna2d1.L	4.18	1.46E-20
dnajc6.S	4.17	1.92E-14
arl8a.S	4.17	7.82E-11

Neurog2 + Co-MO vs CC		
gene	log2FC	padj
bhlhe22.L	4.14	3.01E-11
maneal.S	4.14	5.50E-13
cbfa2t1.S	4.12	1.76E-15
hbg1.L	4.06	3.47E-13
bhlhe22.S	4.03	6.07E-12
pak3.L	4.01	4.96E-12
neurod1.S	3.99	6.37E-11
st8sia1.S	3.98	2.23E-09
celf2.L	3.97	4.19E-09
pkdcc.2.S	3.97	7.88E-13
srrm4.L	3.96	1.71E-31
zic3.L	3.95	6.82E-13
cplx2.L	3.93	1.19E-16
elavl4.S	3.93	2.84E-09
tmem116.L	3.93	4.08E-15
adamtsl1.2.L	3.88	3.64E-11
srrm4.S	3.87	2.38E-14
rundc3a.L	3.86	2.51E-10
mxra7.L	3.86	6.06E-15
zeb2.L	3.86	1.36E-11
cpe.L	3.84	2.65E-19
tuba1b.S	3.83	1.73E-12
pcsk6.S	3.82	6.52E-12
st8sia1.L	3.82	9.38E-14
adcyap1.L	3.81	4.44E-07
tal1.S	3.81	3.14E-07
map3k12.S	3.73	8.56E-10
fbxl16.L	3.72	1.27E-06
pex5l.S	3.72	2.86E-08
npr2.L	3.69	6.72E-07
ror2.S	3.65	9.16E-11
hes5.4.L	3.64	6.12E-17
vamp2.L	3.64	1.24E-10
maneal.L	3.62	7.88E-13
slc45a1.S	3.61	1.67E-06
drgx.S	3.57	7.46E-13
gria1.S	3.57	1.02E-07
cdc42ep3.S	3.56	1.19E-15
insm1.L	3.56	5.28E-11
pdk4.L	3.56	2.85E-15
ppp1r9b.L	3.55	1.72E-07
pros1.S	3.55	1.61E-17
igfals.L	3.54	1.80E-06
emb.L	3.52	6.83E-07
ppp1r9b.S	3.52	1.22E-07
zc3h12c.S	3.49	9.16E-11
ebf3.S	3.48	1.34E-07
tmem178b.S	3.46	6.70E-12
clvs1.L	3.45	5.97E-06
tuba1b.L	3.45	3.53E-12
capn6.L	3.44	1.18E-07
pigz.L	3.44	3.13E-06
stk32a.L	3.44	1.28E-05
cbfa2t3.S	3.43	7.75E-08
dnajc6.L	3.43	3.53E-08
slc18a3.L	3.42	2.73E-05
elavl3.L	3.41	4.38E-08
six1.S	3.41	1.64E-06
hes5.2.L	3.39	7.56E-07
tox2.S	3.39	6.56E-12
b4galnt1.S	3.38	5.03E-10
ulk1.L	3.38	4.71E-12
arid1b.L	3.37	1.17E-26
kcnj4.S	3.34	2.02E-07
erfl.S	3.32	6.05E-11
fitm1.S	3.32	1.45E-06
npr2.S	3.32	1.16E-08
tmem35a.L	3.31	1.27E-06
gfra1.S	3.30	6.38E-09

Neurog2 + Co-MO vs CC		
gene	log2FC	padj
prkce.S	3.30	1.73E-16
rpp25.L	3.30	5.17E-05
amph.L	3.29	1.52E-05
slc3a2.L	3.29	6.56E-08
LOC121394714	3.28	4.13E-17
gabarapl1.S	3.27	1.20E-14
efna5.S	3.26	1.06E-13
sox11.L	3.26	8.18E-13
mmp28.L	3.25	1.04E-05
cacnb1.S	3.24	6.12E-05
adcyap1.S	3.22	1.31E-04
arid1b.S	3.22	6.64E-17
ulk1.S	3.22	5.14E-11
zc3h12c.L	3.22	2.35E-13
abcb9.L	3.21	9.91E-11
fitm1.L	3.21	2.56E-06
pcdh9.L	3.21	6.03E-11
rufy3.S	3.21	3.76E-05
hmx1.L	3.20	7.66E-05
runx1t1.L	3.19	2.58E-10
LOC108718307	3.18	2.90E-05
LOC108708627	3.16	5.35E-08
th.S	3.16	1.49E-05
tuba1a.L	3.16	7.54E-12
ephb1.L	3.14	6.52E-12
olig3.S	3.13	1.13E-04
amigo1.S	3.12	1.36E-04
scn2a.L	3.12	4.44E-07
ap3b2.L	3.11	1.79E-05
dcx.L	3.10	1.03E-06
map1b.L	3.10	1.59E-04
tlx3.S	3.10	1.80E-04
onecut2.S	3.09	4.07E-06
cda.S	3.08	2.71E-04
dbndd1.L	3.08	7.17E-06
sox2.L	3.08	1.80E-06
rassf4.L	3.07	1.12E-07
kcnq3.S	3.05	1.63E-06
nptxr.S	3.05	3.02E-04
tmem178.2.L	3.03	2.64E-08
dpysl4.S	3.02	3.47E-05
sv2b.L	3.01	2.95E-04
scn1a.S	3.01	2.60E-04
snap25.S	3.00	3.34E-04
phox2a.S	2.99	6.64E-09
kif26a.S	2.98	9.00E-08
dnm1.L	2.97	5.03E-04
rtbdn.L	2.97	4.63E-05
nol4.L	2.96	2.93E-09
pdk4.S	2.96	9.96E-19
cpe.S	2.95	1.03E-05
xfrp	2.93	3.58E-17
irx1.L	2.90	1.17E-07
slc16a9.L	2.90	1.09E-06
cbfb.L	2.89	4.68E-11
lrfn1.1.S	2.89	1.11E-04
hs3st3a1.S	2.88	4.05E-09
reep1.L	2.88	4.31E-04
mospd1.L	2.86	4.82E-10
hes5.3.L	2.85	1.89E-08
prdm14.S	2.85	3.99E-04
hes5.5.L	2.84	1.16E-09
pou2f2.S	2.84	2.30E-05
pou4f4.S	2.84	1.06E-03
egln2.L	2.83	4.03E-07
lhx5.L	2.82	4.49E-06
thy1.L	2.82	2.86E-04
zeb2.S	2.82	2.70E-06
nkain4.L	2.81	4.13E-07

Appendix 6.2 Downregulated DEGs: Neurog2 + Co-MO versus CC

Neurog2 + Co-MO vs CC		
gene	**log2FC**	**padj**
bix1.1.L	-2.42	1.42E-05
h4c1.L	-2.40	9.88E-03
bix1.3.L	-1.97	2.33E-02
LOC121403682	-1.92	3.73E-02
sync.S	-1.87	7.83E-03
cd63l.L	-1.84	2.67E-02
cdca8.S	-1.80	4.36E-04
cyp27a1	-1.73	4.31E-03
angptl5.L	-1.71	6.06E-03
LOC121398067	-1.69	4.13E-02
tubal3.2.L	-1.64	2.01E-02
unc93a.2.L	-1.62	1.78E-02
gpr143.L	-1.62	4.27E-04
kit.L	-1.59	4.49E-03
rpn2.S	-1.58	1.28E-02
rpn2.L	-1.55	6.23E-04
frem3.L	-1.55	2.39E-02
klf2.L	-1.53	1.36E-02
b3galt5.L	-1.51	4.11E-02
znf451.L	-1.50	3.58E-02
oat.1.L	-1.49	5.43E-08
LOC108711622	-1.47	4.43E-04
tns2.S	-1.38	4.73E-03
gata5.S	-1.38	4.61E-02
tubal3.1.S	-1.37	3.09E-02
csta.L	-1.36	7.35E-03
slc2a10.S	-1.35	1.59E-02
comt.L	-1.35	2.69E-02
klf2.S	-1.34	4.12E-02
cdh15.L	-1.30	6.80E-03
cdca7.S	-1.28	8.53E-03
ccne2.L	-1.23	7.43E-03
sec14l3.S	-1.20	3.80E-02
bmp7.2.L	-1.20	1.19E-02
tesk1.L	-1.19	4.67E-02
sec24d.S	-1.19	1.78E-02
e2f7.L	-1.18	3.81E-06
cisd1.L	-1.18	3.87E-02
rrm2b.S	-1.17	3.13E-03
LOC108701166	-1.17	1.80E-04
kit.S	-1.17	2.81E-02
tll1.L	-1.15	8.34E-03
apcdd1.L	-1.14	8.65E-03
dhx9.S	-1.13	2.30E-04
ppp1r3c.2.S	-1.12	1.19E-02
faah.1.S	-1.11	9.68E-03
e2f8.L	-1.10	3.19E-04
slc17a9.L	-1.09	4.80E-02
agr2.S	-1.08	4.20E-02
pclaf.S	-1.07	3.33E-02
dmrt2.L	-1.07	2.74E-02
ephb3.S	-1.05	1.06E-02
gk.L	-1.02	3.69E-04
atad2.S	-1.02	3.75E-03
prkd1.S	-1.01	1.31E-02
rock1.L	-1.00	2.19E-03

Appendix 6.3 Gene Ontology analysis of upregulated DEGs: Neurog2 + Co-MO versus CC.

Shown are the top 10 enriched Biological Processes, the genes identified in this term and sorted by enrichment FDR.

1. Nervous system development 4.9E-39
hecw1 gas7 mapk8ip2 fyn rufy3 arid1b nexmif pik3cb cyfip2 ngfr kif26a myo9a ndst1 pak3 dcx fgfr1 map2 cbfa2t2 epb41l3 gnao1 atrn lhx5 sema6a stx1b slc8a3 sall4 jag1 eya1 aplp1 rab3a neurl1 zmiz1 ppp1r9b pmp22 mdk cep85l dpysl3 dbn1 apc2 ccdc88a epha4 dock7 mycl b4galt2 nrp2 klf7 onecut2 neurod4 prex1 chst8 sox4 efnb2 six1 zc4h2 bcl11b chn1 mnx1 plxna3 map1b snap25 nes tspan2 lrp4 msi1 epha7 rapgef5 scn2a stxbp1 tubb2b sulf1 ppp3ca srrm4 tcf12 adcyap1 rnf165 akt1 dmrta2 barhl2 syt2 pomgnt2 ank2 sfrp2 cplx2 notch1 glud1 ncam1 pcdh15 dpysl4 gfra1 pou4f1 prdm8 thy1 robo3 ephb1 ca10 fzd7 kif5a zic3 ssbp3 mmp14 auts2 ppp1r9a kalrn shc1 sh2b2 tal1 elavl4 draxin ntng1 neurod1 nfasc plxnb1 bsn tlx3 cited2 dlc1 lrfn5 phox2a drgx dact1 avpr1a dchs1 rbfox3 shox2 ror2 vxn zeb2 robo1 dclk2 pfkfb3 irx1 emb kcnk3 nhlh1 insm1 sez6l2 lrrn1 rims2 sox11 ulk1 olig3 irx3 neurog2 th fzd2 s1pr5 bhlhe22 tmem132e sox2 amigo1 rgma pcdh9 efna5 pou3f2 prkg1 inka1 zfp36l1 pou3f1 irs2 hmx3 pcdh18 elavl3 lpar1 ncoa6 tox olig2 scrt2 skor2 tmeff1 tubb3 glis2 smn1 dll1 myt1 marcks

2. Neuron differentiation 6.8E-33
hecw1 gas7 mapk8ip2 fyn rufy3 pik3cb cyfip2 ngfr myo9a pak3 dcx fgfr1 map2 cbfa2t2 epb41l3 gnao1 lhx5 sema6a stx1b jag1 eya1 rab3a neurl1 zmiz1 ppp1r9b pmp22 mdk dpysl3 dbn1 ccdc88a epha4 dock7 mycl nrp2 klf7 onecut2 neurod4 prex1 sox4 efnb2 six1 zc4h2 bcl11b chn1 mnx1 plxna3 map1b snap25 tspan2 lrp4 epha7 stxbp1 tubb2b ppp3ca srrm4 tcf12 adcyap1 rnf165 akt1 dmrta2 barhl2 syt2 sfrp2 notch1 ncam1 pcdh15 dpysl4 gfra1 pou4f1 thy1 robo3 ephb1 fzd7 kif5a auts2 ppp1r9a kalrn shc1 tal1 elavl4 draxin ntng1 neurod1 nfasc plxnb1 tlx3 phox2a drgx shox2 ror2 vxn robo1 dclk2 irx1 emb insm1 rims2 sox11 ulk1 olig3 irx3 neurog2 th fzd2 s1pr5 bhlhe22 tmem132e sox2 amigo1 rgma efna5 pou3f2 prkg1 irs2 lpar1 tox olig2 skor2 tmeff1 tubb3 dll1

3. Generation of neurons 1.7E-31
hecw1 gas7 mapk8ip2 fyn rufy3 nexmif pik3cb cyfip2 ngfr myo9a pak3 dcx fgfr1 map2 cbfa2t2 epb41l3 gnao1 lhx5 sema6a stx1b jag1 eya1 rab3a neurl1 zmiz1 ppp1r9b pmp22 mdk cep85l dpysl3 dbn1 ccdc88a epha4 dock7 mycl nrp2 klf7 onecut2 neurod4 prex1 sox4 efnb2 six1 zc4h2 bcl11b chn1 mnx1 plxna3 map1b snap25 tspan2 lrp4 epha7 stxbp1 tubb2b ppp3ca srrm4 tcf12 adcyap1 rnf165 akt1 dmrta2 barhl2 syt2 pomgnt2 sfrp2 notch1 ncam1 pcdh15 dpysl4 gfra1 pou4f1 thy1 robo3 ephb1 fzd7 kif5a auts2 ppp1r9a kalrn shc1 tal1 elavl4 draxin ntng1 neurod1 nfasc plxnb1 tlx3 phox2a drgx shox2 ror2 vxn robo1 dclk2 irx1 emb insm1 rims2 sox11 ulk1 olig3 irx3 neurog2 th fzd2 s1pr5 bhlhe22 tmem132e sox2 amigo1 rgma efna5 pou3f2 prkg1 irs2 lpar1 tox olig2 scrt2 skor2 tmeff1 tubb3 dll1

4. Neurogenesis 2.4E-31
hecw1 gas7 mapk8ip2 fyn rufy3 nexmif pik3cb cyfip2 ngfr myo9a pak3 dcx fgfr1 map2 cbfa2t2 epb41l3 gnao1 lhx5 sema6a stx1b slc8a3 jag1 eya1 rab3a neurl1 zmiz1 ppp1r9b pmp22 mdk cep85l dpysl3 dbn1 ccdc88a epha4 dock7 mycl nrp2 klf7 onecut2 neurod4 prex1 sox4 efnb2 six1 zc4h2 bcl11b chn1 mnx1 plxna3 map1b snap25 tspan2 lrp4 epha7 stxbp1 tubb2b ppp3ca srrm4 tcf12 adcyap1 rnf165 akt1 dmrta2 barhl2 syt2 pomgnt2 sfrp2 notch1 ncam1 pcdh15 dpysl4 gfra1 pou4f1 prdm8 thy1 robo3 ephb1 fzd7 kif5a mmp14 auts2 ppp1r9a kalrn shc1 tal1 elavl4 draxin ntng1 neurod1 nfasc plxnb1 tlx3 phox2a drgx dchs1 shox2 ror2 vxn robo1 dclk2 irx1 emb insm1 rims2 sox11 ulk1 olig3 irx3 neurog2 th fzd2 s1pr5 bhlhe22 tmem132e sox2 amigo1 rgma efna5 pou3f2 prkg1 pou3f1 irs2 lpar1 tox olig2 scrt2 skor2 tmeff1 tubb3 dll1

5. Neuron development 1.7E-24
hecw1 gas7 mapk8ip2 fyn rufy3 pik3cb cyfip2 ngfr myo9a pak3 dcx map2 cbfa2t2 epb41l3 gnao1 sema6a stx1b rab3a neurl1 zmiz1 ppp1r9b pmp22 mdk dpysl3 dbn1 ccdc88a epha4 dock7 nrp2 klf7 onecut2 neurod4 prex1 efnb2 bcl11b chn1 mnx1 plxna3 map1b snap25 tspan2 lrp4 epha7 stxbp1 tubb2b ppp3ca srrm4 adcyap1 rnf165 akt1 barhl2 syt2 sfrp2 notch1 ncam1 pcdh15 dpysl4 gfra1 pou4f1 thy1 robo3 ephb1 kif5a auts2 ppp1r9a kalrn shc1 elavl4 draxin

ntng1 neurod1 nfasc plxnb1 drgx shox2 ror2 robo1 dclk2 emb insm1 rims2 ulk1 th fzd2 tmem132e amigo1 rgma efna5 pou3f2 prkg1 irs2 lpar1 tox skor2 tmeff1 tubb3

6. Cell morphogenesis 2.19E-23
hecw1 gas7 mapk8ip2 fyn rufy3 plekho1 pik3cb cyfip2 ngfr myo9a pak3 dcx map2 epb41l3 cass4 atrn sema6a fgd1 arhgef18 rab3a atrnl1 mdk dbn1 rnd3 epha4 dock7 nrp2 klf7 prex1 efnb2 bcl11b chn1 mnx1 plxna3 map1b nes lrp4 epha7 stxbp1 tubb2b ppp3ca rnf165 wtip barhl2 syt2 prdm14 notch1 fam171a1 ncam1 pcdh15 dpysl4 gfra1 pou4f1 thy1 robo3 ephb1 fzd7 kif5a fmnl2 auts2 ppp1r9a kalrn shc1 tal1 elavl4 draxin ntng1 cdc42ep3 nfasc plxnb1 dlc1 drgx dchs1 shox2 robo1 emb slc26a5 rims2 ulk1 cdc42ep4 amigo1 rgma efna5 pou3f2 irs2 lpar1 skor2 tmeff1 tubb3

7. Neuron projection development 1.19E-22
hecw1 gas7 mapk8ip2 fyn rufy3 pik3cb cyfip2 ngfr myo9a pak3 dcx map2 cbfa2t2 epb41l3 gnao1 sema6a stx1b rab3a neurl1 ppp1r9b pmp22 mdk dpysl3 dbn1 ccdc88a epha4 dock7 nrp2 klf7 prex1 efnb2 bcl11b chn1 mnx1 plxna3 map1b snap25 tspan2 lrp4 epha7 stxbp1 tubb2b ppp3ca adcyap1 rnf165 akt1 barhl2 syt2 sfrp2 notch1 ncam1 pcdh15 dpysl4 gfra1 pou4f1 thy1 robo3 ephb1 kif5a auts2 ppp1r9a kalrn shc1 elavl4 draxin ntng1 nfasc plxnb1 drgx shox2 ror2 robo1 emb rims2 ulk1 amigo1 rgma efna5 pou3f2 prkg1 irs2 lpar1 tox skor2 tmeff1 tubb3

8. Cell projection morphogenesis 5.5E-22
hecw1 gas7 mapk8ip2 fyn rufy3 plekho1 pik3cb cyfip2 ngfr myo9a pak3 dcx map2 epb41l3 sema6a rab3a mdk dbn1 epha4 dock7 nrp2 klf7 efnb2 bcl11b chn1 mnx1 plxna3 map1b nes lrp4 epha7 stxbp1 tubb2b ppp3ca rnf165 barhl2 syt2 notch1 ncam1 dpysl4 gfra1 pou4f1 thy1 robo3 ephb1 kif5a auts2 ppp1r9a kalrn shc1 elavl4 draxin ntng1 nfasc plxnb1 drgx shox2 robo1 emb rims2 ulk1 amigo1 rgma efna5 pou3f2 irs2 skor2 tmeff1 tubb3

9. Cellular component morphogenesis 9.1E-22
hecw1 gas7 mapk8ip2 fyn rufy3 plekho1 pik3cb cyfip2 ngfr myo9a pak3 dcx map2 edn1 epb41l3 sema6a rab3a pmp22 mdk dbn1 epha4 dock7 nrp2 klf7 efnb2 bcl11b chn1 mnx1 plxna3 map1b nes lrp4 pdgfra epha7 stxbp1 tubb2b ppp3ca rnf165 barhl2 syt2 ank2 notch1 ncam1 dpysl4 gfra1 pou4f1 thy1 robo3 ephb1 kif5a auts2 ppp1r9a kalrn shc1 elavl4 draxin ntng1 nfasc plxnb1 drgx shox2 robo1 emb rims2 ulk1 amigo1 rgma efna5 pou3f2 irs2 myh6 skor2 tmeff1 tubb3

10. Cell part morphogenesis 1.6E-21
hecw1 gas7 mapk8ip2 fyn rufy3 plekho1 pik3cb cyfip2 ngfr myo9a pak3 dcx map2 epb41l3 sema6a rab3a mdk dbn1 epha4 dock7 nrp2 klf7 efnb2 bcl11b chn1 mnx1 plxna3 map1b nes lrp4 epha7 stxbp1 tubb2b ppp3ca rnf165 barhl2 syt2 notch1 ncam1 dpysl4 gfra1 pou4f1 thy1 robo3 ephb1 kif5a auts2 ppp1r9a kalrn shc1 elavl4 draxin ntng1 nfasc plxnb1 drgx shox2 robo1 emb rims2 ulk1 amigo1 rgma efna5 pou3f2 irs2 skor2 tmeff1 tubb3

Appendix 6.4 Top 210 upregulated DEGs: Neurog2 + zc3h12c.S-MO versus CC.

Neurog2 + Zc3h12c-MO vs CC		
gene	log2FC	padj
neurog2.L	7.63	2.52E-84
neurod4.S	7.12	6.10E-56
neurod4.L	7.10	2.13E-56
nhlh1.S	6.98	1.16E-39
stxbp1.S	6.80	3.47E-45
LOC108703481	6.52	1.80E-59
neurod1.L	6.40	2.19E-29
celf3.S	6.39	1.06E-51
zc3h12c.S	6.29	1.04E-35
ebf2.L	6.17	6.62E-35
LOC121395160	6.07	2.20E-26
celf3.L	6.02	6.87E-50
neurod1.S	5.99	4.92E-25
onecut2.L	5.84	7.08E-30
spx1.S	5.71	4.88E-20
drgx.L	5.70	1.41E-28
map2.S	5.68	1.30E-31
hes5.2.L	5.64	1.06E-19
gh1.S	5.54	1.94E-17
LOC108702678	5.53	1.89E-21
LOC108714640	5.43	1.17E-29
LOC108716930	5.41	3.17E-29
hbg1.L	5.39	1.64E-23
LOC108717456	5.37	4.37E-26
nes.S	5.36	2.22E-21
ebf2.S	5.34	6.22E-21
abca5.L	5.32	3.78E-21
LOC108715419	5.28	6.24E-24
elavl4.L	5.24	1.09E-25
nhlh1.L	5.22	7.55E-19
myo10.2.S	5.17	1.59E-26
olig2.S	5.17	3.79E-21
dlk2.L	5.11	1.05E-13
maneal.L	5.10	6.36E-26
LOC108695382	5.09	6.75E-24
fitm1.S	5.07	7.14E-16
kank2.L	5.07	9.30E-25
nyx.S	5.06	1.79E-13
bhlhe22.S	5.04	4.83E-19
dpysl3.L	5.01	1.14E-29
nova2.L	5.01	1.15E-27
xfrp	5.01	1.59E-51
sag.L	5.00	2.22E-21
zc3h12c.L	4.93	5.89E-32
LOC108709437	4.89	2.14E-23
LOC108709557	4.78	2.77E-17
MGC53786	4.73	6.36E-17
dbn1.S	4.69	2.01E-34
LOC108708225	4.67	4.77E-16
shd.L	4.67	3.65E-18
prdm14.L	4.66	2.88E-16
slc43a2.S	4.65	3.67E-22
gabarapl1.S	4.64	5.71E-30
capn6.L	4.61	3.59E-14
kcnj9.L	4.60	1.38E-14
pdk4.L	4.60	7.47E-26
pou4f4.L	4.60	7.77E-18
st18.L	4.60	3.09E-17
bhlhe22.L	4.56	6.98E-14
hes2.L	4.52	7.28E-14
drgx.S	4.51	5.45E-21
LOC108699846	4.49	1.20E-20
pou4f1.L	4.48	8.79E-17
hes5.4.L	4.47	6.58E-26
LOC108710959	4.45	1.79E-21
cacna2d1.L	4.43	2.30E-23
LOC108716156	4.43	9.81E-10
mxi1.S	4.36	1.01E-14
rab3b.L	4.36	5.42E-20
ulk1.L	4.35	2.05E-20

Neurog2 + Zc3h12c-MO vs CC		
gene	log2FC	padj
sez6l2.S	4.34	3.51E-11
ebf3.L	4.30	6.66E-11
thy1.L	4.30	1.75E-10
LOC108712815	4.28	3.34E-15
tlx3.L	4.28	2.29E-12
prph.S	4.26	3.00E-13
hes6.2.S	4.25	6.20E-09
zic3.L	4.23	5.34E-15
LOC108699342	4.21	2.05E-18
des.1.L	4.20	1.38E-15
plekhg4.L	4.20	2.80E-21
adamtsl1.2.L	4.18	3.06E-13
LOC108707171	4.14	6.45E-12
map2.L	4.14	6.06E-22
LOC108697150	4.13	1.90E-11
hes5.1.L	4.12	1.10E-17
cbfa2t3.S	4.09	1.72E-11
faxc.L	4.09	3.16E-18
LOC108717058	4.08	2.01E-33
pou5f3.2.S	4.08	4.02E-18
pros1.S	4.08	1.85E-23
LOC108712610	4.07	2.41E-10
tubb3.L	4.07	8.58E-12
hes5.2.S	4.06	1.67E-09
tcf15.S	4.06	1.45E-09
ulk1.S	4.05	8.64E-18
erfl.S	4.03	1.72E-16
LOC108715224	4.03	2.59E-16
sez6l2.L	4.03	2.44E-09
runx1t1.L	4.00	1.46E-16
tubb2b.S	4.00	3.54E-11
lhx5.L	3.99	1.46E-12
ptgds.S	3.97	9.01E-11
LOC108709469	3.96	5.02E-10
rufy2.L	3.94	3.05E-11
tspan18.S	3.94	5.26E-12
LOC121398234	3.92	4.65E-09
st8sia1.S	3.90	2.76E-09
kcnj4.S	3.89	1.99E-10
lgals4.1.s	3.87	1.87E-07
LOC108709888	3.87	1.18E-09
dbn1.L	3.85	2.30E-23
st8sia1.L	3.83	5.45E-14
lrrn1.L	3.81	8.46E-21
pkdcc.2.S	3.81	5.45E-12
prdm8.S	3.81	2.14E-09
otop1.S	3.79	1.05E-11
tnni1.2.L	3.79	6.14E-25
fitm1.L	3.77	4.14E-09
magi1.S	3.77	2.44E-29
dlk2.S	3.76	8.87E-08
paqr9.L	3.76	2.25E-09
map3k12.S	3.75	3.95E-10
mras.S	3.75	1.07E-23
maneal.S	3.74	8.00E-11
nkain1.L	3.74	1.33E-11
pdk4.S	3.74	5.91E-30
aplp1.S	3.72	4.65E-08
LOC108712923	3.72	1.54E-07
LOC108718984	3.72	3.47E-13
LOC108702642	3.70	1.36E-07
LOC108716321	3.70	1.23E-06
lonrf3.S	3.70	8.00E-11
tmem178.2.L	3.70	1.03E-12
LOC108699331	3.69	1.31E-06
hip1.L	3.68	6.52E-18
kcnk13.S	3.66	5.58E-07
mxra7.L	3.66	1.22E-13
pak3.L	3.66	3.19E-10
sag.S	3.66	3.83E-07

Neurog2 + Zc3h12c-MO vs CC		
gene	log2FC	padj
cbfa2t2.L	3.65	2.91E-15
ncam1.L	3.65	6.11E-14
vamp2.L	3.65	6.51E-11
b4galnt1.S	3.64	7.33E-12
map3k12.L	3.64	9.81E-10
cbfa2t2.S	3.63	4.84E-21
LOC108715866	3.63	9.92E-08
slc26a10.S	3.63	1.91E-06
barhl2.L	3.62	8.69E-07
dpysl4.L	3.61	3.11E-07
rgcc.L	3.61	1.37E-15
LOC108702728	3.60	1.07E-08
ehd2.S	3.59	2.26E-07
hbegf.S	3.58	2.11E-13
hes5.6.L	3.58	2.65E-11
sspo.L	3.57	2.84E-17
LOC108709836	3.56	7.13E-11
cttnbp2nl.L	3.55	4.65E-12
LOC108697386	3.55	1.51E-07
abcb9.L	3.54	2.45E-13
LOC108697312	3.54	1.62E-10
rnf165.L	3.54	1.42E-13
zeb2.L	3.54	5.59E-10
ankrd65.L	3.53	3.64E-11
ebf3.S	3.53	4.05E-08
ror2.S	3.50	3.68E-10
XB6050834.S	3.50	4.63E-06
insm1.L	3.49	8.00E-11
lrch2.L	3.49	7.39E-10
abhd1	3.48	1.22E-06
tmem169.L	3.47	1.78E-07
LOC108718307	3.46	1.24E-06
LOC121397699	3.45	1.64E-06
rai2.S	3.45	6.62E-11
cbfb.S	3.44	4.52E-20
pcdh18.L	3.44	5.83E-11
sh3bgr.L	3.44	8.63E-06
scg3.L	3.43	1.77E-06
slc45a1.S	3.43	2.76E-06
dact4.L	3.42	9.65E-12
slc16a9.L	3.42	1.03E-09
LOC121394714	3.41	1.14E-18
hes5.5.L	3.40	4.63E-14
nipa1.L	3.39	7.55E-19
olfml3.L	3.39	7.34E-07
hes5.1.S	3.38	1.40E-11
dcx.L	3.36	2.67E-08
LOC108707093	3.35	2.49E-08
LOC108717735	3.35	4.01E-17
necab3.L	3.35	1.67E-05
cdc42ep3.S	3.33	6.72E-14
pax3.S	3.32	1.86E-06
pex5l.S	3.32	6.16E-07
olig3.S	3.31	1.12E-05
xkr4.S	3.31	1.45E-18
hes5.5.S	3.29	2.81E-12
lrrc8e.2.L	3.29	5.03E-12
rnf151.L	3.29	6.29E-06
LOC108709233	3.28	2.25E-05
LOC108714911	3.28	2.56E-07
LOC108711130	3.27	4.88E-07
LOC108717594	3.27	1.19E-05
mtcl1.L	3.27	1.55E-09
cerk.L	3.26	5.05E-10
dnajc6.L	3.26	9.95E-08
LOC108708445	3.26	5.17E-06
LOC108718675	3.26	1.33E-05
LOC108705236	3.25	2.65E-10
pik3r3.S	3.25	2.45E-14
itgb6.L	3.24	4.30E-07

Appendix 6.5 Top 210 downregulated DEGs: Neurog2 + zc3h12c.S-MO versus CC

Neurog2 + Zc3h12c-MO vs CC		
gene	log2FC	padj
LOC108711805	-3.79	1.00E-11
mmp11.L	-3.60	3.95E-11
capn13.S	-3.24	1.17E-06
heatr4.S	-3.03	6.04E-06
LOC121402204	-3.03	1.34E-12
XB5922676.S	-3.00	2.68E-12
gck.L	-2.99	5.52E-05
LOC121399357	-2.97	1.97E-06
adra2c.L	-2.92	2.91E-05
LOC108716581	-2.92	1.33E-10
atp12a.L	-2.87	4.97E-11
LOC108713766	-2.85	2.97E-17
LOC108697612	-2.84	8.90E-06
c8orf34.S	-2.83	1.57E-13
ppil6.S	-2.82	4.09E-06
arl11.L	-2.81	1.37E-05
tm4sf18.L	-2.81	1.72E-05
hoxa3.L	-2.80	3.29E-05
LOC108714021	-2.78	8.59E-05
LOC108697674	-2.76	4.70E-10
styk1.L	-2.76	6.61E-05
XB5733233.S	-2.76	2.70E-04
LOC108713720	-2.75	6.83E-10
map2k6.L	-2.75	7.11E-10
LOC108711814	-2.73	2.21E-07
LOC121403682	-2.72	1.36E-04
apobec2.L	-2.71	6.88E-04
LOC108717285	-2.70	7.45E-05
sstr5.S	-2.70	6.45E-12
XB5774338.L	-2.69	4.05E-16
stoml3.L	-2.68	8.27E-06
fbxw10.L	-2.67	2.67E-05
LOC108696918	-2.67	1.33E-04
sh3tc2.L	-2.67	1.68E-04
LOC108716578	-2.66	2.34E-04
b4galt4.L	-2.65	4.14E-19
LOC108716766	-2.64	2.69E-08
LOC108711781	-2.63	7.44E-05
psca.S	-2.62	6.81E-05
LOC108711807	-2.61	2.38E-05
scn3b.L	-2.60	7.31E-11
LOC108712705	-2.58	1.53E-14
nr2f5.S	-2.58	6.36E-09
fbxo43.L	-2.57	1.48E-04
dlec1.L	-2.56	1.95E-08
stoml1.L	-2.56	7.36E-05
LOC121394509	-2.55	1.38E-14
LOC108704219	-2.54	1.06E-03
LOC108716526	-2.54	5.92E-04
sp7.L	-2.53	1.91E-13
LOC108701456	-2.52	1.40E-08
gjb2.L	-2.51	6.05E-05
katnip.L	-2.51	4.94E-08
LOC108697575	-2.51	7.35E-05
LOC108699634	-2.51	3.58E-04
steap1.L	-2.50	1.55E-09
dio1.L	-2.49	5.70E-04
LOC108699390	-2.49	2.10E-07
LOC108715714	-2.49	4.99E-05
srpx2.L	-2.49	1.19E-03
tm9sf2.L	-2.48	6.97E-16
dzip1l.S	-2.47	3.05E-11
nwd1.L	-2.47	4.03E-04
slc25a45.L	-2.47	1.71E-04
arhgef37.S	-2.46	4.79E-10
hoxa2.S	-2.46	3.45E-04
LOC108711793	-2.45	5.60E-08
prxl2c.S	-2.45	1.45E-06
tmem38b.L	-2.45	3.29E-10
anxa9.L	-2.44	5.88E-12

Neurog2 + Zc3h12c-MO vs CC		
gene	log2FC	padj
ccdc24.L	-2.43	4.31E-04
LOC108704223	-2.42	1.22E-06
sox21.L	-2.42	7.67E-07
tmc5.L	-2.42	1.76E-06
vwa5a.S	-2.42	5.22E-14
elovl2.L	-2.41	3.90E-09
fucolectin.S	-2.41	1.89E-13
LOC108697308	-2.41	2.10E-05
LOC121401671	-2.41	2.41E-03
gdpd2.L	-2.40	8.27E-09
LOC108712707	-2.40	5.92E-10
LOC108718741	-2.40	2.79E-04
cd38.L	-2.38	1.60E-04
ankar.L	-2.37	2.06E-04
ca2.L	-2.36	9.02E-08
hoxa1.L	-2.36	3.51E-07
klf4.L	-2.36	8.70E-04
XB5864179.L	-2.36	3.71E-04
itln1.L	-2.35	8.88E-09
b3gnt7.L	-2.34	4.14E-19
gal3st1.S	-2.34	2.50E-03
tsga10.L	-2.34	2.43E-07
cdkl2.L	-2.33	5.36E-04
map2k3	-2.33	9.10E-12
sec24d.S	-2.33	1.14E-09
LOC108701370	-2.32	3.20E-04
LOC108714608	-2.32	3.80E-06
LOC108718716	-2.32	2.27E-05
ribc1.L	-2.32	6.99E-08
spaca9.L	-2.32	7.67E-04
cdhr4.L	-2.31	1.25E-03
cyp2d6.S	-2.31	6.00E-04
gjb3l.S	-2.31	3.33E-04
LOC121399341	-2.31	2.28E-03
naalad2.S	-2.31	1.05E-06
XB5717875.L	-2.31	1.49E-05
aldh1l1.L	-2.30	1.37E-08
atp6ap1.1.S	-2.30	2.91E-10
c9orf135.S	-2.30	8.15E-04
ca2.S	-2.30	3.24E-04
capn9.L	-2.30	3.54E-07
g67.L	-2.30	9.31E-04
LOC121395445	-2.30	3.80E-03
tm4sf1.L	-2.30	1.53E-03
add2.S	-2.29	7.80E-07
kdelr3.S	-2.29	2.33E-05
LOC108719860	-2.29	2.29E-05
LOC121393657	-2.29	3.86E-03
LOC121396878	-2.29	8.28E-06
prr15.S	-2.29	8.64E-04
psca.L	-2.29	1.55E-03
sptlc3.L	-2.29	2.81E-04
astl2d.1.L	-2.28	1.35E-12
dgat1.L	-2.28	3.94E-18
LOC108714685	-2.28	1.57E-03
LOC108719843	-2.28	1.00E-03
MGC116505	-2.28	1.65E-03
gk.L	-2.27	8.46E-21
naalad2.L	-2.27	1.53E-09
sybu.S	-2.27	5.43E-04
dnah9.S	-2.26	1.96E-05
LOC108717135	-2.26	2.05E-03
bok.S	-2.25	6.66E-04
gdpd1.L	-2.25	3.17E-09
LOC108717017	-2.25	1.24E-03
LOC121398087	-2.25	5.53E-03
LOC121400504	-2.25	1.90E-03
mcm6.2.L	-2.25	4.02E-10
MGC68910	-2.25	9.30E-09
c6orf118.S	-2.24	2.75E-03

Neurog2 + Zc3h12c-MO vs CC		
gene	log2FC	padj
LOC108701177	-2.24	2.12E-07
LOC108708530	-2.24	3.54E-07
LOC108712708	-2.24	1.72E-03
sp7.S	-2.24	6.98E-14
slc4a9.L	-2.23	2.98E-03
gss.L	-2.22	4.03E-07
LOC108699464	-2.22	3.14E-08
LOC108699929	-2.22	2.42E-08
LOC108708418	-2.22	2.07E-03
LOC108719082	-2.22	1.16E-04
sec14l3.S	-2.22	1.69E-07
slc26a4.3.L	-2.22	4.20E-03
tll1.S	-2.22	1.08E-07
errfi1.S	-2.21	1.44E-04
pou2f3.L	-2.21	3.60E-14
LOC108698436	-2.20	6.56E-04
LOC108709441	-2.20	1.64E-12
mgat4a.S	-2.20	1.47E-03
opn6a.S	-2.20	5.59E-03
pax7.S	-2.20	2.90E-03
pip5kl1.S	-2.20	7.32E-04
sptlc3.S	-2.19	4.44E-10
LOC108696419	-2.18	1.89E-03
LOC108699425	-2.18	3.25E-03
LOC108713173	-2.18	1.35E-08
nipal1.S	-2.18	4.09E-03
otogl2.L	-2.18	4.07E-11
vstm5.L	-2.18	9.88E-04
b4galt1l.L	-2.17	3.03E-07
LOC108698170	-2.17	8.13E-03
LOC108698731	-2.17	2.68E-05
LOC108713813	-2.17	6.72E-04
naga.L	-2.17	1.82E-03
ppp4r4.L	-2.17	1.38E-06
ak1.L	-2.16	7.56E-08
ccdc107.L	-2.16	5.07E-06
clic1.S	-2.16	2.82E-04
LOC108706691	-2.16	1.15E-05
smc2.S	-2.16	7.44E-04
tmprss2.9.L	-2.16	2.04E-03
vill.L	-2.16	2.13E-09
cfap100.L	-2.15	1.53E-08
elmo3.L	-2.15	3.70E-06
gzmak.L	-2.15	8.67E-03
LOC108697608	-2.15	1.48E-04
LOC108699553	-2.15	1.50E-03
LOC108707908	-2.15	1.67E-05
LOC108709769	-2.15	1.24E-06
LOC108718623	-2.15	1.48E-14
lpcat4.L	-2.15	5.75E-05
mcidas.L	-2.15	7.58E-05
prkcd.L	-2.15	3.60E-14
rgs9bpl.L	-2.15	4.09E-03
rpn2.S	-2.15	2.90E-05
slc18a1.S	-2.15	8.42E-09
armh1.L	-2.14	1.67E-04
c20orf85.S	-2.14	2.70E-03
LOC108702843	-2.14	1.67E-07
mcm2.S	-2.14	5.59E-04
pdcl3.S	-2.14	4.59E-03
XB5872372.S	-2.14	8.81E-07
fermt1.S	-2.13	3.21E-06
gas6.S	-2.13	1.59E-03
LOC108700739	-2.13	4.67E-03
odf3.L	-2.13	2.59E-07
rhobtb2.L	-2.13	8.19E-06
scn3b.S	-2.13	1.14E-02
ak8.L	-2.12	1.82E-04
atp2c2.S	-2.12	2.34E-03
LOC108714161	-2.12	1.77E-06

Appendix 6.6 Gene Ontology analysis of upregulated DEGs: Neurog2 + zc3h12c.S-MO versus CC.

Shown are the top 10 enriched Biological Processes, the genes identified in this term and sorted by enrichment FDR.

1. Nervous system development 3.7E-22
cyp51a1 hecw1 syn1 stmn4 gab2 hdac9 arid1b gpc1 bcas1 rora hes2 fgf10 pak3 dcx map2 cbfa2t2 lhx5 phgdh slc8a3 eya1 stk3 prx aplp1 rab3a lhx3 abca2 ppp1r9b pmp22 mdk tcirg1 cep85l tulp1 dpysl3 dbn1 unc5a epha4 arhgef2 mycl satb2 onecut2 cdkn2c neurod4 obsl1 efnb2 barhl1 six1 zc4h2 ell3 dll4 ldlr kif1a mnx1 snap25 nes gdf11 pax3 rapgef5 scn2a bin1 stxbp1 kiaa0319 tubb2b prickle1 srrm4 adcyap1 rnf165 dmrta2 barhl2 crabp2 vash2 syt2 pomgnt2 lrig1 sfrp2 cplx2 nfib notch1 ncam1 doc2a pcdh15 dpysl4 gfra1 pou4f1 prdm8 thy1 robo4 ephb1 ca10 fzd7 zic3 mmp14 auts2 gdpd5 sh2b2 elavl4 ntng1 neurod1 ihh eomes nkx6-1 hesx1 plxnb1 hhip tlx3 cited2 dlc1 pcdh19 phox2a otx2 drgx dchs1 rbfox3 ror2 vxn kcnab1 zeb2 lingo1 gsx1 p2ry1 ywhag dclk2 irx1 emb kcnk3 nhlh1 bcl2 gap43 insm1 lingo2 sez6l2 lrrn1 rims2 cdk5r1 sox11 ulk1 olig3 kcnj10 grb2 neurog2 s1pr5 bhlhe22 sox2 ntm nog tbx1 pcdh9 efna5 pou3f2 zfp36l1 pou3f1 ptch1 irs2 pcdh18 ppia elavl3 ntrk1 tox pjvk olig2 scrt2 skor2 tmeff1 tubb3 lhx1 glis2 smn1 dll1 plppr1 pla2g10 myt1 wnt3

2. Neurogenesis 4.25E-20
hecw1 syn1 stmn4 gab2 hdac9 gpc1 rora hes2 fgf10 pak3 dcx map2 cbfa2t2 lhx5 phgdh slc8a3 eya1 prx rab3a lhx3 abca2 ppp1r9b pmp22 mdk cep85l tulp1 dpysl3 dbn1 unc5a epha4 arhgef2 mycl satb2 onecut2 cdkn2c neurod4 obsl1 efnb2 barhl1 six1 zc4h2 ell3 dll4 ldlr kif1a mnx1 snap25 bin1 stxbp1 kiaa0319 tubb2b srrm4 adcyap1 rnf165 dmrta2 barhl2 crabp2 vash2 syt2 pomgnt2 sfrp2 nfib notch1 ncam1 pcdh15 dpysl4 gfra1 pou4f1 prdm8 thy1 robo4 ephb1 fzd7 mmp14 auts2 elavl4 ntng1 neurod1 ihh nkx6-1 plxnb1 hhip tlx3 phox2a otx2 drgx dchs1 ror2 vxn lingo1 gsx1 p2ry1 ywhag dclk2 irx1 emb bcl2 gap43 insm1 rims2 cdk5r1 sox11 ulk1 olig3 kcnj10 grb2 neurog2 s1pr5 bhlhe22 sox2 ntm nog efna5 pou3f2 pou3f1 ptch1 irs2 ppia ntrk1 tox pjvk olig2 scrt2 skor2 tmeff1 tubb3 lhx1 dll1 pla2g10 wnt3

3. Cell differentiation 2.9E-18
hecw1 tnfrsf12a syn1 stmn4 ehd2 pou2f2 gab2 ros1 hdac9 lmo3 gpc1 cbfb rora hes2 fgf10 fgf22 ap1m1 pak3 dcx map2 cbfa2t2 tp53inp2 runx1t1 rfx3 cass4 lhx5 rcor1 phgdh slc8a3 mospd1 rgcc foxf1 eya1 stk3 prx rab3a lfng lhx3 abca2 ppp1r9b pmp22 mdk calca tcirg1 stx2 cand1 cep85l asf1a tulp1 dpysl3 dbn1 unc5a itgb6 atf2 epha4 arhgef2 mycl ptch2 satb2 onecut2 rdh10 popdc2 cdkn2c neurod4 obsl1 fam210b efnb2 septin6 barhl1 srms tcf15 six1 zc4h2 hip1 ell3 dll4 myod1 cbfa2t3 ldlr gadd45g kif1a mnx1 lrp3 eda2r pyy slc6a6 lgals3 snap25 crp rbm38 aplnr pdgfra tespa1 cnmd gpnmb bin1 stxbp1 kiaa0319 tubb2b brdt prickle1 srrm4 cyp1a1 pcsk6 adcyap1 rnf165 dmrta2 barhl2 crabp2 vash2 syt2 pomgnt2 slc25a38 sfrp2 cplx2 gpc3 prdm14 nfib notch1 herc4 ncam1 fads1 pcdh15 ccdc3 dpysl4 gfra1 pou4f1 prdm8 thy1 robo4 abca5 ephb1 fzd7 gdf6 zic3 mmp14 auts2 npr2 sh2b2 elavl4 ntng1 neurod1 frzb fstl1 ihh eomes nkx6-1 tiparp hesx1 sfmbt1 plxnb1 hhip cartpt tlx3 cited2 osr2 tp53inp1 nfil3 phox2a otx2 drgx dchs1 soat2 ror2 vxn kcnab1 zeb2 lingo1 gsx1 onecut1 p2ry1 ywhag dclk2 irx1 emb dlk2 nhlh1 bcl2 gap43 insm1 ccr9 cd34 btc ctbp2 rims2 cdk5r1 sox11 ulk1 olig3 kcnj10 grb2 neurog2 rnf151 alx1 s1pr5 bhlhe22 sox2 ntm lck nog tbx1 efna5 pou3f2 socs1 zfp36l1 pou3f1 mybl1 ptch1 irs2 bcr foxi2 ppia elavl3 cacna1h ada myh6 s100a10 ntrk1 tox sox18 pjvk olig2 s1pr3 scrt2 skor2 ebf2 nkx1-1 tmeff1 tubb3 pecam1 erfl lhx1 glis2 metrnl dll1 pla2g10 myt1 wnt3 gcnt2

4. Generation of neurons 5.2E-18
hecw1 syn1 stmn4 gab2 hdac9 gpc1 rora hes2 pak3 dcx map2 cbfa2t2 lhx5 phgdh eya1 rab3a lhx3 ppp1r9b pmp22 mdk cep85l tulp1 dpysl3 dbn1 unc5a epha4 arhgef2 mycl satb2 onecut2 neurod4 obsl1 efnb2 barhl1 six1 zc4h2 ell3 dll4 ldlr kif1a mnx1 snap25 bin1 stxbp1 kiaa0319 tubb2b srrm4 adcyap1 rnf165 dmrta2 barhl2 crabp2 vash2 syt2 pomgnt2 sfrp2 nfib notch1 ncam1 pcdh15 dpysl4 gfra1 pou4f1 thy1 robo4 ephb1 fzd7 auts2 elavl4 ntng1 neurod1 ihh nkx6-1 plxnb1 hhip tlx3 phox2a otx2 drgx ror2 vxn lingo1 gsx1 ywhag dclk2 irx1 emb bcl2 gap43 insm1 rims2 cdk5r1 sox11 ulk1 olig3 grb2 neurog2 s1pr5 bhlhe22 sox2 ntm nog efna5 pou3f2 ptch1 irs2 ppia ntrk1 tox pjvk olig2 scrt2 skor2 tmeff1 tubb3 lhx1 dll1 pla2g10 wnt3

5. Cellular developmental process 5.3E-18
hecw1 tnfrsf12a syn1 stmn4 ehd2 pou2f2 gab2 ros1 hdac9 lmo3 gpc1 cbfb rora hes2 fgf10 fgf22 ap1m1 pak3 dcx map2 cbfa2t2 tp53inp2 runx1t1 rfx3 cass4 mapkapk5 lhx5 rcor1 phgdh slc8a3 mospd1 rgcc foxf1 eya1 stk3 prx rab3a lfng lhx3 abca2 ppp1r9b pmp22 mdk calca tcirg1 stx2 cand1 cep85l asf1a tulp1 dpysl3 dbn1 unc5a itgb6 atf2 epha4 arhgef2 mycl ptch2 satb2 onecut2 rdh10 popdc2 cdkn2c neurod4 obsl1 fam210b efnb2 septin6 barhl1 srms tcf15 six1 zc4h2 hip1 ell3 dll4 myod1 cbfa2t3 ldlr gadd45g kif1a mnx1 lrp3 eda2r pyy slc6a6 lgals3 snap25 nes crp rbm38 aplnr pdgfra tespa1 cnmd gpnmb bin1 stxbp1 kiaa0319 tubb2b brdt prickle1 srrm4 cyp1a1 pcsk6 adcyap1 rnf165 dmrta2 barhl2 crabp2 vash2 syt2 pomgnt2 slc25a38 sfrp2 cplx2 gpc3 prdm14 nfib notch1 herc4 ncam1 fads1 pcdh15 ccdc3 dpysl4 gfra1 pou4f1 prdm8 thy1 robo4 abca5 ephb1 fzd7 gdf6 zic3 mmp14 auts2 npr2 sh2b2 elavl4 ntng1 neurod1 frzb fstl1 ihh eomes nkx6-1 tiparp hesx1 sfmbt1 plxnb1 hhip cartpt tlx3 cited2 osr2 tp53inp1 nfil3 phox2a otx2 drgx dchs1 soat2 ror2 vxn kcnab1 zeb2 lingo1 gsx1 onecut1 p2ry1 ywhag dclk2 irx1 emb dlk2 nhlh1 bcl2 gap43 insm1 ccr9 cd34 btc ctbp2 rims2 cdk5r1 sox11 ulk1 olig3 kcnj10 grb2 neurog2 rnf151 alx1 s1pr5 bhlhe22 sox2 ntm lck nog tbx1 efna5 pou3f2 socs1 zfp36l1 pou3f1 mybl1 ptch1 irs2 bcr foxi2 ppia elavl3 cacna1h ada myh6 s100a10 ntrk1 tox sox18 pjvk olig2 s1pr3 scrt2 skor2 ebf2 nkx1-1 tmeff1 tubb3 pecam1 erfl lhx1 glis2 metrnl dll1 pla2g10 myt1 wnt3 gcnt2

6. Neuron differentiation 1.2E-17
hecw1 syn1 stmn4 gab2 hdac9 gpc1 rora pak3 dcx map2 cbfa2t2 lhx5 phgdh eya1 rab3a lhx3 ppp1r9b pmp22 mdk tulp1 dpysl3 dbn1 unc5a epha4 arhgef2 mycl satb2 onecut2 neurod4 obsl1 efnb2 six1 zc4h2 dll4 kif1a mnx1 snap25 bin1 stxbp1 kiaa0319 tubb2b srrm4 adcyap1 rnf165 dmrta2 barhl2 crabp2 vash2 syt2 sfrp2 nfib notch1 ncam1 pcdh15 dpysl4 gfra1 pou4f1 thy1 robo4 ephb1 fzd7 auts2 elavl4 ntng1 neurod1 ihh nkx6-1 plxnb1 tlx3 phox2a otx2 drgx ror2 vxn lingo1 gsx1 ywhag dclk2 irx1 emb bcl2 gap43 insm1 rims2 cdk5r1 sox11 ulk1 olig3 grb2 neurog2 s1pr5 bhlhe22 sox2 ntm nog efna5 pou3f2 ptch1 irs2 ppia ntrk1 tox pjvk olig2 skor2 tmeff1 tubb3 lhx1 dll1 pla2g10 wnt3

7. Anatomical structure morphogenesis 1.7E-14
hecw1 tnfrsf12a celsr3 pik3c2a ehd2 gab2 hdac9 alx4 gpc1 rora fgf10 fgf22 pak3 dcx map2 cass4 lhx5 fgd1 rgcc foxf1 eya1 stk3 aplp1 plekha4 rab3a lmbr1 lfng lhx3 abca2 pmp22 cpe mdk tcirg1 stx2 tulp1 hbegf dbn1 unc5a amotl2 tnnc1 itgb6 rnd3 atf2 epha4 arhgef2 pik3r3 satb2 onecut2 rdh10 obsl1 efnb2 tcf15 six1 dll4 myod1 ldlr kif1a mnx1 nes mical2 aplnr pdgfra ankrd6 amhr2 pax3 pcdh8 cnmd gpnmb stxbp1 kiaa0319 tubb2b cyp1b1 prickle1 rnf165 barhl2 crabp2 vash2 syt2 lrig1 sfrp2 gpc3 prdm14 nfib notch1 ncam1 pcdh15 eps8 dpysl4 gfra1 pou4f1 thy1 robo4 ephb1 fzd7 zic3 mmp14 auts2 carmil2 vav2 elavl4 ntng1 neurod1 frzb cdc42ep3 ihh eomes nkx6-1 tiparp hesx1 plxnb1 hhip cited2 dlc1 osr2 phox2a otx2 drgx dchs1 ror2 lingo1 onecut1 p2ry1 irx1 emb bcl2 gap43 cd34 rims2 cdk5r1 sox11 ulk1 grb2 alx1 sox2 nog tbx1 efna5 pou3f2 fmnl1 zfp36l1 ptch1 irs2 sapcd2 foxi2 gcnt1 stk40 cacna1h ada myh6 s100a10 ntrk1 sox18 s1pr3 skor2 tmeff1 yjefn3 tubb3 gtf2i lhx1 dll1 pla2g10 wnt3

8. Locomotion 1.87E-14
pik3c2a gab2 hdac9 gpc1 pkn2 fgf10 fgf22 pak3 dcx rfx3 cass4 rgcc foxf1 lhx3 ppp1r9b mdk calca bin2 cep85l hbegf dpysl3 unc5a amotl2 itgb6 rnd3 epha4 arhgef2 pik3r3 satb2 onecut2 dbh efnb2 barhl1 six1 dll4 akap12 lgals3 pdgfra lrch1 gpnmb gypc kiaa0319 tubb2b cyp1b1 rnf165 barhl2 pomgnt2 sfrp2 gpc3 prdm14 nfib notch1 ncam1 eps8 dpysl4 gfra1 dst pou4f1 pstpip2 jmy thy1 robo4 ephb1 mmp14 auts2 celf3 carmil2 vav2 sdc3 ntng1 fstl1 nkx6-1 plxnb1 tlx3 cited2 dlc1 tp53inp1 otx2 drgx dchs1 slc3a2 ror2 zeb2 onecut1 p2ry1 emb prkce plekhg5 bcl2 gap43 il16 insm1 ccr9 cd34 btc fosl1 cdk5r1 olig3 grb2 alx1 lck nog tbx1 efna5 pou3f2 pros1 fmnl1 ptch1 irs2 gcnt1 ptprt ppia ada kank2 ntrk1 sox18 scrt2 tmeff1 tubb3 pecam1 lhx1 dach1 chga pla2g10 inpp5d gcnt2

9. Movement of cell or subcellular component 9.61E-14
pik3c2a gab2 hdac9 gpc1 pkn2 fgf10 fgf22 pak3 dcx map2 rfx3 cass4 rgcc foxf1 ap3b2 lhx3 ppp1r9b mdk calca bin2 cep85l hbegf dpysl3 unc5a amotl2 tnnc1 itgb6 rnd3 epha4 arhgef2 pik3r3 satb2 onecut2 dbh efnb2 barhl1 six1 dll4 kif1a akap12 lgals3 pdgfra lrch1 gpnmb bin1 gypc kiaa0319 tubb2b cyp1b1 rnf165 barhl2 arl8a pomgnt2 camk2d sfrp2 gpc3 prdm14 nfib notch1 ncam1 eps8 dpysl4 gfra1 dst pou4f1 pstpip2 jmy cacna2d1 thy1 robo4 ephb1 mmp14 auts2 celf3 carmil2 vav2 sdc3 ntng1 kcnj3 fstl1 nkx6-1 plxnb1 tlx3 cited2 dlc1 tp53inp1 otx2

drgx dchs1 slc3a2 ror2 zeb2 onecut1 p2ry1 emb prkce plekhg5 bcl2 gap43 il16 insm1 ccr9 cd34 btc cdk5r1 olig3 grb2 alx1 lck nog tbx1 efna5 pou3f2 pros1 fmnl1 ptch1 irs2 gcnt1 ptprt ppia ada kank2 myh6 ntrk1 tpm2 sox18 scrt2 tmeff1 tubb3 pecam1 lhx1 dach1 chga pla2g10 inpp5d gcnt2

10.Cell fate commitment 2.7E-12

fgf10 eya1 lhx3 arhgef2 ptch2 satb2 onecut2 six1 dll4 myod1 mnx1 dmrta2 barhl2 sfrp2 prdm14 notch1 pou4f1 fzd7 neurod1 ihh eomes tlx3 ror2 gsx1 onecut1 bcl2 gap43 olig3 sox2 tbx1 pou3f2 ptch1 tox sox18 olig2 ebf2 dll1 wnt3

Appendix 6.7 Top 210 upregulated DEGs: Neurog2 + zc3h12c.S-MO versus Neurog2 + Co-MO

Neurog2 + Z-Mo vs Neurog2 + Co-MO		
gene	log2FC	padj
spx1.S	5.66	2.51E-18
gh1.S	5.48	5.33E-16
LOC121398234	5.17	1.64E-13
abca5.L	5.01	9.53E-18
nyx.S	4.97	3.11E-12
sag.L	4.96	2.25E-19
LOC108709557	4.91	6.89E-17
LOC108708225	4.86	5.33E-16
dlk2.L	4.73	3.82E-11
cand1.L	4.72	4.31E-23
p2ry1.L	4.39	1.45E-17
kcnj9.L	4.33	2.19E-12
hes6.2.S	4.07	1.31E-07
a2ml1.S	4.04	3.03E-10
mxi1.S	3.89	4.36E-11
olfml3.L	3.83	1.11E-07
rab3b.L	3.82	5.06E-15
aplp1.S	3.82	8.83E-08
sag.S	3.81	5.04E-07
crp.L	3.74	3.01E-06
gdf11.S	3.73	7.45E-11
sspo.L	3.61	2.07E-16
itgb6.L	3.59	1.07E-07
rufy2.L	3.53	1.07E-08
mogat1.L	3.53	1.82E-12
chrm5.S	3.53	4.39E-07
ptgds.S	3.52	5.03E-08
masp2.L	3.50	7.77E-06
lrrc8e.2.L	3.50	1.56E-12
ros1.L	3.50	6.57E-06
LOC108709233	3.50	1.60E-05
slc6a6.S	3.49	1.24E-06
LOC108699468	3.46	9.99E-06
hbegf.S	3.43	1.23E-11
trim25.S	3.40	4.93E-06
bin2.S	3.36	3.61E-05
slc6a8l.S	3.35	3.59E-05
lgals4.1.s	3.35	2.38E-05
rdh5.S	3.27	6.48E-05
a2ml1.L	3.25	6.17E-05
LOC108716321	3.21	1.01E-04
ehd2.S	3.20	1.56E-05
alx1.L	3.18	1.01E-04
prss12.L	3.15	5.84E-07
fmnl1.L	3.14	3.73E-06
prx.L	3.13	1.94E-04
nudt8.L	3.12	9.04E-05
spspon.L	3.12	3.91E-07
rnf151.L	3.11	6.58E-05
glra1.S	3.07	3.79E-05
trim25.L	3.05	5.42E-06
hes2.L	3.04	2.96E-06
LOC121395234	3.02	3.55E-04
zg16.S	3.01	1.99E-04
pou5f3.2.S	3.00	2.71E-09
LOC121399870	3.00	4.04E-04
tmem272.S	3.00	5.18E-05
LOC121395171	2.99	3.44E-04
lgals3.S	2.99	6.69E-14
yjefn3.L	2.97	3.05E-05
ngb.S	2.97	4.17E-04
myod1.S	2.97	2.25E-04
ell3.L	2.97	1.32E-08
cdo1.S	2.93	6.01E-07
mcf2l.S	2.92	7.16E-09
bmerb1.L	2.91	1.35E-04
rapsn.L	2.89	1.39E-04
rps6kb2.L	2.89	8.81E-06
crip3.S	2.89	2.74E-07
alx4.L	2.88	7.34E-04

Neurog2 + Z-Mo vs Neurog2 + Co-MO		
gene	log2FC	padj
itga2b.2.L	2.88	7.74E-04
dipk1b.L	2.88	5.64E-04
tubb6.S	2.87	2.31E-04
soat2.S	2.85	6.98E-08
dlgap3.S	2.80	6.53E-04
zc3h12c.S	2.79	7.94E-08
scp2.S	2.79	1.11E-07
klf2.S	2.79	1.18E-08
LOC108711399	2.78	1.08E-03
sox18.S	2.77	7.48E-04
LOC108714911	2.77	4.75E-05
sema4d.S	2.76	8.41E-08
ptpn1.L	2.75	8.21E-04
fcn1.S	2.75	1.21E-03
ccdc3.L	2.75	1.14E-04
ncf1.S	2.72	1.69E-03
LOC121398286	2.72	6.38E-05
htr7.L	2.72	1.37E-06
smtn.S	2.69	2.26E-07
map1lc3c.L	2.68	1.55E-03
LOC121395589	2.68	2.11E-03
LOC100192369	2.68	4.91E-05
cnmd.L	2.68	4.72E-04
bix1.3.L	2.67	2.31E-04
ntm.L	2.66	3.02E-06
gtf2i.S	2.66	3.61E-05
fgf22.L	2.66	3.61E-05
LOC121398973	2.65	2.07E-03
tnfrsf12a.L	2.64	2.67E-04
timm50.S	2.64	3.35E-08
sh3bgr.L	2.63	2.25E-03
necab3.L	2.63	2.32E-03
LOC108698216	2.63	1.32E-03
ccdc106.S	2.63	1.65E-04
dpys.L	2.62	2.93E-04
c1qtnf7.S	2.61	1.28E-03
plekha4.S	2.60	4.37E-04
vstm2l.L	2.59	2.57E-04
pou5f3.2.L	2.59	3.27E-12
znrd2.L	2.58	7.72E-05
LOC108718675	2.57	1.73E-03
LOC108717594	2.57	1.90E-03
frzb.S	2.57	3.39E-03
plin2.L	2.56	1.28E-13
s6a13.S	2.56	3.09E-03
snx5.L	2.55	1.52E-12
pecam1.S	2.54	3.03E-03
dlk2.S	2.54	1.27E-03
ccna2.L	2.54	1.79E-12
slc26a10.S	2.53	3.11E-03
pkib.S	2.53	2.21E-03
gdpd5.S	2.52	1.49E-04
tp53i11.S	2.52	1.13E-04
elf5l.L	2.52	1.08E-03
b3galt1.S	2.52	2.09E-03
entpd2.S	2.51	8.03E-07
rgs10.S	2.50	2.11E-04
LOC108703769	2.50	7.74E-04
rgl2.L	2.50	4.39E-03
pla2g10.L	2.49	4.22E-03
adam28.2.L	2.49	4.48E-03
LOC121396841	2.48	1.93E-04
lrig1.S	2.47	3.85E-07
kiaa0319.S	2.47	1.58E-03
sgtb.L	2.46	1.49E-03
LOC121402202	2.46	5.46E-03
LOC121400594	2.46	3.28E-03
hal.2.L	2.46	2.72E-04
bcas4.L	2.46	6.04E-04
pla1a.L	2.45	4.27E-03

Neurog2 + Z-Mo vs Neurog2 + Co-MO		
gene	log2FC	padj
tp53inp1.S	2.44	1.31E-07
s1pr3.L	2.44	2.69E-03
mastl.L	2.43	1.20E-10
LOC121393606	2.43	4.92E-03
mtarc1.L	2.43	6.34E-03
LOC108699698	2.43	2.23E-03
lhcgr-A	2.43	6.31E-03
kank2.S	2.43	5.99E-03
h4c4.L	2.43	6.26E-03
cd274.L	2.43	2.80E-03
pstpip2.L	2.42	6.49E-03
pif1.L	2.42	3.87E-08
lonrf3.L	2.42	1.60E-03
LOC121393622	2.42	6.32E-03
lsmem1.L	2.42	5.93E-04
dcaf10.S	2.42	4.99E-07
cdkn2c.L	2.42	1.36E-05
btc.L	2.42	3.95E-03
tspan1.S	2.41	3.95E-03
pjvk.S	2.41	1.50E-03
phgdh.S	2.41	1.22E-09
lhx5.S	2.41	8.96E-05
agpat1.S	2.41	1.22E-05
sync.S	2.40	1.11E-04
socs1.L	2.40	4.02E-03
nipa1.L	2.40	9.61E-10
slc52a2.L	2.40	7.00E-03
cenpa.L	2.40	4.14E-06
LOC121396852	2.39	7.32E-03
tyr.L	2.39	5.10E-03
tars1.L	2.38	2.83E-05
folr1.L	2.38	4.85E-04
LOC108711198	2.36	4.87E-15
LOC108710854	2.36	9.04E-05
klf2.L	2.36	5.42E-06
hes7.1.L	2.36	8.04E-03
abhd1	2.36	3.10E-03
myo15a.L	2.35	3.21E-03
cgas.S	2.35	8.54E-03
metrnl.S	2.35	9.13E-04
carmil2.L	2.35	2.80E-03
cldn10.L	2.35	3.74E-03
nlrp12.S	2.34	7.91E-03
LOC108697429	2.34	8.64E-03
adamts8.L	2.34	8.34E-03
plekhg4.L	2.33	2.28E-06
mras.S	2.33	7.16E-09
eomes.L	2.33	9.36E-03
ccna2.S	2.33	1.63E-12
zar1l.S	2.32	9.24E-03
tyw3.L	2.31	6.69E-06
spdya.L	2.31	1.02E-02
znf385c.L	2.31	9.91E-03
LOC108696899	2.31	3.23E-03
atp4b.L	2.31	1.03E-02
pax3.S	2.30	3.36E-03
marchf4.L	2.30	1.02E-02
LOC108704851	2.30	1.04E-02
LOC108701308	2.30	9.64E-03
eda2r.L	2.30	2.31E-04
thsd1.L	2.29	1.12E-02
shisa2.S	2.29	1.11E-02
nexn.L	2.29	2.49E-03
eva1c.S	2.29	1.10E-02
shox.L	2.29	4.27E-03
gpr1.S	2.29	4.73E-03
gpnmb.L	2.29	3.53E-12
tcirg1.L	2.28	6.62E-06
prkar2b.S	2.28	8.13E-05
slc25a15.L	2.28	1.04E-03

Appendix 6.8 Top 210 downregulated DEGs: Neurog2 + zc3h12c.S-MO versus Neurog2 + Co-MO

Neurog2 + Z-Mo vs Neurog2 + Co-MO		
gene	log2FC	padj
coe3l.L	-3.86	1.07E-07
fbxl16.L	-3.39	1.87E-05
mllt11.S	-3.37	8.32E-06
LOC121401564	-3.32	1.70E-06
tal1.S	-3.02	1.12E-04
igfbpl1.S	-2.99	1.78E-05
cd38.L	-2.94	4.75E-06
gbx2.2.L	-2.82	2.63E-14
slitrk6.S	-2.81	1.60E-04
adra2c.L	-2.72	3.13E-04
tm4sf18.L	-2.72	9.74E-05
scn3b.L	-2.68	1.05E-10
map2k6.L	-2.67	1.17E-08
mapk8ip2.S	-2.66	6.53E-04
rasl10b.L	-2.66	2.55E-04
XB5735880.S	-2.63	4.93E-04
dbndd1.L	-2.62	2.52E-04
cpe.S	-2.61	1.61E-04
eepd1.L	-2.56	2.94E-03
fign.S	-2.55	6.37E-05
map1b.L	-2.55	2.61E-03
epb41.S	-2.52	9.07E-08
stoml1.L	-2.52	2.49E-04
LOC108716581	-2.48	3.85E-07
kctd18.S	-2.44	1.47E-03
heatr4.S	-2.42	1.12E-03
pltp.L	-2.42	6.53E-03
tulp4.S	-2.42	2.23E-03
tll2l.L	-2.41	1.47E-03
LOC108714021	-2.40	2.01E-03
mmp11.L	-2.40	1.05E-04
p2ry4.L	-2.40	1.11E-10
nr2f5.S	-2.38	4.62E-07
tm4sf1.L	-2.38	2.09E-03
rasef.S	-2.37	4.88E-04
dse.L	-2.36	1.81E-03
sulf1.L	-2.36	6.74E-06
hmx1.L	-2.35	6.17E-03
pnpla8.L	-2.35	5.78E-04
slit2.S	-2.35	3.02E-06
f13b.L	-2.34	2.89E-03
foxe1.L	-2.33	8.45E-03
amigo1.S	-2.32	7.04E-03
arnt2.L	-2.32	5.08E-03
mapk8ip2.L	-2.32	5.89E-03
tmem38b.L	-2.32	1.55E-08
fbxw10.L	-2.31	9.68E-04
plcb4.L	-2.31	5.17E-03
c11orf53.S	-2.29	2.64E-03
gatad2b.L	-2.29	2.07E-03
b3galt5.L	-2.28	4.02E-04
atp12a.L	-2.27	1.61E-06
LOC108697612	-2.27	1.47E-03
map2k3	-2.26	2.73E-10
cda.S	-2.25	1.19E-02
LOC108715719	-2.25	1.10E-02
LOC121400504	-2.25	3.95E-03
prph.S	-2.25	7.64E-04
trh.L	-2.25	1.30E-02
LOC108696918	-2.24	3.98E-03
rhobtb2.L	-2.24	7.34E-06
adam11.L	-2.23	1.32E-02
dclk1.L	-2.23	9.02E-03
gng13.S	-2.23	7.06E-07
rnf32.L	-2.23	1.87E-03
plcb2.L	-2.23	3.73E-04
pdcl3.S	-2.22	6.03E-03
slc20a2.L	-2.22	3.19E-03
foxa1.L	-2.21	1.55E-07
gbx2.2.S	-2.21	3.73E-03

Neurog2 + Z-Mo vs Neurog2 + Co-MO		
gene	log2FC	padj
gpr37.L	-2.21	1.11E-05
styk1.L	-2.21	4.20E-03
gzmak.L	-2.20	1.25E-02
LOC121402204	-2.20	2.77E-06
mgat4a.S	-2.20	3.02E-03
enox1.S	-2.19	3.90E-03
plscr1.L	-2.19	5.94E-06
pkhd1.L	-2.19	4.19E-04
astl2d.1.L	-2.18	8.14E-11
garem2.S	-2.18	1.66E-02
spsb3.L	-2.18	2.05E-09
muc2.L	-2.18	5.27E-10
pmp22.L	-2.18	3.74E-03
sipa1.L	-2.18	1.03E-03
ucma.S	-2.18	1.17E-02
igfbpl1.L	-2.17	7.72E-03
LOC108713720	-2.17	7.57E-06
rflb.L	-2.17	9.27E-03
tecta.1.L	-2.17	5.56E-03
greb1.L	-2.16	1.16E-04
hoxa3.L	-2.16	4.29E-03
LOC108709626	-2.16	1.05E-05
apc2.L	-2.14	3.94E-03
map3k7.S	-2.14	1.07E-11
cav3.S	-2.14	6.04E-06
klf4.L	-2.13	6.10E-03
LOC108719843	-2.13	4.70E-03
slc4a9.L	-2.13	9.60E-03
ak1.L	-2.12	4.60E-07
cdhr4.L	-2.12	6.96E-03
gfi1b.L	-2.12	2.46E-05
mgll.S	-2.11	4.10E-07
capn13.S	-2.10	6.41E-03
pou2f3.L	-2.10	4.42E-12
sulf1.S	-2.10	3.03E-03
lrrc31.L	-2.09	5.96E-03
LOC121399357	-2.09	3.34E-03
htr3a.L	-2.08	5.35E-04
pou2f3.S	-2.08	6.12E-05
fignl2.S	-2.07	1.35E-02
LOC108702891	-2.07	1.21E-02
kif5a.L	-2.07	1.34E-02
rab33a.L	-2.07	1.30E-02
cldn1.L	-2.06	4.03E-06
irx3.L	-2.06	2.13E-02
c11orf53.L	-2.05	1.00E-03
cldn34.L	-2.05	1.82E-02
srap.L	-2.05	2.19E-02
reep1.L	-2.05	1.65E-02
hoxa2.L	-2.04	1.22E-02
LOC108699297	-2.04	6.39E-03
kiaa2012.L	-2.04	2.51E-05
ppil6.S	-2.04	3.16E-03
rgs9bpl.L	-2.04	1.29E-02
slc27a2.L	-2.04	2.10E-06
aldh18a1.L	-2.03	4.33E-05
cdkl2.L	-2.03	6.45E-03
col14a1.L	-2.03	1.36E-02
hoxa2.S	-2.03	8.21E-03
wdr72.L	-2.03	1.37E-02
opn8.L	-2.03	1.53E-02
XB5774338.L	-2.03	1.46E-08
bok.S	-2.02	5.21E-03
hoxa1.L	-2.02	6.11E-05
LOC108704223	-2.02	2.11E-04
fign.L	-2.02	9.60E-03
LOC121395440	-2.02	1.52E-06
nwd1.L	-2.02	9.83E-03
rpp25.L	-2.02	2.43E-02
tal1.L	-2.02	2.44E-02

Neurog2 + Z-Mo vs Neurog2 + Co-MO		
gene	log2FC	padj
abcd2.L	-2.01	2.84E-02
get1.S	-2.01	3.40E-05
pkib.L	-2.01	2.88E-02
arhgef37.S	-2.00	3.02E-06
hace1.L	-2.00	1.68E-03
lmcd1.S	-2.00	2.30E-02
mbnl2.L	-2.00	2.80E-02
enpp2.L	-1.99	4.33E-03
g67.L	-1.99	9.64E-03
nptxr.S	-1.99	2.89E-02
sstr5.S	-1.99	4.03E-06
tp63.L	-1.99	1.90E-05
rnf223.L	-1.98	1.50E-02
adam12.S	-1.98	2.28E-02
myo10.L	-1.98	1.75E-03
nipal1.S	-1.98	1.80E-02
wnk4.L	-1.98	1.92E-02
c9orf135.S	-1.97	1.02E-02
cat.1.L	-1.97	1.51E-02
fbxo6.S	-1.97	1.05E-02
gal3st1.S	-1.97	2.40E-02
slc18a1.L	-1.97	3.23E-02
pm20d1.L	-1.97	2.26E-04
abcc5.L	-1.96	2.11E-05
akap11.S	-1.96	2.01E-02
ccn5.L	-1.96	2.43E-02
h1-0.S	-1.96	6.10E-03
golga6l7.L	-1.96	2.11E-04
add2.S	-1.95	1.15E-04
gss.L	-1.95	3.67E-05
ccdc27.S	-1.95	8.68E-05
unc13a.S	-1.95	3.41E-02
LOC108708418	-1.95	1.47E-02
samd8.S	-1.95	8.39E-03
c8orf34.S	-1.94	5.10E-06
dlec1.L	-1.94	1.16E-04
katnip.L	-1.94	1.35E-04
ncs1.S	-1.94	7.91E-06
slc1a3.S	-1.94	2.21E-02
dcdc2.S	-1.93	9.25E-03
MGC68910	-1.93	4.90E-06
ribc1.L	-1.93	3.88E-05
slc52a1.L	-1.93	4.60E-07
sp7.L	-1.93	2.16E-07
arid1b.S	-1.92	4.50E-06
cebpa.L	-1.92	1.31E-03
LOC108700234	-1.92	3.05E-02
tex47.L	-1.92	4.33E-05
LOC108715780	-1.91	1.67E-02
stoml3.L	-1.91	5.18E-03
ccdc107.L	-1.90	2.32E-04
erich3.S	-1.90	7.56E-03
ghrh.L	-1.90	3.83E-02
LOC108714343	-1.90	4.20E-02
LOC108717135	-1.90	2.11E-02
MGC84752	-1.90	8.06E-05
vwa5a.S	-1.90	4.32E-08
dzip1l.L	-1.89	2.08E-02
LOC108698443	-1.89	1.88E-02
LOC108709387	-1.89	2.35E-02
c17orf98.S	-1.89	1.64E-03
ppp1r2.L	-1.89	2.46E-04
kif26a.S	-1.88	2.28E-03
sh3bgrl.S	-1.88	3.39E-02
wfs1.L	-1.88	1.09E-03
avpr2.S	-1.87	1.93E-02
b4galt4.L	-1.87	6.63E-09
glb1l.L	-1.87	2.68E-02
mlycd.S	-1.87	9.82E-03
ndnfl2.S	-1.87	3.86E-02

Appendix 6.9 Gene Ontology analysis of zc3h12c.S-MO inhibited Neurog2 downstream genes.

The 78 genes are derived from the Venn Diagram in Fig. 23. Shown are the top 10 enriched Biological Processes, the genes identified in this term and sorted by enrichment FDR.

1. Neuron differentiation 7.7E-06
mapk8ip2 rufy3 myo9a pmp22 dock7 map1b snap25 tubb2b ppp3ca sfrp2 ncam1 kif5a tal1 irx3 tmem132e amigo1 prkg1 olig2 tubb3

2. Generation of neurons 7.69E-06
mapk8ip2 rufy3 nexmif myo9a pmp22 dock7 map1b snap25 tubb2b ppp3ca sfrp2 ncam1 kif5a tal1 irx3 tmem132e amigo1 prkg1 olig2 tubb3

3. Neurogenesis 1.54E-05
mapk8ip2 rufy3 nexmif myo9a pmp22 dock7 map1b snap25 tubb2b ppp3ca sfrp2 ncam1 kif5a tal1 irx3 tmem132e amigo1 prkg1 olig2 tubb3

4. Neuron projection development 4.0E-05
mapk8ip2 rufy3 myo9a pmp22 dock7 map1b snap25 tubb2b ppp3ca sfrp2 ncam1 kif5a amigo1 prkg1 tubb3

5. neuron development 4.0e-05
mapk8ip2 rufy3 myo9a pmp22 dock7 map1b snap25 tubb2b ppp3ca sfrp2 ncam1 kif5a tmem132e amigo1 prkg1 tubb3

6. Cell morphogenesis 3.4E-04
mapk8ip2 rufy3 myo9a arhgef18 dock7 map1b tubb2b ppp3ca ncam1 kif5a tal1 slc26a5 amigo1 tubb3

7. Cellular component morphogenesis 5.0E-04
mapk8ip2 rufy3 myo9a pmp22 dock7 map1b tubb2b ppp3ca ncam1 kif5a amigo1 tubb3

8. Neuron projection morphogenesis 5.5E-04
mapk8ip2 rufy3 myo9a pmp22 dock7 map1b snap25 tubb2b ppp3ca sfrp2 ncam1 kif5a amigo1 prkg1 tubb3

9. Cell projection morphogenesis 5.6E-04
mapk8ip2 rufy3 myo9a dock7 map1b tubb2b ppp3ca ncam1 kif5a amigo1 tubb3

10. Plasma membrane bounded cell projection morphogenesis 5.6E-04
mapk8ip2 rufy3 myo9a dock7 map1b tubb2b ppp3ca ncam1 kif5a amigo1 tubb3

Appendix 6.10 The overlapping genes from the Venn diagram in Fig. 23 are listed below.

Zc3h12c.S-MO inhibited Neurog2 downstream genes:
Total: 78 genes

garem2.S mllt11.S atg4c.L cpe.S gng13.S tmem132e.S myo9a.S sfrp2.S pmp22.L zfhx4.Samigo1.S ppp3ca.S kif26a.S atp13a3.L zfhx4.L fignl2.S opn8.L irx3.L arhgef18.L tal1.Skif5a.L reep1.L ndnfl2.S prph.S tmem65.L sulf1.L enox1.S LOC108709387 prph.L igfbpl1.Lrpp25.L nptxr.S arid1b.S cda.S prkg1.S snap25.L fam83b.L abcc5.L enox1.LLOC108698396 gbx2.1.L dock7.L slc7a8.S tal1.L fign.L clip2.S apc2.L hmx1.L rufy3.Ldbndd1.L coe3l.L tubb3.L gbx2.2.L bsn.L tubb2b.S znf385a.L slc26a5.L igfbpl1.S gipr.Lfmn1.L adam11.L XB5735880.S olig2.L fmn2.L mapk8ip2.L rab33a.L nexmif.L atp6v1fnb.L map1b.L rasef.S LOC121401564 sulf1.S ncam1.S slc18a3.L pigz.L sipa1.L fbxl16.L eya2.S

Zc3h12c.S -MO enhanced Neurog2 downstream genes:
Total: 37 genes

zc3h12c.L hes5.6.L hes5.2.L acer2.L neurod1.S jpt1.L auts2.S plekhg4.L sez6l2.S cbfb.S mras.S cbfa2t2.Lplk3.S gabarapl1.S prdm8.S dact4.L tnni1.2.L pds5b.L shox.L tcf15.S neurog2.Lcbfa2t2.S tmem116.L tspan18.S dlb.S fitm1.S ca10.L hes5.1.L otop1.S xfrp s1pr5.S maneal.L plekhg4.S mcf2l.S lrrn1.L zc3h12c.S magi1.S

Appendix 6.11 Gene Ontology analysis of upregulated DEGs: Neurog2 + zc3h12c.S-MO versus Neurog2 + Co-MO.

Shown are the top 10 enriched Biological Processes, the genes identified in this term and sorted by enrichment FDR.

1. Mitotic cell cycle 5.3E-11
akap8l brca1 mnat1 parp3 rad51 fgf10 hmmr tipin wdr62 cdc14b pds5b birc5 nudc cdc6 rae1 psmd10 rgcc ccne1 rpa3 ezh2 ube2s nup88 ncapg ripor2 fbxo5 kif20a ect2 cenpa phf13 cdc20 nup43 mastl khdrbs1 cit cdkn2c cks2 psmb2 prmt1 dlgap5 gnai1 pcna ccnb1 cdca8 mdm2 ckap2 gpnmb nusap1 kif23 nabp2 cyp1a1 ticrr tp53 kif2c nuf2 dis3l2 ccna2 plk2 ccnb3 mki67 incenp eif4e eps8 haus1 ccnb2 npm2 dbf4b racgap1 spc24 ccnf spdya pttg1 gem melk ska3 cenpn fam107a bub1 cdk1 cks1b znrd2 plk3 btc ube2c ccne2 tubb6 pole pidd1 aurkb cib1 ptch1 sapcd2 kank2 cenpw dhfr psmb8 kifc1 cdk11b wee2 h4c4 prkar2b psme1

2. Mitotic cell cycle process 8.5E-10
akap8l brca1 mnat1 parp3 rad51 fgf10 hmmr tipin wdr62 cdc14b pds5b birc5 nudc cdc6 rae1 psmd10 rgcc ccne1 ezh2 ube2s ncapg ripor2 fbxo5 kif20a ect2 cenpa phf13 cdc20 nup43 mastl khdrbs1 cit cdkn2c cks2 psmb2 prmt1 dlgap5 gnai1 pcna ccnb1 cdca8 mdm2 ckap2 gpnmb nusap1 kif23 nabp2 cyp1a1 ticrr tp53 kif2c nuf2 dis3l2 ccna2 plk2 ccnb3 mki67 incenp eif4e eps8 haus1 ccnb2 npm2 dbf4b racgap1 spc24 ccnf spdya pttg1 melk cenpn fam107a bub1 cdk1 plk3 btc ube2c ccne2 pole pidd1 aurkb sapcd2 kank2 dhfr psmb8 kifc1 h4c4 prkar2b psme1

3. Cell cycle process 1.8E-09
akap8l brca1 mnat1 parp3 rad51 tp53bp1 fgf10 hmmr mov10l1 tipin wdr62 pold3 cdc14b pds5b birc5 nudc phgdh cdc6 cbx5 rae1 psmd10 rgcc ccne1 rpa3 ezh2 ube2s ncapg ripor2 fbxo5 kif20a msh3 ect2 cenpa msh6 phf13 sfpq cdc20 nup43 mastl khdrbs1 cit cdkn2c cks2 psmb2 prmt1 dlgap5 gnai1 sox15 pcna rfc3 ccnb1 cdca8 mdm2 kiaa1614 ckap2 gpnmb nusap1 kif23 brdt nabp2 cyp1a1 ticrr tp53 kif2c mael nuf2 dis3l2 ccna2 plk2 ccnb3 terf1 mki67 incenp eif4e eps8 haus1 tdrd9 ccnb2 npm2 alkbh4 dbf4b racgap1 spc24 ccnf spdya rfc4 pttg1 gem melk cenpn mcm7 pclaf fam107a mn1 bub1 cdk1 plk3 phc3 btc ube2c ccne2 pole pidd1 aurkb sapcd2 kank2 rnf212b dhfr psmb8 kifc1 wee2 h4c4 prkar2b psme1

4. Cell cycle 1.2E-08
akap8l brca1 mnat1 parp3 rad51 tp53bp1 rassf1 mapk6 fgf10 hmmr mov10l1 tipin wdr62 pold3 epb41l2 cdc14b pds5b birc5 nudc phgdh cdc6 cbx5 rae1 psmd10 rgcc ccne1 rpa3 ezh2 urgcp ube2s nup88 ncapg cdca3 ripor2 fbxo5 kif20a msh3 ect2 cenpa msh6 phf13 sfpq cdc20 nup43 mastl khdrbs1 cit cdkn2c cks2 stk35 mcm8 psmb2 prmt1 dlgap5 gnai1 sox15 gadd45g pcna rfc3 ccnb1 cdca8 mdm2 kiaa1614 ckap2 gpnmb nusap1 kif23 brdt nabp2 cyp1a1 ticrr tp53 prkacb kif2c mael nuf2 dis3l2 ccna2 plk2 ccnb3 terf1 mki67 gas2 incenp eif4e eps8 haus1 suv39h2 tdrd9 ccnb2 npm2 alkbh4 dbf4b racgap1 spc24 ccnf spdya rfc4 pttg1 gem melk ska3 mettl3 cenpn mcm7 pclaf chaf1a fam107a mn1 bub1 cdk1 cks1b znrd2 plk3 phc3 btc ube2c ccne2 tubb6 pole pidd1 exd1 aurkb cib1 ptch1 sapcd2 kank2 cenpw rnf212b dhfr psmb8 kifc1 cdk11b wee2 h4c4 prkar2b psme1

5. Cell division 2.2E-07
tipin epb41l2 cdc14b pds5b birc5 nudc orc6 cdc6 rae1 ccne1 numbl ube2s ncapg cdca3 fbxo5 kif20a ect2 cenpa phf13 cdc20 nup43 mastl cit cks2 gnai1 ccnb1 cdca8 ckap2 nusap1 kif23 kif2c nuf2 dis3l2 ccna2 plk2 ccnb3 terf1 incenp haus1 ccnb2 alkbh4 racgap1 spc24 ccnf pttg1 ska3 bub1 cdk1 cdca4 cks1b znrd2 plk3 btc ube2c ccne2 aurkb cib1 ptch1 sapcd2 cenpw kifc1

6. Chromosome segregation 1.8E-06
akap8l brca1 pum2 pds5b birc5 nudc cdc6 ccne1 ncapg fbxo5 ect2 phf13 sfpq cdc20 nup43 dlgap5 ccnb1 cdca8 nusap1 kif23 kif2c mael nuf2 dis3l2 terf1 mki67 incenp racgap1 pttg1 gem ska3 cenpn bub1 cdk1 ube2c ccne2 aurkb cenpw rnf212b kifc1 h4c4

7. Mitotic cell cycle phase transition 1.1E-05
brca1 mnat1 fgf10 hmmr cdc14b cdc6 psmd10 rgcc ccne1 ezh2 ube2s fbxo5 cdc20 mastl khdrbs1 cdkn2c cks2 psmb2 prmt1 dlgap5 pcna ccnb1 mdm2 gpnmb nabp2 cyp1a1 ticrr tp53 ccna2 plk2 ccnb3 eif4e eps8 haus1 ccnb2 npm2 dbf4b ccnf spdya melk fam107a bub1 cdk1 plk3 ube2c ccne2 pole pidd1 aurkb kank2 dhfr psmb8 prkar2b psme1
8. Nuclear division 2.7E-05
akap8l rad51 mov10l1 cdc14b pds5b nudc cdc6 rgcc ccne1 ube2s ncapg ripor2 fbxo5 msh3 phf13 cdc20 nup43 cks2 dlgap5 ccnb1 cdca8 nusap1 kif23 brdt kif2c mael nuf2 dis3l2 terf1 mki67 incenp eps8 tdrd9 ccnb2 npm2 racgap1 spdya pttg1 bub1 cdk1 btc ube2c ccne2 aurkb rnf212b kifc1 wee2 h4c49

9. Cell cycle phase transition 6.8E-05
akap8l brca1 mnat1 tp53bp1 fgf10 hmmr tipin cdc14b cdc6 psmd10 rgcc ccne1 ezh2 ube2s fbxo5 cdc20 mastl khdrbs1 cdkn2c cks2 psmb2 prmt1 dlgap5 pcna ccnb1 mdm2 gpnmb nabp2 cyp1a1 ticrr tp53 ccna2 plk2 ccnb3 eif4e eps8 haus1 ccnb2 npm2 dbf4b ccnf spdya melk fam107a mn1 bub1 cdk1 plk3 ube2c ccne2 pole pidd1 aurkb kank2 dhfr psmb8 prkar2b psme1

10. Mitotic sister chromatid segregation 8.0E-05
akap8l pds5b nudc cdc6 ncapg fbxo5 phf13 cdc20 dlgap5 ccnb1 cdca8 nusap1 kif23 kif2c nuf2 dis3l2 incenp racgap1 pttg1 bub1 cdk1 ube2c aurkb kifc1 h4c4